UNIVERSITY OF ALBERTA

LOW TEMPERATURE OXIDATION OF METHANOL USING HYDROPHOBIC CATALYSTS

by

DAVID SPAGNOLO ©

A thesis submitted to the Faculty of Graduate Studies and Research in partial fulfillment of the requirements for the degree of **DOCTOR OF PHILOSOPHY**.

Department of Chemical and Materials Engineering

Edmonton, Alberta

Spring 1997

National Library of Canada
Acquisitions and Bibliographic Services
395 Wellington Street
Ottawa ON K1A 0N4
Canada

Bibliothèque nationale du Canada
Acquisitions et services bibliographiques
395, rue Wellington
Ottawa ON K1A 0N4
Canada

Your file Votre référence

Our file Notre référence

The author has granted a non-exclusive licence allowing the National Library of Canada to reproduce, loan, distribute or sell copies of his/her thesis by any means and in any form or format, making this thesis available to interested persons.

The author retains ownership of the copyright in his/her thesis. Neither the thesis nor substantial extracts from it may be printed or otherwise reproduced with the author's permission.

L'auteur a accordé une licence non exclusive permettant à la Bibliothèque nationale du Canada de reproduire, prêter, distribuer ou vendre des copies de sa thèse de quelque manière et sous quelque forme que ce soit pour mettre des exemplaires de cette thèse à la disposition des personnes intéressées.

L'auteur conserve la propriété du droit d'auteur qui protège sa thèse. Ni la thèse ni des extraits substantiels de celle-ci ne doivent être imprimés ou autrement reproduits sans son autorisation.

0-612-21640-3

Canada

UNIVERSITY OF ALBERTA

LIBRARY RELEASE FORM

Name of Author: **David Spagnolo**

Title of Thesis: **Low Temperature Oxidation of Methanol using Hydrophobic Catalysts**

Degree: **Doctor of Philosophy**

Year this Degree Granted: **1997**

Permission is hereby granted to the University of Alberta Library to reproduce single copies of this thesis and to lend or sell such copies for private, scholarly, or scientific research purposes only.

The author reserves all other publication and other rights in association with the copyright in the thesis, and except as hereinbefore provided, neither the thesis nor any substantial portion thereof may be printed or otherwise reproduced in any material form whatever without the author's prior written permission.

Signed: D. Spagnolo

547 RH, Michener Park
Edmonton, AB
T6H 4M5

DATE: Jan. 21/97

UNIVERSITY OF ALBERTA

FACULTY OF GRADUATE STUDIES AND RESEARCH

The undersigned certify that they have read, and recommended to the Faculty of Graduate Studies and Research for acceptance, a thesis entitled **Low Temperature Oxidation of Methanol using Hydrophobic Catalysts** submitted by **David Spagnolo** in partial fulfillment of the requirements for the degree of **Doctor of Philosophy**.

K. T. Chuang (supervisor)

R. R. Hudgins (external examiner)

M. Cowie

S. E. Wanke

A. E. Mather

DATE: Jan. 14/97

ABSTRACT

Hydrophobic catalysts, namely platinum supported on fluorinated carbons, were investigated for the low temperature oxidation of methanol in air. The catalysts are characterized in terms of their pore size distribution, surface area, platinum dispersion and wettability. To obtain a quantitative measure of the wettability of the hydrophobic supports, an equation that relates the contact angle and the heat of immersion is developed which enables the calculation of the contact angle from heat of immersion data for hydrophobic powders. The heat of immersion method has many advantages over the conventional methods for measuring contact angle.

A mechanism for the low temperature oxidation of methanol in air is proposed which explains the temperature dependence of the various products of the oxidation reaction. The presence of internal mass transfer limitations on the catalysts is investigated in order to collect accurate kinetic data. A first order rate equation is developed using Langmuir-Hinselwood kinetics to successfully describe the overall methanol conversion. The kinetic parameters for the rate equation are determined for all four catalysts studied.

Hydrogen adsorption studies and reaction rate experiments indicate the presence of platinum-fluoride interactions on the highly fluorinated carbon catalysts which negatively affect the catalyst performance for the oxidation of methanol. The activity of these catalysts is improved by heat treatment which eliminates much of the fluoride from the catalyst surface.

It is shown that the hydrophobic catalysts are stable in wet feed conditions, where as, the hydrophilic catalyst continually loses activity. There is some loss of activity for the hydrophobic catalysts in wet feed conditions. The highly fluorinated carbon catalysts show a reversible and irreversible deactivation mechanism in the presence of water vapor. These mechanisms are attributed to competitive adsorption and strongly adsorbed intermediates caused by the platinum-fluoride interaction.

ACKNOWLEDGEMENT

The author wishes to thank Dr. K. T. Chuang and Dr. S. E. Wanke for their guidance and valuable criticism throughout this program.

The author is grateful to Dr. B. Zhou, Dr. Y. Maham, and Mr. A. Afacan for their encouraging friendship, which made the time spent at the university more enjoyable.

The author's greatest personal debt is to his wife, Maria, and daughter, Yvonne, whose support and unfailing patience were invaluable for the completion of this work.

The author is also indebted to his mother, Linda, and father, Dino, whose inspiration and encouragement led to the initiation of the program.

The author is sincerely grateful for the financial support provided by the Department of Chemical and Materials Engineering at the University of Alberta.

TABLE OF CONTENTS

CHAPTER			PAGE
1.0	**INTRODUCTION TO THE CATALYTIC OXIDATION OF VOLATILE ORGANIC COMPOUNDS**		1
	1.1	INTRODUCTION	2
	1.2	CONVENTIONAL CATALYSTS USED IN THE CATALYTIC OXIDATION OF VOCs	5
	1.3	HYDROPHOBIC CATALYSTS	6
	1.4	SCOPE OF THE PRESENT WORK	8
	1.5	REFERENCES	9
2.0	**CATALYST PREPARATION**		10
	2.1	INTRODUCTION	11
	2.2	IMPREGNATION OF PLATINUM ON SUPPORTS	13
	2.3	COATING THE POWDER CATALYST ON CERAMIC SPHERES	15
	2.4	REFERENCES	16
3.0	**CATALYST CHARACTERIZATION**		17
	3.1	INTRODUCTION	18
	3.2	SURFACE AREA AND PORE SIZE DISTRIBUTION	18
	3.3	DETERMINING PLATINUM DISPERSION	20
		3.3.1 X-ray Diffraction	20
		3.3.2 Pulse Chemisorption	21
	3.4	COMPARISON OF THE PLATINUM DISPERSIONS	25
	3.5	HYDROPHOBICITY OF SUPPORTS	28
	3.6	REFERENCES	30
4.0	**RELATIONSHIP BETWEEN HEAT OF IMMERSION AND CONTACT ANGLE**		31
	4.1	INTRODUCTION	32
	4.2	DERIVATION OF THE THEORETICAL RELATIONSHIP BETWEEN THE CONTACT ANGLE AND THE HEAT OF IMMERSION	36

4.3	INTRODUCTION TO THE PRINCIPLES OF HEAT-FLOW CALORIMETRY	39
4.4	EXPERIMENTAL EQUIPMENT	43
	4.4.1 The C-80 Micro-calorimeter	43
	4.4.2 Calorimetry Cell and Experimental Procedure	47
4.5	RESULTS AND DISCUSSION	49
4.6	CONTACT ANGLE MEASUREMENTS USING THE COMPRESSED POWDER METHOD	51
	4.6.1 Introduction	51
	4.6.2 Experimental Procedure and Apparatus	53
	4.6.3 Results and Discussion	55
4.7	CONCLUSIONS	59
4.8	NOTATION	60
4.9	REFERENCES	62
5.0	**CATALYTIC OXIDATION OF METHANOL**	64
5.1	INTRODUCTION	65
5.2	PROPOSED MECHANISMS FOR THE CATALYTIC OXIDATION OF METHANOL	65
5.3	COMPARISON OF THE PROPOSED MECHANISMS	69
5.4	MODIFIED MECHANISM FOR THE OXIDATION OF METHANOL	71
5.5	EFFECT OF WATER ON THE CATALYTIC OXIDATION OF METHANOL	74
5.6	REFERENCES	78
6.0	**EXPERIMENTAL EQUIPMENT AND OPERATIONS**	80
6.1	EXPERIMENTAL EQUIPMENT	81
	6.1.1 Feed Section	81
	6.1.2 Reaction Section	86
	6.1.3 Feed and Product Analysis	88
6.2	OPERATING OF EQUIPMENT AND EXPERIMENTAL PROCEDURES	89
6.3	REFERENCES	93

7.0 EVALUATING THE KINETICS FOR THE OXIDATION OF METHANOL 94
7.1 INTRODUCTION 95
7.2 CATALYST STABILITY IN DRY CONDITIONS 95
7.2.1 Hydrophobic Catalysts 96
7.2.2 Hydrophilic Catalysts 102
7.3 INTERNAL MASS TRANSFER EFFECT 105
7.4 EVALUATION OF THE KINETIC PARAMETERS 110
7.5 SELECTIVITY OF THE METHANOL OXIDATION REACTION 122
7.6 REFERENCES 128

8.0 EFFECT OF WATER ON THE METHANOL OXIDATION REACTION 129
8.1 INTRODUCTION 130
8.2 CATALYST STABILITY IN WET FEED CONDITIONS 130
8.2.1 Hydrophobic Catalysts 130
8.2.2 Hydrophilic Catalyst 140
8.3 EFFECT OF WATER ON FLUORINATED CARBON CATALYSTS 143

9.0 CONCLUSIONS AND RECOMMENDATIONS 146
9.1 CONCLUSIONS 147
9.2 RECOMMENDATIONS 149

APPENDICES 150

A. CALCULATIONS FOR THE CHARACTERIZATION OF CATALYSTS 151

B. HEAT OF IMMERSION DATA 154

C. DERIVATION OF THE RATE EQUATION FOR THE OXIDATION OF METHANOL 155

D.	**CATALYST STABILITY DATA**	159
E.	**THEORETICAL CALCULATION OF THE EFFECTIVENESS FACTOR**	164
F.	**EXPERIMENTAL DATA FROM THE KINETIC STUDY**	169
G.	**CONVERSION AND SELECTIVITY DATA**	182
H.	**CATALYST STABILITY DATA (WET AND DRY CONDITIONS)**	186
I.	**RATE DATA FOR WET FEED CONDITIONS**	197

LIST OF TABLES

		Page
Table 3.1	Pore Size Distribution of Catalysts	19
Table 3.2	Characterization of Catalysts	19
Table 3.3	Pre-treatment Procedure for Pulse Chemisorption Experiments	24
Table 4.1	Enthalpy of Immersion and Contact Angle of Hydrophobic Powders	52
Table 4.2	Contact Angle Measured Using Compressed Powder Method	58
Table 7.1	Effect of Active Layer Thickness	108
Table 7.2	Results of the Kinetic Study on Various Catalysts	115
Table 7.3	Reaction Order as a Function of Temperature for Pt/FC28	117

LIST OF FIGURES

		Page
Figure 2.1	TEM Photograph of FC28 Powder	12
Figure 2.2	Rotary Incline Evaporator	14
Figure 2.3	Cross-section of the Catalyst Particle	16
Figure 3.1	X-ray Diffraction Peaks for the Platinum Powder Catalysts	22
Figure 3.2	The Contact Angle (θ) for a Drop on a Flat Smooth Surface	29
Figure 4.1	Principle of Heat-fluxmeter	40
Figure 4.2	Schematic Diagram of the C-80 Micro-Calorimeter	44
Figure 4.3	Block Diagram of the C-80 and Accessories	46
Figure 4.4	Schematic Diagram of the Calorimetry Cell	48
Figure 4.5	Enthalpy of Immersion vs Concentration of n-propanol	50
Figure 4.6	Apparatus for Sessile Drop Measurements	54
Figure 4.7	Image of a Water Drop on Various Compressed Powder Discs as Reproduced on a Laser Printer	56
Figure 5.1	Modified Mechanism for the Oxidation of Methanol	72
Figure 6.1	Schematic Diagram of Reaction Apparatus	82
Figure 6.2	Inlet Methanol Concentration vs Time	84
Figure 6.3	Inlet Water Concentration vs Time	85
Figure 6.4	Schematic Diagram of the Berty Reactor	87
Figure 6.5	Component GC Peak Area vs Concentration	90
Figure 6.6	Methanol Conversion vs Rotation Speed	92
Figure 7.1	Methanol Conversion vs Time for Pt/FC10 Catalyst in Dry Conditions	97

Figure 7.2	Methanol Conversion vs Time for Pt/FC28 Catalyst in Dry Conditions	98
Figure 7.3	Methanol Conversion vs Time for Pt/FC65 Catalyst in Dry Conditions	99
Figure 7.4	Product Yield vs Time for Pt/FC28 Catalyst in Dry Conditions	100
Figure 7.5	Methanol Conversion vs Time for Pt/Al_2O_3 Catalyst in Dry Conditions	103
Figure 7.6	Product Yield vs Time for Pt/Al_2O_3 Catalyst in Dry Conditions	104
Figure 7.7	Arrhenius Plot for Various Thicknesses of the Active Phase Layer	109
Figure 7.8	Arrhenius Plot for Pt/FC10 Catalyst	112
Figure 7.9	Arrhenius Plot for Pt/FC65 Catalyst	113
Figure 7.10	Arrhenius Plot for Pt/Al_2O_3 Catalyst	114
Figure 7.11	Reaction Rate vs Temperature for the Fluorinated Carbon Catalysts	119
Figure 7.12	Comparison of Heat Treated Pt/FC28 to Pt/FC10 and Regular Pt/FC28	121
Figure 7.13	Selectivity versus Temperature for Pt/FC10 Catalyst	123
Figure 7.14	Selectivity versus Temperature for Pt/FC28 Catalyst	124
Figure 7.15	Selectivity versus Temperature for Pt/FC65 Catalyst	125
Figure 7.16	Selectivity versus Temperature for Pt/Al_2O_3 Catalyst	126
Figure 8.1	Methanol Conversion vs Time for Pt/FC10 Catalyst in Wet Conditions	131
Figure 8.2	Methanol Conversion vs Time for Pt/FC28 Catalyst in Wet Conditions	132
Figure 8.3	Methanol Conversion vs Time for Pt/FC65 Catalyst in Wet Conditions	133
Figure 8.4	Cyclic Behavior of the Pt/FC10 Catalyst	135

Figure 8.5	Cyclic Behavior of the Pt/FC28 Catalyst	136
Figure 8.6	Cyclic Behavior of the Pt/SDB Catalyst	138
Figure 8.7	Product Yield vs Time for Pt/FC28 Catalyst in Wet Conditions	139
Figure 8.8	Methanol Conversion vs Time for Pt/Al_2O_3 Catalyst in Wet Conditions	141
Figure 8.9	Product Yield vs Time for Pt/Al_2O_3 Catalyst in Wet Conditions	142
Figure 8.10	Reaction Rate vs Temperature for Pt/FC10 Catalyst in Wet Conditions	144
Figure 8.11	Reaction Rate vs Temperature for Pt/FC28 Catalyst in Wet Conditions	145

CHAPTER 1

INTRODUCTION TO CATALYTIC OXIDATION OF VOLATILE ORGANIC COMPOUNDS

1.1 INTRODUCTION

Volatile organic compounds (VOCs) are hydrocarbons (halogenated and nonhalogenated) having boiling points below 138 °C.[1] They are among the most common pollutants emitted by the chemical process industries and are precursors to ground-level ozone which is a major component in the formation of smog. VOCs include most solvents, thinners, degreasers, cleaners, lubricants and liquid fuels. The discharge of VOCs to the environment is regulated by local, provincial and federal laws. In the United States, the Clean Air Act Amendments of 1990, require a 90% reduction of 189 hazardous air pollutants, most of which are included under the definition of VOCs. Because of the increasing attention being given to VOC control, the search for efficient and economical technologies that will effectively remove these contaminants from waste gas streams is extremely important.

There are several methods for removal of VOCs. These technologies can be separated into two categories. The first category includes destructive methods such as thermal oxidizers, catalytic oxidizers, flares, boilers/process heaters, biofilters, ultraviolet oxidizers and corona destruction reactors. The second category includes recovery devices such as condensers, adsorbers, absorbers, membrane separators and plasma technology devices. The selection of a destruction versus recovery device is based on the economic benefit of recovering the VOCs in the waste gas stream. Absorbers and boiler/process heaters are not often used for VOC control. In general, absorbers are less effective than the other technologies and are used more for the removal of inorganic compounds. Boilers and process heaters are not solely used for VOC removal but they can be used to destroy the VOCs as long as this function does not compromise the safety and reliability of the primary purpose of the unit. Biofiltration, membrane separation and ultraviolet oxidation are new technologies that have only recently become commercially available. Biofiltration involves the use of soil or compost beds containing microorganisms to

convert VOCs into carbon dioxide, water, and mineral salts. Membrane separation refers to the use of a semi-permeable polymeric membrane to separate VOCs from a waste gas stream. Ultraviolet oxidation uses oxygen-based oxidants such as ozone, peroxide and OH^- and O^- radicals to convert VOCs into carbon dioxide and water in the presence of UV light. The newest technologies, which are not yet commercially available, are corona destruction and plasma technology. In corona destruction, energetic electrons are generated in a high-intensity reactor, where they collide with the VOCs to produce non-reactive compounds such as carbon dioxide and water. The exact mechanism by which the excited electrons react with the VOCs is not well understood but it does not appear to produce hazardous intermediate compounds that would require disposal as hazardous waste. The reactor operates at ambient temperature and can treat halogenated and nonhalogenated compounds. Plasma technology is not yet well known as a VOC abatement technology, although research and development are underway in the United States and Europe. Thermal and catalytic oxidizers, adsorbers, and condensers are the most popular VOC controls in use today because of their broad applicability to a wide variety of VOC emission streams.[2]

The driving force for condensation is over-saturation which is achieved by cooling or pressurization (or both) of the waste gas stream. Condensation is most efficient for VOCs with boiling points above 37°C at relatively high concentrations of above 5,000 ppm.[3] Low boiling VOCs require extensive cooling or pressurization which greatly increases the operating costs. Condensation produces a liquid product that must be treated to remove condensed water and possibly to separate various chemical species. One of the advantages of this technology is that the VOCs can be recovered and reused in the process. Because of the nature of the condensation system, it is important that polymerizing materials not be present in the waste stream due to the potential for fouling of the heat-transfer surfaces.

The other major recovery technology used for waste streams containing VOCs is adsorption. Carbon is the most commonly used adsorbent. The VOCs are removed from the waste stream by adsorption onto the surface of the carbon. Adsorption systems can be designed to handle VOC concentrations from 20 to 5,000 ppm.[3] The installation costs are often lower than those for other technologies and the operating costs are relatively low. One of the disadvantages of carbon adsorption is carbon attrition. In order to regenerate the carbon, the VOCs must be removed from the carbon by heating. This desorption process can only be carried out at temperatures of a few hundred degrees because the carbon is flammable. When the temperatures are insufficient to desorb the VOCs, the adsorption sites are no longer available and the performance of the bed is drastically decreased. The waste carbon must then be disposed of and in most cases, it is considered a hazardous waste which requires expensive disposal costs. Another disadvantage of the adsorption systems is that they are very sensitive to the moisture content of the gas stream being treated. The ability of the carbon to absorb the VOCs decreases as the relative humidity of the gas stream exceeds 50%. This is most likely due to capillary condensation in the carbon bed which blocks the adsorption sites. This may be an area in which a hydrophobic adsorbent could be used to reduce the effect of humidity on the adsorption process.

For waste gas streams that contain small amounts of VOCs, recovery of the VOCs is not economical and therefore one of the destructive technologies is favored. Thermal oxidation systems combust VOCs at temperatures from 700°C to 980°C depending on the type and concentration of the materials in the waste stream. Compounds that are difficult to combust or are present at low inlet concentrations will require greater heat input and retention time in the combustion zone to ensure that the desired destruction and removal efficiency is accomplished. Thermal oxidizers are designed to accomplish from 95% to 99+% destruction of virtually all VOCs. These systems can be designed to handle VOC concentrations ranging from 100 to 2,000 ppm.[3] There are some drawbacks to thermal

oxidation. For example, operating temperatures near 980°C can produce elevated levels of nitrogen oxides which may, in turn, require further treatment such as selective catalytic reduction. The high temperatures also make it necessary to use expensive material in the construction of the oxidizing unit. Another disadvantage of thermal oxidizers is the supplemental fuel cost associated with burning VOCs when they are present below the lower flammable limit.

Catalytic oxidation systems directly combust VOCs similar to that of thermal oxidizers. The major difference is that catalytic systems operate at lower temperatures, between 370°C and 480°C. This is made possible by the use of catalysts, which avoid the use of supplemental fuel. Destruction efficiencies in excess of 90% are common with a maximum destruction and removal efficiency in the order of 95%. Catalytic systems can be designed to handle VOC concentrations from 100 to 2,000 ppm.[3] The catalytic system is well suited for low concentration streams where the flow rates and VOC contents are variable. The lower operating temperature reduces the amount of nitrogen oxides produced and reduces the startup fuel requirement compared to the thermal oxidizers. However, there is a high cost associated with the catalyst replacement. The catalysts used in the oxidation of VOCs constitute a large portion of the operating costs. For this reason, there is great incentive to develop more efficient catalysts that keep their activity for a longer period of time. There is also incentive to reduce the operating temperature of the catalytic oxidizers which will also lower the operating cost associated with this process.

1.2 CONVENTIONAL CATALYSTS USED IN THE CATALYTIC OXIDATION OF VOCs

Supported noble metal catalysts have been found to have higher activity for the oxidation of VOCs than their metal-oxide counterparts.[4] The conventional noble metal catalysts are Pt or Pd supported on γ-Al_2O_3 or SiO_2. For catalytic reactions, the rate of

reaction is generally proportional to the metal area accessible to the reactants. To maximize the area, it is common practice to disperse the metal on a high surface area support. The use of high porous supports such as Al_2O_3 and SiO_2 is to provide a large surface area for metal deposition. The majority of waste gas streams contain water vapor as well as the organic pollutants. Water is also produced as a by-product in the oxidation of VOCs. Once water is present in the catalyst bed, it can adsorb on the catalyst support or condense in the pores of conventional catalysts through capillary condensation. This water is believed to affect the activity of the catalyst by inhibiting the mass transfer of reactants, such as oxygen and VOCs, to the catalyst sites. The above mentioned supports are hydrophilic and therefore are susceptible to capillary condensation and water adsorption. To prevent the water from condensing in the pores, it is necessary to operate the reactor at temperatures above the critical point of water (approximately 374 °C). The reason that the catalytic oxidizers operate between 370 and 480 °C is to retain the catalytic activity in the presence of water vapor. If water was not present in the feed stream the catalytic oxidizers could achieve the required destruction efficiency at temperatures below 300 °C depending on the VOCs present in the feed. According to Kosusko et al.[5], complete oxidation of most organic pollutants can take place below 170 °C. Catalysts that could resist the effects of water at low temperatures would enable the operating temperature of the catalytic oxidizers to be reduced. This could be achieved by the introduction of hydrophobic supports which allow the catalyst surface to stay "dry" in the presence of water and/or water vapor. This increases the activity of the catalyst by allowing higher concentrations of reactants at the active sites and by reducing mass transfer limitations.

1.3 HYDROPHOBIC CATALYSTS

The development of hydrophobic catalysts began in the early 1970s for the isotopic exchange reaction between hydrogen and water vapor[6-8] to avoid the condensation of

water in the pores of metal-supported catalysts. Recently, hydrophobic catalysts have been tested for the oxidation of various VOCs, including, benzene, toluene, xylene, CO and formaldehyde.[9-11] The literature on hydrophobic catalysts can be divided into two categories: (i) noble metals dispersed on a hydrophilic support coated with a hydrophobic material such as polytetrafluoroethene (PTFE) or silicon oil; (ii) noble metals dispersed on a hydrophobic support such as styrene-divinylbenzene (SDB) copolymer or fluorinated carbon (FC).

The development of hydrophobic catalysts was based on the theory of capillary condensation. When a metal supported catalyst is exposed to water vapor, it can become "wet" due to capillary effects. In such a case, the gaseous reactants must dissolve in the liquid in order to reach the metal surface. Since some gases, such as oxygen, are sparsely soluble in aqueous solutions, the rate determining step is often the mass transfer of reactants to the reaction sites. The combination of low solubility with low liquid phase diffusion coefficients of reactants, results in low apparent catalytic activity. To overcome the mass transfer limitations, a hydrophobic support may be used.

When a conventional catalyst is exposed to aqueous solutions, capillary condensation takes place until it reaches thermodynamic equilibrium dictated by the Kelvin equation.

$$\ln(P_o / P) = \frac{2V_m \gamma \cos\theta}{rRT} \qquad (1.3\text{-}1)$$

where r = the radius of the capillary
R = the gas constant
T = the temperature
V_m = the molar volume of liquid at T
γ = the surface tension of the liquid
θ = the contact angle
P_o = the saturation pressure over a flat surface
P = the saturation pressure over a curved surface

For conventional catalyst supports the material is hydrophilic which means the contact angle with water is below 90° and usually close to zero. Thus, the entire catalyst will be wet when exposed to the liquid. The Kelvin equation implies that increasing the contact angle reduces pore condensation. In the presence of a liquid, P is equal to P_o and if a hydrophobic material with a contact angle of greater than 90° is selected as a catalyst support, its pores will remain dry and accessible to the gaseous reactants. In this way the concentration of reactants at the active sites in the pores is increased. Also, the rate of diffusion in the gas phase is approximately 1000 to 10 000 times higher than that in the liquid phase. A combination of these two improvements by using hydrophobic catalyst supports can increase the activity of the catalyst substantially in the presence of water.

1.4 SCOPE OF THE PRESENT WORK

The use of hydrophobic catalysts is growing. It is the purpose of this thesis to study the fundamental aspects involved with using hydrophobic catalysts for the oxidation of VOCs at concentrations less than 3000 ppm. This includes a description of the preparation and characterization of the catalysts as well as the determination of the kinetics of the catalyst in both dry and wet feed conditions. The reaction studied is the gas phase oxidation of methanol. The reason for choosing this specific reaction is discussed in detail in Chapter 5. The hydrophobic catalyst is compared to a conventional catalyst in terms of activity and its ability to retain its activity in the presence of water. Much of the work in this study has been focused on the characterization of the hydrophobicity of the catalyst support and on the kinetics of the methanol oxidation reaction.

The following is a list of objective for this thesis.

1. Characterize the hydrophobic catalysts in terms of surface area, pore size distribution, platinum dispersion and hydrophobicity.
2. Develop a method for determining the contact angle of hydrophobic powders.

3. Propose a mechanism for the low temperature oxidation of methanol.
4. Compare the stability and reaction rate of the different catalysts studied in both dry and wet feed conditions.

1.5 REFERENCES

1. Tessitore, J., J. Pinion, E. DeCresie, *Pollution Engineering*, **1990**, March, 62.
2. Moretti, E. C., and N. Mukhopadhyay, *Chemical Engineering Progress*, **1993**, July, 20.
3. Ruddy, E. N., and L. A. Carroll, *Chemical Engineering Progress*, **1993**, July, 28.
4. Spivey, J.J., *Ind. Eng. Chem. Res.*, **1987**, 26, 2165.
5. Kosusko, M., M. E. Mullins, K. Ramanathan, T. N. Rogers, *Environ. Prog.*, **1988**, 7(2), 136.
6. Enright, J. T., and K. T. Chuang, *Can. J. Chem. Eng.*, **1978**, 56, April, 246.
7. Suppiah, S., and K. T. Chuang, *Can. J. Chem. Eng.*, **1987**, 65, Feb., 42.
8. Suppiah, S., K. T. Chuang, J. H. Rolston, *Can. J. Chem. Eng.*, **1987**, 65, April, 256.
9. Chuang, K. T., S. Chen, S. Tong, *Ind. Eng. Chem. Res.*, **1992**, 31, (11), 2466.
10. Yaparpalvi, R., and K. T. Chuang, *Ind. Eng. Chem. Res.*, **1991**, 30, (9),2219.
11. Chuang, K. T., B. Zhou, S. Tong, *Ind. Eng. Chem. Res.*, **1994**, 33, (7), 1680.

CHAPTER 2

CATALYST PREPARATION

2.1 INTRODUCTION

The hydrophobic catalysts developed for this work are platinum supported on fluorinated carbon. Fluorinated carbon (FC) is a very hydrophobic powder with large specific surface area and particle sizes less than 1 μm. Three FC powders were purchased from Allied Corporation with varying degrees of fluorination. The designation given to each of the fluorinated carbons indicates the weight percent of fluoride. For example, FC10 represents a fluorinated carbon with 10 wt% fluoride. It follows that FC28 and FC65 have 28 and 65 wt% fluoride respectively. The fluorinated carbon was made by contacting elemental fluorine with carbon black. The greater the fluorination, the more hydrophobic the powder. The thermal stability of the FC powders is also related to the degree of fluorination. The decomposition temperature of FC10, FC28 and FC65 is 380, 450 and 500 °C respectively. Calculation of the mean particle size of the powder, using surface area measurements and assuming the powder is non-porous and spherical, gives a particle size of 18 nm. Figure 2.1 show a photograph of the FC28 powder taken using a transmission electron microscope (TEM). The particles are in the range of 10 to 100 nm and appear to be agglomerates of smaller particles. It seems that the large surface area of the fluorinated carbon is caused by the extremely small particle size.

The hydrophilic catalyst used in this study is platinum supported on gamma alumina powder. Alumina (Al_2O_3) is one of the most widely used catalyst supports because of its high specific surface area and good thermal and mechanical stability. The high surface area is a result of its porous nature. Alumina is known to be a very hydrophilic material and has been used as a drying agent for many decades.[1,2]

Figure 2.1 TEM Photograph of FC28 Powder

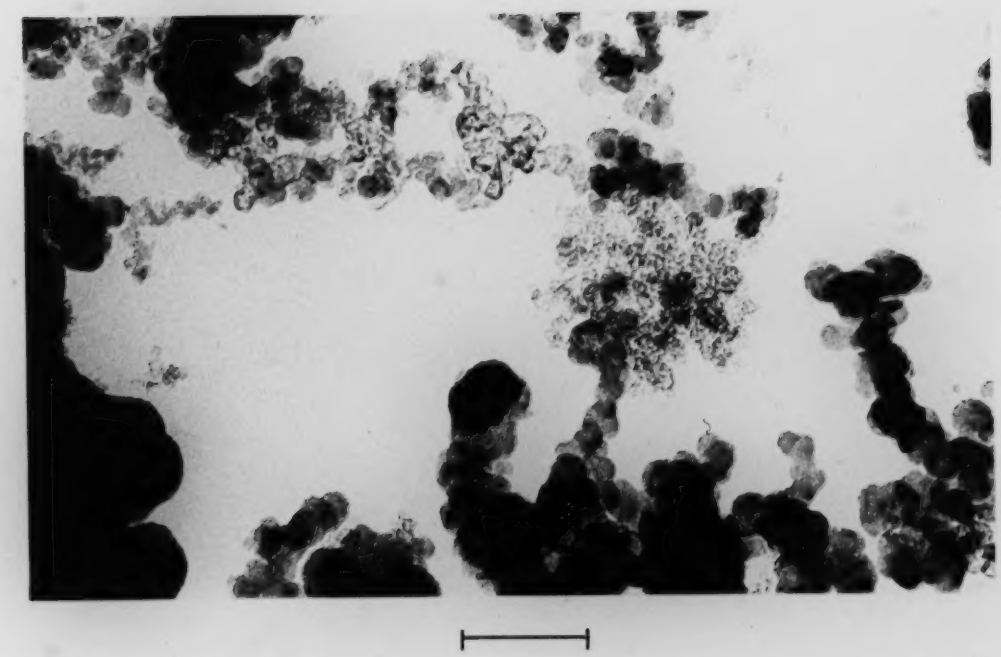

2.2 IMPREGNATION OF PLATINUM ON SUPPORTS

Platinum was impregnated on the fluorinated carbon using a 4% Pt solution of tetraammine platinum (II) nitrate in water. Since the fluorinated carbon is not wetted by water, the platinum solution was added to a mixture of 50% methanol and 50% water. The mixture of methanol, water and platinum solution was mixed in a beaker for 20 minutes before the powder support was added. The slurry was then mixed for another 20 minutes. The beaker was placed on an incline rotary evaporator under a heat lamp (see Figure 2.2) until all the liquid had evaporated (~ 5 h). Periodically, a small amount of methanol was used to rinse the sides of the beaker so that all the powder was being contacted by the liquid. This is important because as the liquid evaporates, the concentration of platinum ions in the liquid phase increases. Powder that is left on the sides of the beaker early in the evaporation process will not have the same concentration of platinum ions as the powder that is in contact with the liquid near the end of the process. By rinsing the sides of the beaker, the impregnated powder is more homogeneous. The procedure described above was also used for the Pt/Al_2O_3 catalyst. The impregnated fluorinated carbon powder was placed in a 1.27 cm diameter U-tube at 300 °C for 12 hours in 76 mL/min flowing hydrogen to reduce the platinum. In the case of the Pt/Al_2O_3 catalyst, the platinum was reduced at 400 °C for 12 hours with the same flow rate of hydrogen. The lower reduction temperature used for the fluorinated carbon catalysts was necessary because of the lower thermal stability of the support material. The platinum loading of the catalysts was determined from the initial amounts of platinum and powder support placed in the beaker. All the catalyst powders were made with 10% platinum loading. This is a relatively large loading of platinum, however, the powders were then coated on ceramic spheres before being placed in the Berty reactor. By coating the powders onto the ceramic support, the overall platinum loading of the final catalysts is quite small. It was necessary to coat the powder catalyst on larger supports so that it

Figure 2.2 Rotary Incline Evaporator

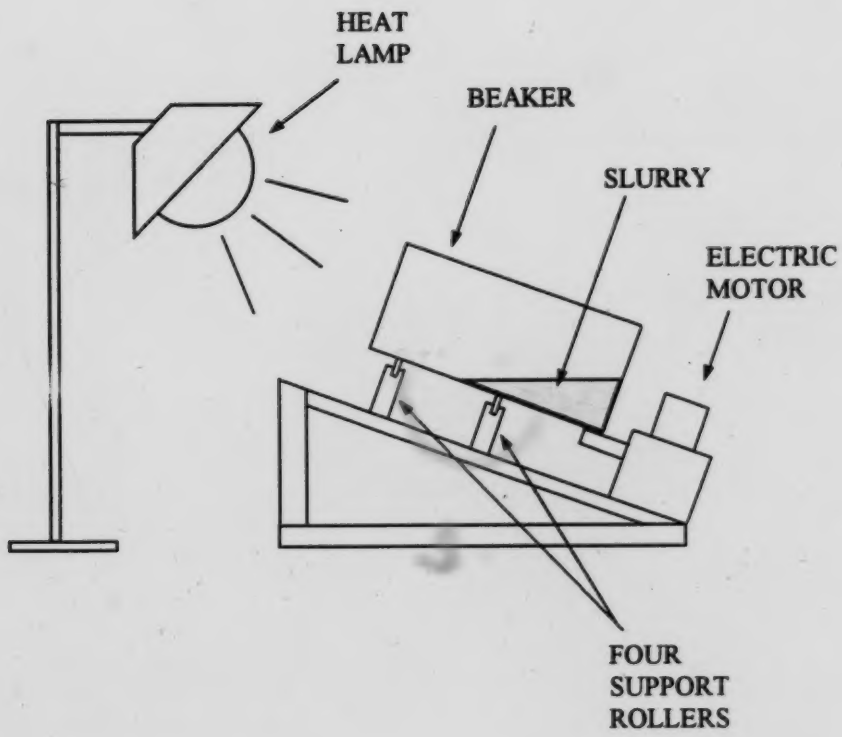

would not be blown out of the reactor. A description of the reactor and its operation is given in Chapter 6.

2.3 COATING THE POWDER CATALYST ON CERAMIC SPHERES

The powder catalyst was coated on 0.64 cm diameter ceramic spheres which were pre-washed with methanol and water and dried at 200 °C for 24 hours. To achieve a uniform layer of catalyst powder on the spheres, the catalyst powder had to be well dispersed in a liquid solution. A small amount of Triton surfactant was added to water and stirred until a uniform emulsion was obtained (~ 20 min). The powder catalyst was added to the emulsion and stirred for 20 minutes. The ceramic spheres were then added to the emulsion and the beaker was placed on the incline rotary evaporator under the heat lamp until the catalyst was completely dry (~3 h). The coated spheres were then placed in a 1.27 cm diameter U-tube and calcined at 300 °C for 3 hours in 100 mL/min flowing air. This calcination step was required to remove nitrates left behind after the impregnation of platinum. The calcination also changes the oxidation state of the surface platinum, as well as removes the Triton surfactant.

Figure 2.3 shows the cross section of the final catalyst. The catalyst is similar to an eggshell type catalyst with the active phase confined to a thin layer around the sphere. The thickness of this layer is important when determining the kinetics of a reaction. If the layer is too thick, mass transfer effects may cause the observed reaction rate to be less than the specific rate for the particular reaction of interest. This internal mass transfer phenomenon was observed for the first fluorinated carbon catalyst made. A more in-depth discussion on the effect of the active layer thickness is given in Chapter 7.

Figure 2.3 Cross-section of the Catalyst Particle

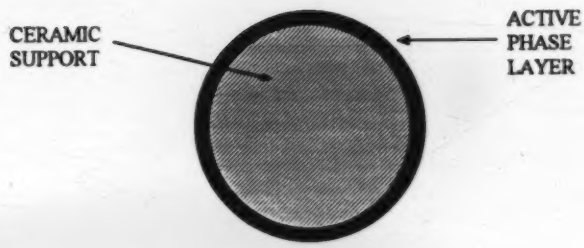

2.4 REFERENCES

1. Kotoh, K., M. Endoeda, T. Matsui, M. Nishikana, *J. Chem. Eng. Japan*, **1993**, 26, (4), 355.

2. Desai, R., M. Hussain, D. M. Ruthven, *Can. J. Chem. Eng.*, **1992**, 70, 699.

CHAPTER 3

CATALYST CHARACTERIZATION

3.1 INTRODUCTION

To better understand heterogeneous catalytic reactions, researchers must determine the characteristics of the catalyst which have the greatest influence on the activity. Factors such as metal dispersion, pore size distribution, and metal crystallite size have been found to be the most influential characteristics for supported noble metal catalysts. Many well established methods to characterize these catalysts exist. To characterize the catalysts used in this work the following methods were used: nitrogen BET surface area, nitrogen pore size distribution, X-ray diffraction and hydrogen pulse chemisorption. These characterization techniques determine the physical differences between the catalysts.

3.2 SURFACE AREA AND PORE SIZE DISTRIBUTION

The surface area and pore size distribution of each powder catalyst was measured using an Omnisorp 360 analyzer. The results of the pore size distribution and nitrogen BET surface area measurements are shown in Table 3.1 and 3.2 respectively. Table 3.1 shows that the fluorinated carbon catalysts have much larger pores than the alumina catalyst. The percent of the total pore volume from pores larger than 5 nm is 81.9%, 83.6% and 71.5% for the Pt/FC10, Pt/FC28 and Pt/FC65 catalysts, respectively. The Pt/Al_2O_3 catalyst has only 5.2% of its pore volume from pores larger than 5 nm. The pores of the fluorinated carbon catalysts are formed by the agglomeration of the small particles and are not from pores internal to the particle itself. Table 3.1 also shows the pore size distribution of fresh FC28 powder. There are no pores smaller then 5 nm before the impregnation of the platinum. This suggests that the fluorinated carbon powder becomes more closely packed after the impregnation process. The smaller pores of the alumina catalyst are more susceptible to pore condensation than the larger pores of the fluorinated carbon catalyst. With the production of water at the catalyst sites, the Kelvin

Table 3.1 Pore Size Distribution of Catalysts

Pore Radius (nm)	Pore Volume (mL/g)				
	10%Pt/FC10	10%Pt/FC28	10%Pt/FC65	10%Pt/Al_2O_3	Fresh FC28
>30	0.0	0.0	0.003	0.0	0.01367
30-20	0.03939	0.04372	0.04417	0.00263	0.03143
20-10	0.1177	0.1203	0.1253	0.00944	0.07186
10-5	0.1079	0.1008	0.1109	0.01177	0.03251
5-4	0.01522	0.01345	0.02474	0.01558	0.0
4-3	0.01345	0.01202	0.02457	0.2052	0.0
3-2	0.015	0.01446	0.03489	0.1966	0.0
2-1	0.01465	0.01195	0.02866	0.01495	0.0
Total pore volume above 1 nm	0.3234	0.3167	0.3962	0.4562	0.1495

Table 3.2 Characterization of Catalysts

Catalyst	BET Surface Area (m^2/g)	Pt Disperson by XRD	Pt Dispersion by Chemisorption
10wt% Pt/FC10	188	6.2%	13.5%
10wt% Pt/FC28	157	7.5%	3.7%
10wt% Pt/FC65	291	5.3%	2.0%
10wt% Pt/Al_2O_3	237	7.8%	13.8%

equation (1.3-1) predicts that the pores of the alumina catalyst will become filled with water thereby blocking access of the reactants to the active sites.

3.3 DETERMINING PLATINUM DISPERSION

An important characteristic of supported metal catalysts is the amount of metal atoms exposed to the reactant molecules. The reason for supporting a noble metal on a high surface area support is to increase the amount of the metal surface area for reaction. The parameter used to describe this characteristic of the catalyst is called the metal dispersion. The metal dispersion is defined as the number of metal surface atoms divided by the total number of metal atoms impregnated on the catalyst. It is conventionally reported as a percent dispersion which requires that the ratio be multiplied by 100. Since the dispersion is a ratio between the surface area of metal and the volume of metal on the support, it follows that the dispersion of a catalyst increases with decreasing metal crystallite size. For this reason, the impregnated metal is more effective if the dispersion is high.

Two methods have been used to determine the dispersion of the catalysts used in this study. The first method is an X-ray diffraction technique which uses the metal crystallite size to calculate the dispersion. The second method, and more commonly used technique for determining the dispersion, is pulse chemisorption. Both methods are described in detail in the following sections.

3.3.1 X-ray diffraction

X-ray diffraction (XRD) may be used to obtain information about the structure and composition of crystalline material. The mean crystallite size of a material can be determined from the broadening of an X-ray diffraction peak. In the context of a supported metal catalyst, the size of the metal crystallites can be used to estimate the metal dispersion. A Philips X-ray diffractometer was used for the X-ray diffraction experiments.

Figure 3.1 shows the X-ray diffraction intensity as a function of the diffraction angle, 2θ, for the platinum catalyst powders. The peak broadening is inversely proportional to the crystallite size and the two are related by the Scherrer formula[1,2]:

$$t = \frac{0.9 \times \lambda}{B \cos \theta_B} \qquad (3.3.1\text{-}1)$$

where t = the diameter of the crystal particle
λ = the wave length of the X-ray emission
B = the breadth of the diffraction peak at half its maximum intensity in radians
θ_B = the angle at which the maximum intensity occurs (Bragg angle)

Appendix A.1 and A.2 show the calculation of the platinum particle size using the XRD data and the calculation of the platinum dispersion, respectively. The platinum dispersion determined by XRD on these catalysts is quite low as seen in Table 3.2. However, this low dispersion is not uncommon for catalysts with such high platinum loading.[3-5] It is important to note that the XRD data show that the platinum dispersion is similar for each catalyst.

3.3.2 Pulse Chemisorption

There are many types of pulse chemisorption that can be used to determine the dispersion of a supported metal catalyst. The most popular method uses hydrogen as the adsorption gas. With hydrogen pulse chemisorption, the dispersion of the metal is determined by the amount of hydrogen that can be adsorbed by the catalyst sample. The hydrogen is thought to adsorb on a one to one basis (i.e. one hydrogen atom adsorbs on one platinum surface atom). The moles of hydrogen adsorbed on the catalyst sample is measured and converted to an equivalent number of moles of platinum surface atoms. The metal dispersion is calculated by dividing the number of platinum surface atoms by the total number of platinum atoms in the catalyst sample. A sample calculation of the dispersion is shown in Appendix A.3 for the platinum/alumina catalyst. It is extremely

Figure 3.1 X-ray Diffraction Peaks for the Platinum Powder Catalysts

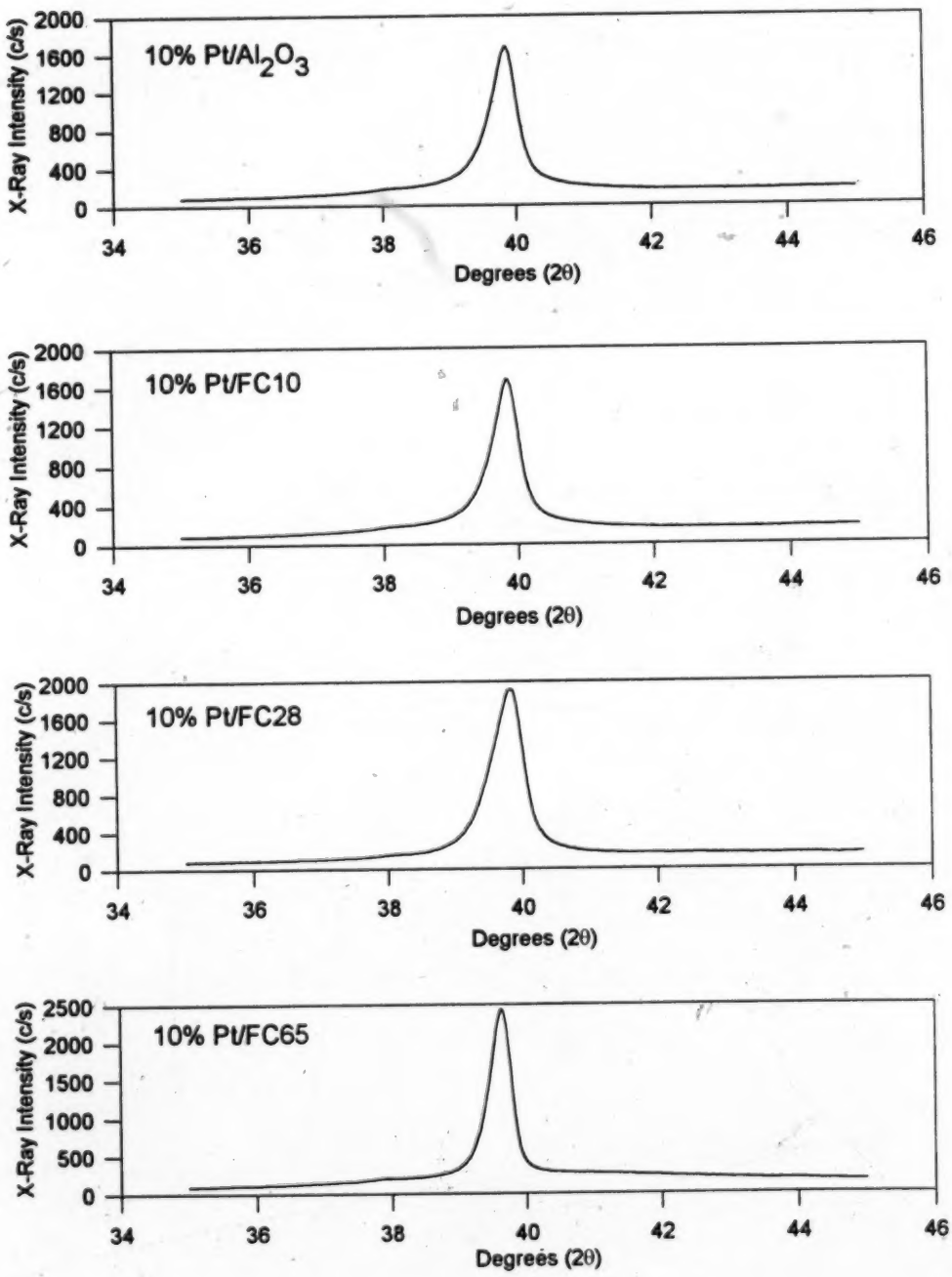

important that the surface of the catalyst is completely cleaned of any physically or chemically adsorbed species prior to the pulse chemisorption.

The apparatus used for the chemisorption experiments was an Altamira AMI-1 machine which is capable of running in situ pre-treatment steps on the catalyst sample. The pre-treatment procedure was needed to clean the surface of the catalyst and was the same for each catalyst tested. However, because of the thermal instability of the fluorinated carbon catalysts the pre-treatment temperatures where different. Table 3.3 shows each pre-treatment step and the temperatures at which they were carried out. The first step in the pre-treatment procedure is to purge all the lines with argon including the catalyst sample. This step removes any gas present from previous experiments and removes all the moisture and oxygen (air) from the system. The next few steps involving hydrogen, at various temperatures, are required to remove any chemisorbed oxygen from the platinum surface. The system is then purged with argon to remove all the hydrogen from the system including any which is adsorbed on the platinum. The catalyst sample is then exposed to pulses of hydrogen at room temperature and the amount of hydrogen adsorbed is measured.

Table 3.2 shows the dispersion results from the chemisorption experiments. Initial experiments on the Pt/FC28 and Pt/FC65 supported catalysts showed no adsorption of hydrogen. To increase the sensitivity of the hydrogen pulse chemisorption technique, the Pt/FC28 and Pt/FC65 catalysts were tested using a hydrogen titration method. In this method, the catalyst sample is exposed to oxygen so that the platinum surface atoms are bonded to an oxygen atom. This technique increases the sensitivity of the pulse chemisorption experiment because the ratio between the hydrogen atoms consumed and the surface platinum atoms is increased from 1:1 to 3:1. Two hydrogen atoms form water with the adsorbed oxygen on the platinum and the other hydrogen atom adsorbs on the vacant platinum site. These experiments also proved to be inconclusive with very little hydrogen being consumed.

Table 3.3 Pre-treatment Procedure for Pulse Chemisorption Experiments

Platinum on Fluorinated Carbon Catalysts:					
Step	Gas	Flow rate (mL/min)	Time (min)	Temperature (°C)	Rate (°C/min)
1	Ar	30	15	25	-
2	H_2	30	-	25→150	20
3	H_2	30	15	150	-
4	H_2	30	-	150→300	10
5	H_2	30	60	300	-
6	Ar	30	120	300	-
7	Ar	30	20	300→25	-
Platinum on Alumina Catalyst:					
1	Ar	30	15	25	-
2	H_2	30	-	25→400	10
3	H_2	30	-	400→450	5
4	H_2	30	60	450	-
5	Ar	30	120	450	-
6	Ar	30	35	450→25	-

The three fluorinated carbon catalysts were then sent to the Atomic Energy of Canada Ltd. (AECL) laboratory in Chalk River, Ontario. The AECL lab is equipped with a static chemisorption apparatus which is more accurate when dealing with weakly chemisorbed species or low adsorption samples. The results from the static chemisorption experiments for the fluorinated carbon catalysts are the values shown in Table 3.2.

3.4 COMPARISON OF THE PLATINUM DISPERSIONS

The dispersion for the Pt/FC10 and Pt/Al_2O_3 catalysts determined from the chemisorption technique is 13.5% and 13.8% respectively. This is approximately two times that evaluated from the XRD technique. The Pt/FC28 and Pt/FC65 catalysts show a much lower dispersion with 3.7% and 2.0% respectively, which is less than half the value found using XRD. All four catalyst powders have similar platinum crystallite size as shown by the XRD results, which is to be expected, since all the catalysts were prepared in the same manner. Adams et al.[6] point out that the X-ray diffraction technique yields a volume averaged crystallite size given by

$$\bar{d}_v = \frac{\sum n_i d_i^4}{\sum n_i d_i^3} \qquad (3.4\text{-}1)$$

where there are n_i crystallites of volume d_i^3. The chemisorption technique, however, yields a surface averaged crystallite size given by

$$\bar{d}_s = \frac{\sum n_i d_i^3}{\sum n_i d_i^2} \qquad (3.4\text{-}2)$$

In both Equations 3.4-1 and 3.4-2, the variable d represents the crystallite diameter. A direct comparison between these two techniques for the determination of the platinum dispersion is not valid unless the platinum crystallite size distribution is vary narrow.[6,7] Adams et al.[6] show that the X-ray diffraction technique yields a dispersion less than the

adsorption technique with the limit going to equal dispersions when all the metal crystallites on the support are the same size. The Pt/FC28 and Pt/FC65 show unexpected results with the XRD technique yielding larger dispersions than the chemisorption technique. These results suggest that the surface platinum on the Pt/FC28 and Pt/F65 catalysts is unable to adsorb hydrogen with the same effectiveness as the platinum on the Pt/FC10 and Pt/Al_2O_3 catalysts.

The inability to adsorb hydrogen on the two highly fluorinated catalysts indicates a possible metal-support interaction. The relatively large amount of fluoride present on the support may have the ability to affect the adsorption capacity of the dispersed platinum through electronic interactions. These electronic interactions may be strong enough to reduce the ability of the surface platinum to induce the dissociative adsorption of hydrogen. The fluoride on the surface of the support is thought to only affect the platinum atoms in the immediate vicinity of the fluoride. This would still allow for some adsorption of hydrogen on the platinum crystallites and would explain the low chemisorption dispersion values for the Pt/FC28 and Pt/FC65 catalysts.

The observation that impurities, such as halogens, poison supported noble metal catalysts has been documented in the literature.[5,8-13] The majority of the studies focus on the poisoning effects of chloride on platinum and palladium supported catalysts. Two potential mechanisms have been used to explain the loss of activity. (1) The halide either blocks or distorts the surface electronic properties of the catalytic species leading to poor performance. (2) The halide forms a platinum or palladium oxide-halogen species which are more stable and consequently less reactive than the oxygen species. Platinum oxifluorides may be formed during the calcination step described in Chapter 2, similar to that reported by Barbier et al.[8] with chloride containing Pt/Al_2O_3 catalysts. Lieske et al.[9] and Barbier et al.[8] found that the presence of platinum oxichlorides had little affect on the hydrogen adsorption capacity of the platinum compared to catalysts containing no chloride. The Cl/Pt atomic ratio in these studies varied between 0 and 6 for the catalysts

reported. These results agree well with the chemisorption experiments described above for the Pt/FC10 catalyst which has a F/Pt atomic ratio of 9.2. The hydrogen adsorption capacity of the Pt/FC10 catalyst was similar to that of the Pt/Al_2O_3 catalyst in the present study. However, the Pt/FC28 and Pt/FC65 catalysts have F/Pt atomic ratios of 25.9 and 60.1 respectively. The larger F/Pt ratio could account for the drop in the hydrogen adsorption capacity of these catalysts. The platinum oxichloride species described in the literature are stable up to 727 °C. If analogous species exist on the Pt/FC28 and Pt/FC65 catalysts, it is unlikely that heat treatments up to 500 °C would remove the fluoride. Thermal gravimetric analysis (TGA) experiments on the 10%Pt/FC28 catalyst showed that approximately 20% of the mass was lost upon heating the powder at a rate of 20 °C/min in nitrogen from 25 to 500 °C. The majority of the mass loss occurred above 400 °C which is in agreement with the thermal stability data provided by the supplier of the fluorinated carbon (450 °C). The amount of mass lost and the temperature of the decomposition, suggest that the loss in mass is caused by the removal of fluoride. Since there is a loss of fluoride, it is unlikely that a platinum oxifluoride species was present on the catalyst. It is more probable that the fluoride on the catalyst support blocks or distorts the surface electronic properties of the platinum leading to poor hydrogen adsorption. The results reported by Simone et al.[10] strongly suggest that localized site blockage and/or inductive effects are responsible for poor performance of chloride containing palladium/alumina catalysts for the oxidation of methane. Marécot et al.[11] also describe similar halogen-metal interactions on platinum/alumina catalysts used for the oxidation of propane and propene. The effect of the heat treatment on the activity of the Pt/FC28 catalyst for the oxidation of methanol is presented in Chapter 7.

Metal-support interactions are considered to be chemical characteristics of the catalyst. They can greatly affect the reaction kinetics. However, to compare catalysts only physical characteristics must be used to evaluate which support gives the most

favorable results. For this reason, the dispersions evaluated from the XRD data are used to calculate and compare the reaction rates in Chapter 7.

3.5 HYDROPHOBICITY OF SUPPORTS

With the introduction of hydrophobic catalysts, an important characteristic that greatly affects the activity in the presence of water is the hydrophobicity of the support. The degree of hydrophobicity, therefore, becomes an important characteristic of these catalysts. To fully characterize the hydrophobic catalysts, it is necessary to quantify the degree of wettability (hydrophobicity).

The most widely used parameter for describing the wettability of a solid is the contact angle. The contact angle is conceptually easy to understand when put in the context of a flat smooth surface (see Figure 3.2). In fact, there are several well known methods for measuring the contact angle of liquids on flat surfaces. However, most catalyst supports are in the form of porous pellets, spheres, or powders. In these cases, the concept of a contact angle becomes difficult to envision, especially when dealing with powders. Most powders have particle sizes in the micron range and are non-spherical. With the introduction of porous powders, the concept of a contact angle becomes even more complicated. Despite this fact, there are some methods for determining the contact angle of powders. There are also many problems associated with these methods because of the nature of powders. Chapter 4 describes some of the conventional techniques used to evaluate the contact angle of powders and develops a novel method for determining the contact angle of hydrophobic powders.

Figure 3.2 Contact Angle (θ) for a Drop on a Flat Smooth Surface

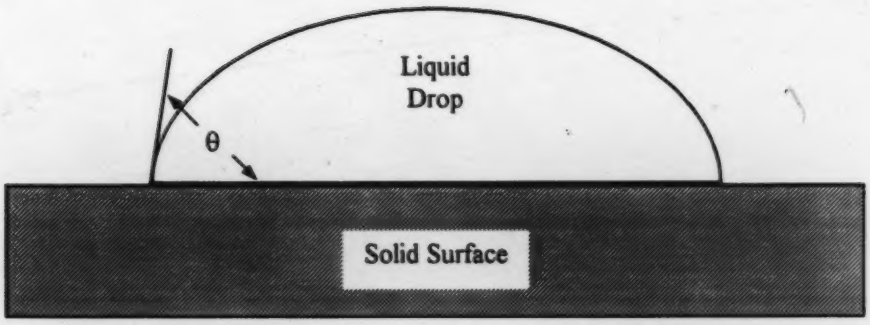

3.6 REFERENCES

1. Cullity, B.D., *Elements of X-ray Diffraction*, Addison-Wesley Publishing Company Inc., **1967**, 99.
2. Klug, H.P., and L.E. Alexander, *X-ray Diffraction Procedures*, John Wiley & Son Inc., **1970**, 491.
3. Otto, K., J.M. Andino, C.L. Parks, *J. Catal.* **1991**, 131, 243.
4. Hubbard, C.P., K. Otto, H.S. Gandhi, Y.S. Ng, *J. Catal.* **1993**, 144, 484.
5. Hicks, R.F., H. Qi, M.L. Young, R.G. Lee, *J. Catal.* **1990**, 122, 280.
6. Adams, C.R., H.A. Benesi, R.M. Curtis, R.G. Meisenheimer, *J. Catal.* **1962**, 1, 336.
7. Dorling, T.A., and R.L. Moss, *J. Catal.* **1966**, 5, 111.
8. Barbier, J., D. Bahloul, P. Marécot, *Catal. Lett.* **1991**, 8, 327.
9. Lieske, H., G. Lietz, H. Spindler, J. Völter, *J. Catal.* **1983**, 81, 8.
10. Simone, D.O., T. Kennelly, N.L. Brungard, R.J. Farrauto, *Appl. Catal.* **1991**, 70, 87.
11. Marécot, P., A. Fakche, B. Kellali, G. Mabilon, M. Prigent, J. Barbier, *Appl. Catal. B* **1994**, 3, 283.
12. Cullis, C.F., and B.M. Willatt, *J. Catal.* **1984**, 86, 187.
13. Barbier, J., D. Bahloul, R. Szymanski, *Bull. Soc. Chim. Fr.* **1988**, 3, 478.

CHAPTER 4

RELATIONSHIP BETWEEN HEAT OF IMMERSION AND CONTACT ANGLE

A version of this chapter has been published in the Journal of Physical Chemistry , 1996, 100, 6626-6630.

4.1 INTRODUCTION

Two of the oldest methods used for the measurement of the contact angle of powders are the Washburn method and the Bartell method.[1-3] They are based on the same assumptions and equations, with the main difference being that the Washburn technique is a dynamic method while the Bartell technique is a static method. In the Washburn and Bartell methods the liquid is allowed to penetrate into a packed bed of powder. In the derivation of the theory, the bed of powder is conceived to be a bundle of parallel capillaries of constant radius (r). This assumption is an oversimplification of the tortuous path in which the liquid must travel in the bed. For the model to approach this assumption the packed bed must be homogeneous and stay that way during the wetting process. If the characteristics of the packed bed do not change during the wetting process, the bed is said to be stable. It could be argued whether any packed bed of powder is truly stable when it becomes wetted for the simple reason that the wetting phenomenon changes the surface characteristics of the particles, which in turn, changes the interparticle interactions in the bed.

Both the Washburn and Bartell methods are based on the following equation

$$v = \frac{dl}{dt} = \frac{r^2 \Delta P}{8 \eta l} \qquad (4.1\text{-}1)$$

which describes the rate of penetration of a liquid into a capillary under laminar flow conditions. A list of symbol definitions is given at the end of the chapter. The pressure term can be expressed as

$$\Delta P = \frac{2\gamma_{lv} \cos\theta}{r} + \Delta p \qquad (4.1\text{-}2)$$

if the liquid penetration proceeds exclusively under the influence of the surface tension and a threshold pressure difference Δp over the capillary. Substituting Equation 4.1-2 into Equation 4.1-1 and integrating with the boundary condition l=0 at t=0 gives

$$l^2 = \frac{r^2}{4\eta}\left\{\frac{2\gamma_{lv}\cos\theta}{r} + \Delta p\right\}t \qquad (4.1\text{-}3)$$

Since the bed is not made up of constant radii capillaries, an effective radius r_e is substituted for r and a constant C is used to take into account other errors introduced by the simplifying assumptions. With these adjustments to Equation 4.1-3, the equation used for estimating the contact angle is

$$l^2 = \frac{Cr_e^2}{\eta}\left\{\frac{2\gamma_{lv}\cos\theta}{r_e} + \Delta p\right\}t \qquad (4.1\text{-}4)$$

In the Washburn method, l^2 is measured as a function of time at a given value of Δp. This yields a straight line with slope m which, from Equation 4.1-4, is given by

$$m = \frac{Cr_e^2}{\eta}\left\{\frac{2\gamma_{lv}\cos\theta}{r_e} + \Delta p\right\} \qquad (4.1\text{-}5)$$

As mentioned above C and r_e depend on the packing of the powdered bed. In most cases, experiments are done with Δp=0 and therefore,

$$m = A\frac{\gamma_{lv}}{\eta}\cos\theta \qquad (4.1\text{-}6)$$

where $A = 2Cr_e$

The value of A can be obtained by using a liquid that is known to completely wet the powder (i.e. θ=0). For θ=0, cosθ=1 and A can be calculated from the slope m and the values of γ_{lv} and η for the liquid. One problem that exists when evaluating A is knowing whether the contact angle of the powder-liquid system used is indeed zero.

The task of determining the bed constants becomes even more difficult if the powder has a large contact angle with the liquid of interest. For example, if the contact angle of a hydrophobic powder is required, one must use a threshold pressure (Δp) in order to get the water to penetrate the packed bed. In this case, experiments with a liquid that has θ=0 must be done at two different pressures in order to evaluate both C and r_e

as separate variables. The problem is that the characteristics of the packed bed may change when exposed to different external pressures. Also, by having large pressure differences across the packed bed when measuring the rate for large contact angle systems, liquid channeling may occur and the packed bed may become unstable. This is where the greatest difficulty arises when attempting to measure the contact angle of very hydrophobic powders using pure water.

The Bartell method is a static method where v=0 and therefore:

$$\Delta p = \frac{2\gamma_{lv}\cos\theta}{r_e} \qquad (4.1\text{-}7)$$

White[4] proposed that

$$r_e = \frac{2(1-\phi)}{\phi\rho_s A_s} \qquad (4.1\text{-}8)$$

In the Bartell method, the pressure difference required to stop the liquid flow in the packed bed is measured and the contact angle can be calculated based on the characteristics of the powder and the packed bed porosity. However, in most cases the packing density changes with exposure to the liquid, which makes the calculated value of r_e suspect. As with the Washburn method, problems arise when the contact angle of the system is large because of instability in the bed and liquid channeling.

In both methods, obtaining representative data is very difficult and some investigators have been unable to obtain reproducible results.[5,6] The beds must be packed uniformly in order to get a uniform liquid level in the bed. When pressure is needed to force the liquid into the bed, the bed becomes unstable and channeling occurs. These methods are not suitable for large contact angle systems. In order to avoid these problems some authors have used several concentrations of binary solutions (i.e. alcohol/water) to decrease the contact angle and then extrapolate the data to the pure liquid of interest.[7] However, the problem of an unstable bed still exists, making the experiments tedious and time consuming.

Several other methods have been used to assess the wettability of small particles such as, the compressed powder method[8], the sedimentation volume method[9], the film flotation method[10], the solidification front technique[11], and the centrifugation method.[12] The most direct method of measuring the contact angle is the compressed powder method. This method consists of compressing the powder into flat discs and measuring the contact angle from a drop of liquid placed on the pellet. Many authors have criticized the compressed pellet method.[7,8] Neumann and Good[8] pointed out that the surface formed by compression of the particles may have different properties than those of the single crystals because of the plastic distortion of the topmost particles during compression. There are also problems obtaining flat smooth surfaces from the compression of powders and it is well known that this surface roughness affects the observed contact angle.

Calorimetry has been used to characterize the chemistry of solid surfaces and its interactions with any molecules that contact it. More specifically, immersion calorimetry is a valuable means of investigating the solid surface properties. The heat of immersion is defined as the heat released or adsorbed when a clean solid is immersed in a liquid. The use of immersion calorimetry has increased significantly over the past decade with the advancements in heat flow calorimeters. Recent developments in micro-calorimeters have made it possible to measure very small changes in heat over long periods of time. It is, therefore, possible to measure the heat of immersion of low energy surfaces with accuracy. The relationship between the contact angle and the heat of immersion as shown by Adamson and Ling[13] and Melrose[14] is

$$\Delta H_{im} = T\gamma_{lv}\frac{d\cos\theta}{dT} - \left(\gamma_{lv} - T\frac{d\gamma_{lv}}{dT}\right)\cos\theta \qquad (4.1\text{-}9)$$

In theory, it should be possible to calculate the contact angle by using heat of immersion data. However, as seen from Equation 4.1-9, the first term on the right side poses a problem. Equation 4.1-9 has been used to calculate the heat of immersion from contact angle data but not vice-versa[15]. It is therefore, necessary to derive an equation which

relates the heat of immersion and contact angle in such a way that the contact angle can be calculated from heat of immersion data.

4.2 DERIVATION OF THE THEORETICAL RELATIONSHIP BETWEEN THE CONTACT ANGLE AND THE HEAT OF IMMERSION

Let g_i be the change in Gibbs energy for immersion.

Let h_i be the change in enthalpy for immersion.

By definition, $g_i = \gamma_{sl} - \gamma_s$ (4.2-1)

and $h_i = g_i - T\frac{dg_i}{dT}$ (4.2-2)

Substituting Eqn. 4.2-1 into 4.2-2

$$h_i = \gamma_{sl} - \gamma_s - T\left(\frac{d\gamma_{sl}}{dT} - \frac{d\gamma_s}{dT}\right) \quad (4.2\text{-}3)$$

Young's equation is given by,

$$\gamma_{lv}\cos\theta = \gamma_s - \gamma_{sl} - \pi_e \quad (4.2\text{-}4)$$

where $\pi_e = \gamma_s - \gamma_{sv}$

Substituting Eqn. 4.2-4 into 4.2-3

$$h_i = -\gamma_{lv}\cos\theta - \pi_e - T\left(\frac{d\gamma_{sl}}{dT} - \frac{d\gamma_s}{dT}\right) \quad (4.2\text{-}5)$$

For low energy surfaces, $d\gamma_s/dT$ can be taken to be approximately -0.07 ± 0.02 mJ/m^2 K according to Neumann[15], Schonhorn[16], Dettre and Johnson[17,18] and Starkweather.[19] For large contact angle systems there is little interaction between the solid and the liquid. Only London dispersion forces operate across the solid/liquid interface. If it is assumed that the solid/liquid surface tension of these systems is independent of temperature then Equation 4.2-5 becomes

$$h_i = -\gamma_{lv}\cos\theta - \pi_e - 0.07T \quad (4.2\text{-}6)$$

Rearranging Eqn. 4.2-6 yields,

$$\cos\theta = \frac{-0.07T - h_i - \pi_e}{\gamma_{lv}} \qquad (4.2\text{-}7)$$

Equation 4.2-7 gives a simple relationship between the contact angle and the heat of immersion for low energy surfaces. For systems with large contact angles, π_e can be considered negligible and Equation 4.2-7 becomes

$$\cos\theta = \frac{-0.07T - h_i}{\gamma_{lv}} \qquad (4.2\text{-}8)$$

It should be noted that h_i is the enthalpy change upon immersion. Many authors quote the heat of immersion (ΔH_{im}) as being the negative of h_i (i.e. $\Delta H_{im} = -h_i$). An uncertainty of ± 0.02 mJ/m^2 K in the value of $d\gamma_s/dT$ can lead to a 5° error in the contact angle.

Equation 4.2-8 was used to predict the contact angle of hydrophobic powders found in the literature. One of the most studied hydrophobic powders is graphon. The heat of immersion of graphon in water is 32.2 mJ/m^2 at 25°C as determined by Young et al.[20] Using this value in the above equation, the contact angle is calculated to be 81°. Young et al.[20] measured a contact angle of 82° for water on a pelletized button of graphon.

Hansford et al.[21] measured the heat of immersion and the contact angle of a hydrophobic powder called griseofulvin. The heat of immersion was reported to be 5.7 mJ/m^2 and the contact angle was found to be 101.9°, based on the Washburn method. In order to obtain the contact angle of the griseofulvin/water system, Hansford and co-workers used binary solutions of ethanol/water. Because of the difficulties in measuring large contact angle systems using the Washburn method, the contact angle between the griseofulvin and several concentrations of ethanol/water mixtures was determined. The value of the contact angle at low concentrations of ethanol in water were then extrapolated to pure water. The experimental value of 101.9° is the extrapolated value of the contact angle. Using the experimental heat of immersion, Equation 4.2-8 predicts a value of 102°.

In these two cases, Equation 4.2-8 accurately predicts the contact angle of hydrophobic powders using heat of immersion data. Another hydrophobic material that can be used to verify Eqn. 4.2-8 is Teflon. Chessick et al.[22] measured the heat of immersion of Teflon powder and the contact angle on a chip of Teflon pressed from the powder. They report a heat of immersion value of 6 mJ/m^2 and a contact angle of 110°. Many other authors have reported results for the contact angle of water on Teflon. Ellison and Zisman[23] reported a contact angle of 108°, which is often cited in literature. However, there is a range of values reported by other workers. For example, Dann[24] reported a contact angle of 112° and Hu and Adamson[25] reported a value of 98°. Tarasevich[26] reported an equilibrium contact angle of 102° based on the equation $\theta = 0.5(\theta_A + \theta_R)$, where θ_A and θ_R are the advancing and receding contact angles respectively. Using the heat of immersion value given by Chessick et al.[22], Equation 4.2-8 predicts a contact angle of 102°. It is important to remember that the derivation of Equation 4.2-8 incorporates Young's equation in which the phases are in equilibrium. Therefore, the contact angle calculated from Equation 4.2-8 is the equilibrium contact angle.

Using Equation 4.2-8, a criterion can be established to determine whether a material has a contact angle larger than 90°. The criterion is sensitive to temperature but can be stated at conditions of 25 °C. For $\theta > 90°$, $h_i > -20.9$ mJ/m^2. The criterion is in terms of h_i and not ΔH_{im} so that the exothermic or endothermic nature of the wetting process is easily distinguishable. From the above criterion, it can be seen that any endothermic wetting process ($h_i > 0$) must have a contact angle greater than 90°.

To determine the hydrophobicity of the catalyst supports, the heat of immersion for the three fluorinated carbon powders is measured using a heat-flow calorimeter. The ΔH_{im} values are used to calculate the contact angle associated with the hydrophobic powders. The next section describes the principles of the heat-flow calorimeter used in this study.

4.3 INTRODUCTION TO THE PRINCIPLES OF HEAT-FLOW CALORIMETRY

There have been many types of calorimeters developed to study the thermal energy changes of various processes. Of the several types of calorimeters available, the Tian-Calvet heat flow calorimeter has shown to be adaptable to many applications.[27] Similar to many other types of calorimeters, the heat-flow calorimeter is composed of an inner vessel (cell), in which the thermal phenomenon to be studied occurs, and a surrounding medium (thermostat). However, in heat-flow calorimetry a thermal fluxmeter surrounds the calorimeter cell to detect the heat flow between the cell and the thermostat. The fluxmeter consists of thermopiles (batteries of differential thermocouples), which are connected in series so that they thermally connect the cell to the thermostat. When a thermal phenomenon is produced in the calorimetric cell, the thermal power flows through the thermopiles to the thermostat (see Figure 4.1).

In order to determine the amount of heat generated in the calorimetric cell, it is convenient to consider a situation where there is a constant and continuous heat flux occurring in the cell at a constant temperature. When a constant thermal power, W, is produced in the cell, energy is transferred to the surrounding medium through the thermopiles. Each thermopile delivers an elementary thermal power, W_i, which is represented by

$$W_i = \kappa_i (T_i - T_e) \qquad (4.3\text{-}1)$$

In heat-flow calorimetry, the difference between T_i and T_e is very small. This elementary power exchange then produces an elementary electromotive force (emf), e_i

$$e_i = \varepsilon_i (T_i - T_e) \qquad (4.3\text{-}2)$$

Combining Equations 4.3-1 and 4.3-2 gives

$$e_i = \frac{\varepsilon_i}{\kappa_i} W_i \qquad (4.3\text{-}3)$$

Figure 4.1 Principle of Heat-fluxmeter

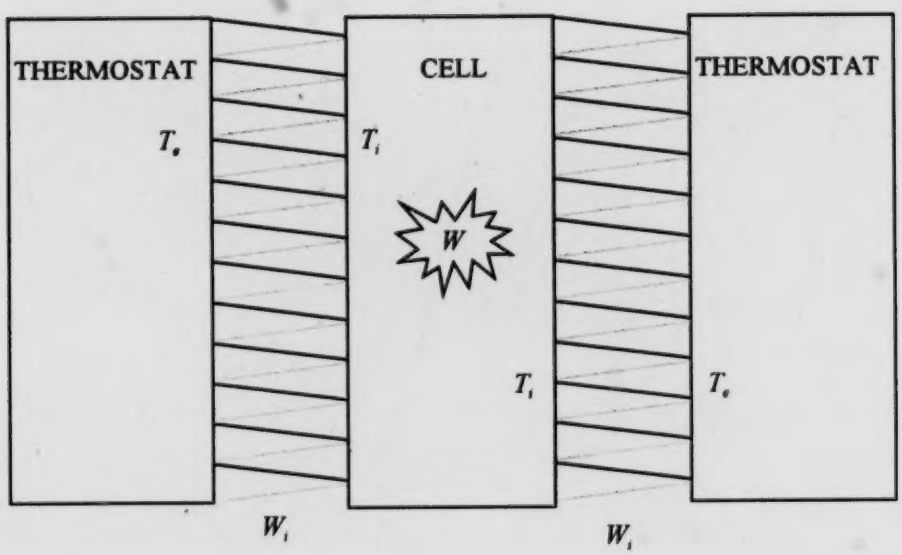

Since all the thermocouples are connected in series, the total power transferred (W) and the total emf produced (E) are given by

$$W = \sum_{i=1}^{n} W_i = n\kappa_i (T_i - T_e) \qquad (4.3\text{-}4)$$

$$E = \sum_{i=1}^{n} e_i = n\varepsilon_i (T_i - T_e) \qquad (4.3\text{-}5)$$

Since all the thermocouples are identical, ε_i and κ_i are the same for each thermocouple. Therefore,

$$E = \frac{\varepsilon}{\kappa} \sum_{i=1}^{n} W_i = \frac{\varepsilon}{\kappa} W \qquad (4.3\text{-}6)$$

Equation 4.3-6 indicates that the total emf generated by the thermopiles is proportional to the heat flux (i.e. the thermal power generated in the cell).

In practice, measurements are usually carried out with variable thermal power produced in the calorimetric cell. If a thermal power (W) is produced in the cell at time t and the temperature difference between the cell and the thermostat is (T_i-T_e), part of the power is transferred to the thermostat through the fluxmeter and part remains in the cell at time t. The power exchanged through the thermocouples (W_t) is given by Equation 4.3-4 and the remaining part of W increases the temperature of the cell. If it is assumed that the temperature increase of the cell, $d(T_i - T_e)$, during the time interval dt is uniform, then the remaining power (W_r) is given by

$$W_r = C_p \frac{d(T_i - T_e)}{dt} \qquad (4.3\text{-}7)$$

The total thermal power at time t can be represented by

$$W = W_t + C_p \left(\frac{d(T_i - T_e)}{dt} \right) \qquad (4.3\text{-}8)$$

Combining Equations 4.3-4 and 4.3-8 gives

$$W = n\kappa_i(T_i - T_e) + C_p \frac{d(T_i - T_e)}{dt} \qquad (4.3\text{-}9)$$

This equation is the fundamental equation of heat-flow calorimetry and is called the Tian equation. The combination of Equations 4.3-5 and 4.3-9 leads to

$$W = S\left(E + \tau \frac{dE}{dt}\right) \qquad (4.3\text{-}10)$$

where S and τ are the constants of calorimetry. S represents the static calibration constant of the calorimeter; it depends only on the heat fluxmeter. The symbol τ represents the dynamic calibration constant and is called the calorimeter time constant since it has the dimension of time. This constant depends upon both the fluxmeter and the heat capacity of the cell.

The amount of heat generated (Q) by a thermal process over a period of time can be obtained from the electrical signal by integration of Equation 4.3-10.

$$Q_t^{t'} = S\int_t^{t'} E dt + S\tau\int_t^{t'} dE \qquad (4.3\text{-}11)$$

If the integration time limits t and t' are chosen such that the entire thermal process is included, the second term on the right hand side of Equation 4.3-11 becomes zero. Equation 4.3-11 reduces to

$$Q_{process} = S \int_{process} E dt \qquad (4.3\text{-}12)$$

where $Q_{process}$ represents the total heat developed by the thermal process in the cell. The term $\int E dt$ is equal to the area under the curve of the recorded electrical signal over the time interval (t'-t). The calibration constant, S, is obtained from the integration of the electrical signal produced from a calibration experiment.

To obtain accurate measurements of the thermal power generated in the calorimetric cell it is necessary to eliminate any electrical signals produced by sources

other than the phenomenon being studied in the cell. If the temperature of the calorimetric block, T_e, changes due to a residual instability of the regulator, or as a result of temperature programming, the temperature of the cell will follow the temperature change and move towards the temperature of the block. As a result of this temperature variation, thermal power is transmitted through the fluxmeter, producing an electrical signal which is not related to the thermal process being studied in the cell. To reduce the electrical signal due to the temperature fluctuations in the calorimeter block, a second identical cell is fitted in the calorimeter surrounded by a second fluxmeter connected differentially to the first fluxmeter. This cancels the electrical signal caused by temperature variations not related to the phenomenon being studied in the first cell (sample cell). A more detailed description of the Tian-Calvet heat flow principles is given by Calvet and Part[28] and Gravelle.[29]

4.4 EXPERIMENTAL EQUIPMENT

4.4.1 The C-80 Micro-calorimeter

The micro-calorimeter used in the heat of immersion experiments was a Setaram C-80 differential calorimeter. The C-80 calorimeter is based on Tian-Calvet heat flow principles described in the previous section. The C-80 calorimeter is shown in Figure 4.2. The calorimeter is cylinder-shaped with a massive aluminum block in its center which is used as a calorimetric thermostat. Two identical cylindrical cavities, symmetrically located from the center line, house two removable calorimetric cells. The cells, identical in design, are machined to fit snugly into the cavities in the aluminum block. One cell acts as a sample/measurement cell and the other as a reference cell. When placed in the calorimetric block, each cell is surrounded by a thermopile (fluxmeter). The two fluxmeters are designed identically and are connected in opposition to give a differential thermopile output. This arrangement cancels interfering signal disturbances caused by the

Figure 4.2 Schematic Diagram of the C-80 Micro-calorimeter

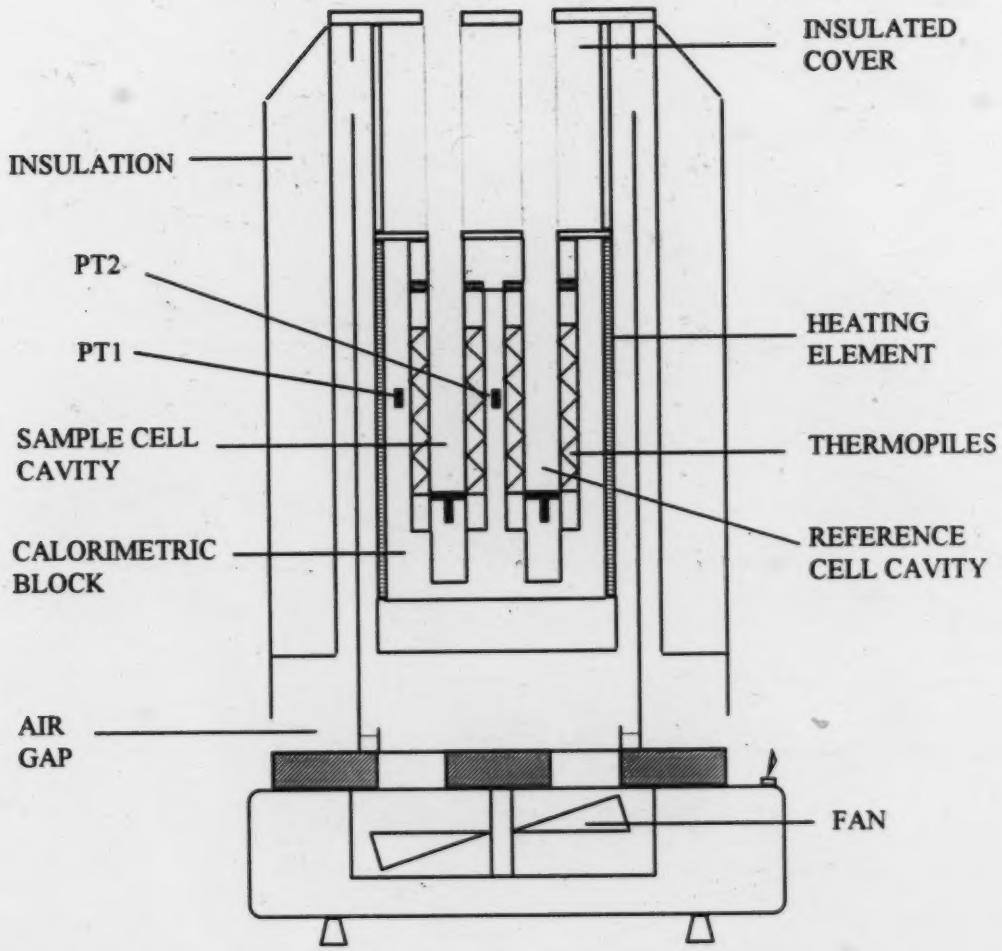

presence of residual temperature instability or temperature programming. The fluxmeters thermally connect the two cells to the calorimetric block. Any thermal exchange between the cells and the calorimetric block, cause the fluxmeter to output a proportional signal, which is channeled to a digital voltmeter.

Two platinum resistance probes are located within the calorimeter. Probe PT1 is used to control the temperature of the calorimetric block. A heater wrapped around the outside of the aluminum block and connected to a temperature control unit, maintains the set experimental temperature of the calorimeter. The second platinum probe (PT2) is used to obtain the temperature of the cells within the calorimeter. It is located on the center line of the aluminum block between the two cells.

Surrounding the block is an air gap that provides thermal insulation. Outside the air gap is a layer of insulating material. This arrangement provides excellent temperature control and stability. Air cooling is used to reduce the calorimeter temperature when required. This is achieved with the assistance of an electrical fan that is located in the base of the calorimeter and provides circulation of air in the air gap. The main body of the calorimeter is attached to a rocking motor. The rocking mechanism rotates the entire calorimeter 180°. The rotation is needed to increase the mixing required for measurements such as the heat of mixing, the heat of solution, and the heat of wetting. The calorimeter is enclosed in a thermally insulated sheet metal box. This box shields the calorimeter from the effects of disruptive thermal currents present in the laboratory.

To simplify the operation of the calorimeter, it is connected to an HP-86B minicomputer using an HP-1B interface. A block diagram of the calorimeter and all its accessories is shown in Figure 4.3. This set-up provides an easy method of monitoring, collecting and integrating the differential fluxmeter output. The software necessary to control the operation of the calorimetric system and manipulate the data was written in-house, using Hewlett Packard BASIC. The computer is also connected to an HP-9121

Figure 4.3 Block Diagram of the C-80 and Accessories

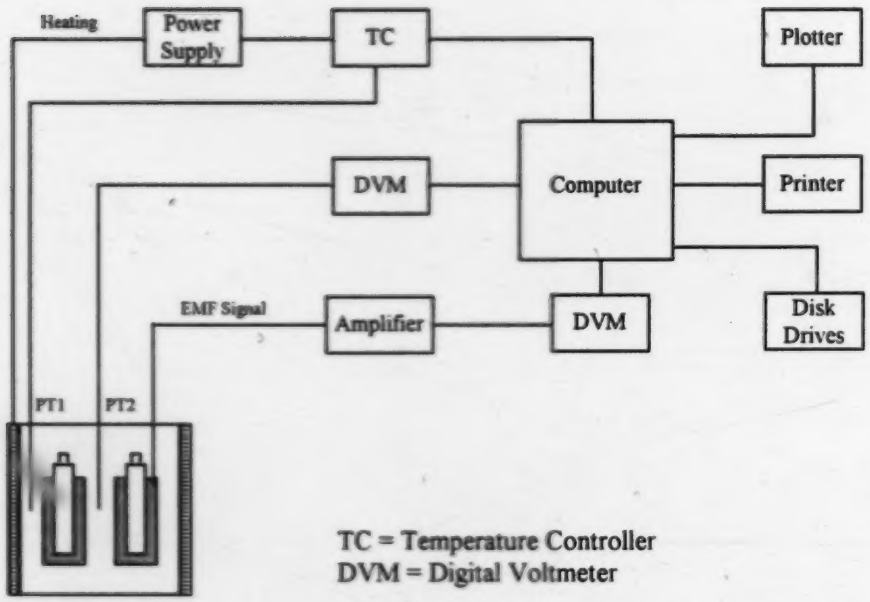

3.5" dual disc drive which permits the storage of collected data. Hard copies of the results are obtained from an HP-82906A printer, supported by an HP-7470A multi-pen plotter.

4.4.2 Calorimetry Cell and Experimental Procedure

Figure 4.4 shows the calorimetric cell which was designed for the heat of immersion experiments. The wetting chamber is made of stainless steel with a threaded opening. The upper body consists of three separate pieces; two of which are made of Orlon and one of stainless steel. All three pieces were designed and built in the Chemical and Materials Engineering machine shop at the University of Alberta. A Teflon o-ring fitted between the upper and lower body of the cell provides a seal that prevents any loss of liquid or vapor from the cell. A 1.6 mm diameter breaking rod is passed through the center of the assembly. A rubber o-ring is used to seal the annulus between the rod and the upper body. The o-ring is held tight by another threaded piece of stainless steel. The sample and reference cells were made identical.

Glass sample bulbs were made by the glass blowing shop in the Department of Chemistry at the University of Alberta to hold the powder samples. Each bulb (~11.5 mm diameter) was made with a very thin wall to reduce the amount of energy associated with breaking the bulb. If there is a heat effect associated with the breaking of the bulb, it would be necessary to place an empty glass bulb in the reference cell. The heat associated with breaking the bulb in the reference cell would then cancel the heat associated with breaking the sample bulb. Initial experiments using an empty glass bulb in the sample cell and no bulb in the reference cell, showed that there was no heat effect when the bulb was broken. Therefore, it was not necessary to place a bulb in the reference cell during the heat of immersion experiments.

Prior to the experiments, the three fluorinated carbon powders were heated to 195 °C for 24 hours and kept in a glove box under a nitrogen atmosphere to prevent any adsorption of water. In the glove box, the sample powder (≈0.1 g) was placed in the glass

Figure 4.4 Schematic Diagram of the Calorimetry Cell

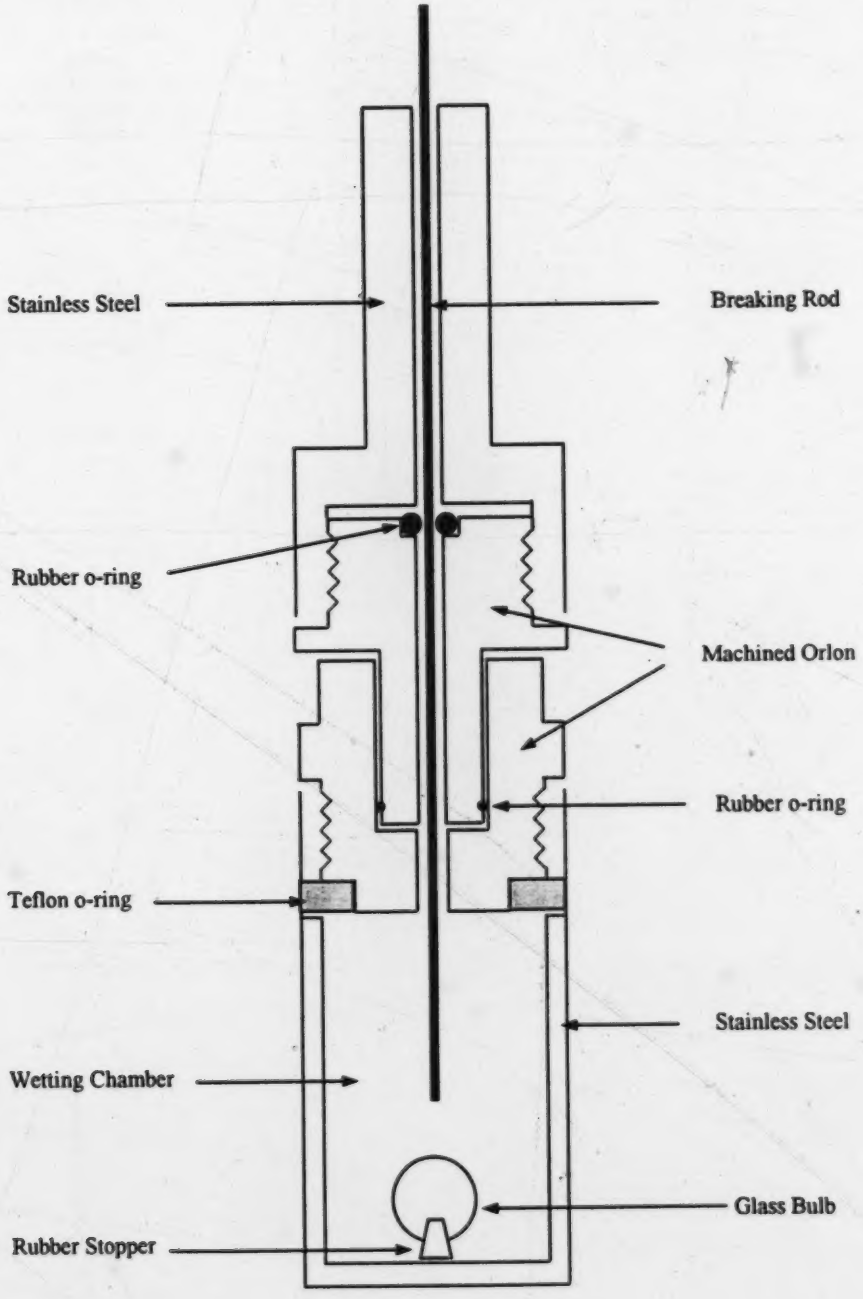

bulb and sealed with a rubber stopper. The bulb was then placed in the sample cell and the cell was filled with approximately 5 mL of liquid. The same amount of liquid was placed in the reference cell. Both cells were sealed immediately after the liquid was added. The two cells were placed in the C-80 micro-calorimeter and the temperature of the calorimeter block was set to 30 °C. The calorimeter was allowed to reach the equilibrium temperature over a 3 hour period at which point the sample bulb was broken and the rotation of the calorimeter was set in motion.

The fluorinated carbon powders tested in this study are very hydrophobic which made it difficult to wet the entire surface of the powder with pure water. For this reason, mixtures of n-propanol and water were used as the wetting solution and the heat of immersion values were extrapolated to the value for pure water. A similar approach was adopted by Hansford et al.[21] when studying the griseofulvin powder by the Washburn method. At each concentration the heat of immersion was measured at least three times to ensure reproducibility. The solutions used in the experiments were made from de-ionized, distilled water and research grade n-propanol of 99.98% purity obtained from Fisher Scientific.

4.5 RESULTS AND DISCUSSION

Figure 4.5 shows the enthalpy of immersion as a function of the n-propanol concentration in water. For the FC10 powder, direct measurement of the heat of immersion in pure water was possible. As seen from the graph, there is a linear relationship between the heat of immersion and the concentration of n-propanol at low concentrations. This linear relationship was also observed by Young et al.[30] for aqueous solutions of n-butyl alcohol on graphon and by Hansford et al.[21] for aqueous solutions of ethanol on griseofulvin. This shows that the extrapolation of the heat of immersion data is a valid method for obtaining the heat of immersion of hydrophobic powders in water in which direct measurement with pure water is not possible.

Figure 4.5 Enthalpy of Immersion vs Concentration of n-Propanol

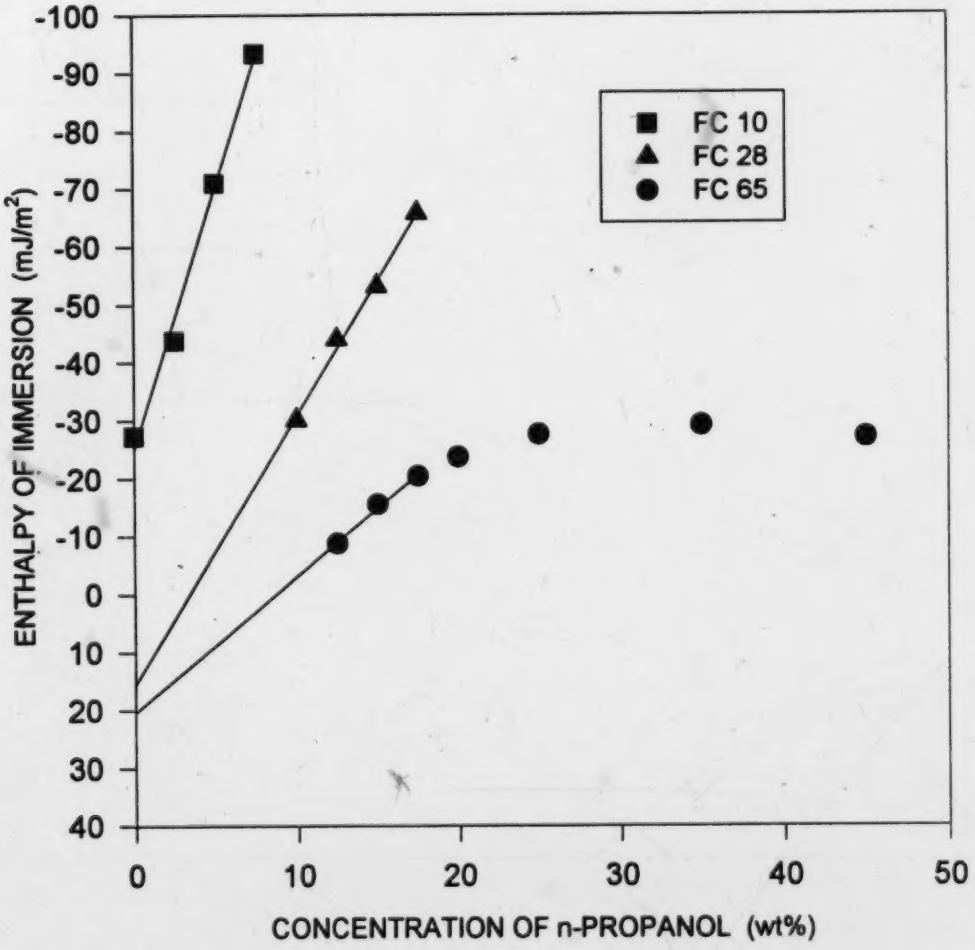

It was not possible to completely wet the surface of the FC28 or the FC65 powders with n-propanol concentrations less than 10 wt% and 12.5 wt% respectively. However, extrapolation of the measured values gives a ΔH_{im} of -15.5 mJ/m² for FC28 and -20.4 mJ/m² for FC65. The standard error arising from extrapolation to zero percent n-propanol for both the FC28 and FC65 is 3.4 mJ/m².

Table 4.1 shows the change in enthalpy upon immersion (h_i), the calculated contact angle and the contact angle obtained from literature for a number of hydrophobic powders. The estimated errors for FC28 and FC65 arise from the extrapolation to zero percent n-propanol. Table 4.1 shows that the wetting process for FC28 and FC65 is endothermic, where as the wetting process for all other hydrophobic powders is exothermic. This is not the first identification of an endothermic wetting process. Tovbin et al.[31] established that the forced flow of water onto hydrophobic sites on PbI_2 surfaces is an endothermic process. Ideally, a measure of the contact angle for the fluorinated carbons using one of the conventional methods described earlier would solidify the validity of Equation 4.2-8. Attempts to measure the contact angle using the Washburn and Bartell methods were unsuccessful because of the nature of the fluorinated carbon. The very small particle sizes, along with their extremely hydrophobic nature, made the packed beds very unstable. Experiments using the compressed powder method are described in the next section.

4.6 CONTACT ANGLE MEASUREMENTS USING THE COMPRESSED POWDER METHOD

4.6.1 Introduction

The problems associated with the compressed powder method have been described in Section 4.1. Despite the many drawbacks with this method, the experimental procedure

Table 4.1 Enthalpy of Immersion and Contact Angle of Hydrophobic Powders

Powder	h_i (mJ/m²)	Calculated θ using Eqn. 4.2-8 (°)	Measured θ from literature (°)	Reference
Graphon	-32.2	81	82	17
Griseofulvin	-5.7	102	101.9	18
Teflon	-6	102	110	19
			102 (equil.)	23
			108	20
			98	22
			112	21
FC 10	-27.3	85		
FC 28	15.5 ± 3.4	120		
FC 65	20.4 ± 3.4	125		

is quite simple. For this reason, the compressed powder method was used to obtain a visual representation of the extremely hydrophobic nature of the fluorinated carbon material. This section briefly describes the experimental apparatus used for the measurement of the contact angle and shows the problems associated with the compressed powder method. The contact angle of water on the various fluorinated carbon powders as well as a Teflon powder is measured.

4.6.2 Experimental Procedure and Apparatus

The compressed discs were formed using a 150 tonne hydraulic press. The mold used to form the discs was made up of six stainless steel pieces which formed a rectangular box. A piece of chart recorder paper was placed on the bottom face of the mold. Chart paper was used because of its smooth surface. The powder was then added (~ 1 g) and another piece of chart paper was placed on the top of the powder. The pieces of chart paper also permitted easy removal of the compressed disc from the mold. To achieve a stable disc, a small amount of methanol was added to the powder. This helped increase the packing density of the disc by wetting the particles and reducing the electrostatic repulsion between the particles. It was not necessary to use methanol in the preparation of the Teflon disc. The hydraulic press was increased to 100 tonnes and left for 10 minutes. The pressure was slowly released so as not to break the compressed disc. After the disc was formed, the methanol was evaporated at room temperature for 120 hours in a fume hood.

The apparatus used to measure the contact angle of a water drop on the compressed discs is shown in Figure 4.6. The apparatus was designed and built by Professor D. Li of the Mechanical Engineering Department at the University of Alberta. The technique uses an Axisymmetric Drop Shape Analysis-Profile (ASDA-P) program to determine the liquid-fluid interfacial tension and contact angle from the shape of a sessile drop on the surface of the compressed disc. A small drop of distilled water is placed on

Figure 4.6 Apparatus for Sessile Drop Measurements

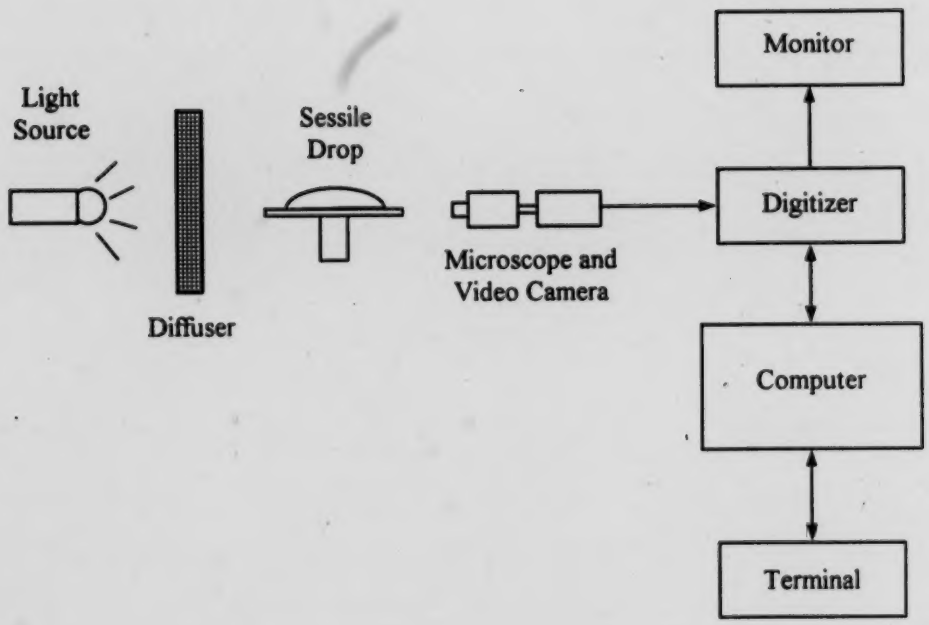

the disc using a syringe. A magnified video camera is used to produce an analog signal containing the image data. The analog signal is transmitted to the image processor and converted to a digital signal containing the image data in the form of pixels. The digital pixel data are stored in the computer memory and can be accessed for display or additional computer processing. Display circuitry transforms the digital data stored in memory back into an analog signal which is displayed on a video monitor. Once the image is obtained and stored in the computer memory, the ASDA-P FORTRAN program calculates the surface tension and the contact angle of the sessile drop. The ASDA-P program constructs an objective function which expresses the deviation of the physically observed image from a theoretical curve satisfying the Laplace equation of capillarity. The objective function is minimized numerically with the liquid surface tension as one of the adjustable parameters. A detailed description of the principles of ASDA-P are given elsewhere.[32,33]

4.6.3 Results and Discussion

Figures 4.7(a)-(d) show the image of a water droplet on various fluorinated carbon discs as well as a Teflon disc. The Teflon disc was used to show the effect the compressed powder method has on the measured contact angle. Table 4.2 shows the contact angle calculated by the ASDA-P program based on the images in Figures 4.7(a)-(d). The contact angles measured using the compressed powder method are significantly higher than the values found using the heat of immersion technique. This is to be expected, since the surface formed by the compression of the powder is rough and heterogeneous. Surface roughness has been shown to greatly affect the apparent or macroscopic contact angle.[34-37] The contact angle of the Teflon disc (124°), which had the smoothest surface of the four materials, is much higher than the reported literature values (98-112°). Another problem encountered with the compressed powder method is that some small particles of fluorinated carbon were found to float on the surface of the water drop. This affects the surface tension of the liquid which is one of the parameters

Figure 4.7 Image of a Water Drop on Various Compressed Powder Discs as Reproduced on a Laser Printer

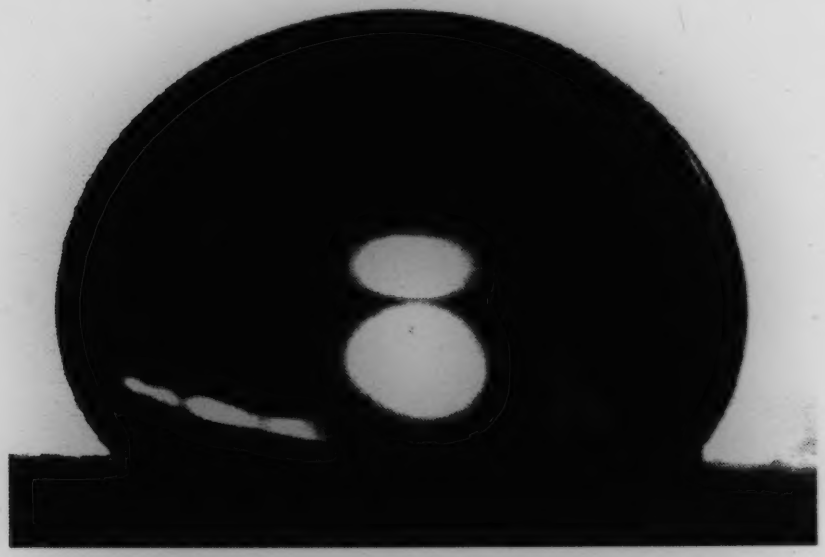

(a) FC10 compressed disc.

(b) FC28 compressed disc.

(c) FC65 compressed disc.

(d) Teflon compressed disc.

Table 4.2 Contact Angle Measured Using Compressed Powder Method

Compressed Disc	Measured Contact Angle (°)
FC10	134
FC28	166
FC65	166
Teflon	124

used in the ASDA-P technique to determine the contact angle. It is extremely difficult to obtain a smooth homogeneous surface using the fluorinated carbon powders. For this reason, the compressed powder method used in this study is for the purpose of giving a visual representation of the hydrophobicity of these powders. The contact angles shown in Table 4.2 are not to be taken as quantitative results.

4.7 CONCLUSIONS

One of the advantages of using the heat of immersion method for evaluating the wettability of powders is that the preparation of the sample is relatively easy compared to the conventional methods for measuring contact angle. This results in much more reproducible data and a much higher experimental success rate than for the Washburn or Bartell methods. Also, the heat of immersion method is not susceptible to problems such as contact angle hysteresis, surface roughness or drop size, as is the case with the compressed powder method. The principal disadvantage of the heat of immersion method is that the solid must have a large specific surface area. At present, most heat flow calorimeters have a sample capacity of approximately 7 mL. This volume is used for both the wetting liquid and the solid sample. This limits the amount of powder which can be used in an experiment. If the powder has a small specific surface area, the amount of heat exchanged upon wetting will be small. This of course is also dependent on the surface energy of the solid. With hydrophobic materials (low surface energy), the problem becomes one of sample size. If the powder of interest has a low specific surface area and is hydrophobic, as is the case for Teflon, it becomes necessary to use a larger sample of powder (≈5 g). In many of the heat flow calorimeters in use today, it is not possible to use this large a sample. The calorimeter used by Chessick et al.[22] for the measurement of Teflon was capable of holding up to 8 g of powder. This larger sample size enabled

Chessick and co-workers to measure the heat of immersion of Teflon whereas it is not possible using the C-80 micro calorimeter used in this work.

The heat of immersion method has many advantages over the conventional methods of measuring the contact angle of hydrophobic powders. But, it must be noted that the heat of immersion method is limited for use with large contact angle systems because of the assumptions made in the derivation of Equation 4.2-8.

4.8 NOTATION

A = parameter as defined by Eqn. 4.1-6

A_s = surface area per gram of solid

C = constant

C_p = heat capacity of the cell

E = total electromotive force

e_i = elementary electromotive force

g_i = Gibbs energy change upon immersion

h_i = enthalpy change upon immersion

ΔH_{im} = heat of immersion defined as ($\Delta H_{im} = - h_i$)

l = length through which the liquid has penetrated the bed

n = number of thermocouples in the fluxmeter

m = slope as defined by Eqn. 4.1-5

Δp = threshold pressure difference across the packed bed

ΔP = total pressure difference across the packed bed

Q = heat generated

r = radius of capillary

r_e = effective radius

S = static calibration constant of calorimetry

T = temperature

T_e = temperature of the thermostat

T_i = temperature of the cell

t = time

W = total thermal power

W_i = elementary thermal power

W_r = power remaining in the cell

W_t = power exchanged through the thermocouples

Greek Symbols:

γ = surface tension

ε_i = thermoelectric power of the thermocouple

η = liquid viscosity

θ = equilibrium contact angle

θ_A = advancing contact angle

θ_R = receding contact angle

κ_i = thermal conductivity of the thermocouple

ν = rate of flow of liquid through the packed bed

π_e = equilibrium film pressure

ρ_s = mass density of solid

τ = dynamic calibration constant of calorimetry

ϕ = volume fraction of solid in the packed bed

Subscripts:

s = solid interface

sl = solid/liquid interface

lv = liquid/vapor interface

sv = solid/vapor interface

4.9 REFERENCES

1. Washburn, E. W., *Phys. Rev.* **1921**, 17, 273.
2. Bartell, F. E., and E. J. Merril, *J. Phys. Chem.* **1932**, 36, 1178.
3. Bartell, F. E., and C. E. Whitney, *J. Phys. Chem.* **1932**, 36, 3115.
4. White, L. R., *J. Colloid Interface Sci.* **1982**, 90, 536.
5. Heertjes, P. M., and N. W. F. Kossen, *Powder Technol.* **1967**, 1, 33.
6. Studebaker, M. L., and C. W. Snow, *J. Phys. Chem.* **1955**, 59, 973.
7. Hansford, D. T., J. W. Grant, J. M. Newton, *Powder Technol.* **1980**, 26, 119.
8. Neumann, A. W., and R. J. Good, *Surface and Colloid Science*, Good, R. J., and R. R. Stromberg, Eds., Plenum: New York, **1979**, Vol. 11, 72.
9. Vargha-Butler, E. I., T. K. Zubovits, M. K. Weibel, D. R. Absolom, A. W. Neumann, *Colloids and Surfaces* **1985**, 15, 233.
10. Fuerstenau, D. W., J. Diao, M.C. Williams, *Colloids and Surfaces* **1991**, 60, 127.
11. Vargha-Butler, E. I., M. R. Soulard, A. W. Neumann, *CIM Bulletin* **1981**, 74, (836), 54.
12. Huethorst, J. A. M., and A. F. M. Leenaars, *Colloids and Surfaces* **1990**, 50, 101.
13. Adamson, A. W., and I. Ling, *Advan. Chem.* **1964**, 43, 57.
14. Melrose, J. C., *J. Colloid Sci.* **1965**, 20, 801.
15. Neumann, A. W., *Adv. Colloid Interface Sci.* **1974**, 4, 105.
16. Schonhorn, H., *J. Phys. Chem.* **1966**, 70, 4086.
17. Dettre, R. H., and R. E. J. Johnson, *J. Colloid Interface Sci.* **1966**, 21, 367.
18. Dettre, R. H., and R. E. J. Johnson, *J. Phys. Chem.* **1967**, 71, 1529.

19. Starkweather, H. W., *SPE Trans.* **1965**, Jan., 5.

20. Young, G. J., J. J. Chessick, F. H. Healey, A.C. Zettlemoyer, *J. Phys. Chem.* **1954**, 58, 313.

21. Hansford, D. T., J. W. Grant, J. M. Newton, *J.C.S. Faraday I* **1980**, 76, 2417.

22. Chessick, J. J., F. H. Healey, A. C. Zettlemoyer, *J. Phys. Chem.* **1956**, 60, 1345.

23. Ellison, A. H., and W. A. Zisman, *J. Phys. Chem.* **1954**, 58, 260.

24. Dann, J. R., *J. Colloid Interface Sci.* **1970**, 32, 302.

25. Hu, P., and A. W. Adamson, *J. Colloid Interface Sci.* **1977**, 59, 605.

26. Tarasevich, Y. I., *Kolloidnyi Zhurnal* **1991**, 53, 1111.

27. Gravelle, P. C. *Catal. Rev. - Sci. Eng.* **1977**, 16, 37.

28. Calvet, E., and H. Part, *Recent Progress in Microcalorimetry*, Skinner, H.A. ed. Pergamon Press, New York **1963**.

29. Gravelle, P.C., *Adv. Catal.*, **1972**, 22, 191 .

30. Young, G. J., J. J. Chessick, F. H. Healey, *J. Phys. Chem.* **1956**, 60, 394.

31. Tovbin, M. V., E. P. Skorobagat'ko, G. G. Buderashaya, L. V. Savchuk, E. N. Nikolaets, *Kolloidnyi Zhurnal* **1982**, 44, 1199.

32. Li, D., P. Cheng, A. W. Neumann, *Advances in Colloid and Interface Sci.* **1992**, 39, 347.

33. Cheng, P., D. Li, Y. Boruvka, A. W. Neumann, *Colloids and Surfaces* **1990**, 43, 151.

34. Wenzel, R.N., *Ind. Eng. Chem.* **1936**, 28, 988.

35. Good, R.J., *J. Amer. Chem. Soc.* **1952**, 74, 5041.

36. Neumann, A.W., *Advances in Colloid and Interface Sci.* **1974**, 4, 105.

37. Huh, C., and S. G. Mason, *J. Colloid Interface Sci.* **1977**, 60, 11.

CHAPTER 5

CATALYTIC OXIDATION OF METHANOL

5.1 INTRODUCTION

The oxidation of methanol has become a much studied reaction since the early 1980's. Interest arose from the introduction of methanol fueled vehicles. With the increasingly stringent air pollution standards for vehicles, methanol has become an alternative to gasoline. Methanol is a high-octane fuel which can produce less carbon monoxide, reactive hydrocarbons, and oxides of nitrogen when combusted than does gasoline. To obtain the greatest possible emission reduction from methanol, the methanol vehicles require an emission control catalyst which has been optimized to convert the products of methanol combustion. Methanol exhaust components of particular concern are formaldehyde and unburned methanol because of their adverse affect on the environment. Recently, methanol has been targeted as a major pollutant with 30 622 tonnes released to the environment in Canada during 1993 (Environment Canada national pollutant release inventory summary 1993). This made methanol the second most released pollutant behind sulfuric acid. Half of the methanol release was to the air which could be removed using a catalytic oxidizing unit.

5.2 PROPOSED MECHANISMS FOR THE CATALYTIC OXIDATION OF METHANOL

Most of the studies concerning the gas-phase oxidation of methanol have been interested in the production of partial oxidation products such as formaldehyde and methyl formate using metal oxide catalysts.[1,2] The oxidation of methanol over transition metals has received less attention. Firth[3] was the first to study the catalytic oxidation of methanol over platinum. The study focused on the kinetics of the methanol oxidation reaction in excess oxygen over a platinum supported on alumina catalyst. The reactions were performed at atmospheric pressure, with temperatures below 60 °C and methanol concentrations up to 3 vol%. No partial oxidation products were detected and the

reaction was found to be first order in methanol. Firth[3] determined the reaction order, with respect to oxygen, to be -0.5 which indicated the adsorbed oxygen competes with methanol for adsorption sites on the catalyst surface. Extrapolation of the data to infinite oxygen pressure suggested that there are some sites still available for the adsorption of methanol. Therefore, the methanol is thought to adsorb on two types of sites, one of which can adsorb oxygen atoms and one which cannot. This leads to two parallel mechanisms, one which is inhibited by oxygen and one which is not. Firth[3] proposed a kinetic equation of the form

$$-r_{CH_3OH} = \frac{k_1 P_{CH_3OH}}{P_{O_2}^{\frac{1}{2}}} + k_2 P_{CH_3OH} \qquad (5.2\text{-}1)$$

where k_1 and k_2 are rate constants for the inhibited and uninhibited reactions respectively. Arrhenius plots of the results showed an apparent activation energy for the inhibited reaction of 42 ± 5 kJ/mol and 46 ± 5 kJ/mol for the uninhibited portion of the reaction. Firth[3] proposed a model for the reaction in which the inhibited reaction proceeds on a platinum metal surface not covered by oxygen and the uninhibited reaction proceeds on the oxygen-covered surface. The reaction on the oxygen-covered surface is thought to involve the rupture of an oxygen to metal bond in the rate determining step while the reaction on the bare metal surface does not involve the rupture of such a bond.

Hodges and Roselaar[4] were the next to study the gas-phase oxidation of methanol. They used a flow reactor with platinum discs at temperatures from 150 to 500 °C with oxygen-lean feed mixtures. Oxygen-lean feeds were used to examine the product distribution under conditions of incomplete combustion. They found that between 150 and 190 °C formaldehyde and water were the only products and that the platinum lost activity after being in use for some time. No significant deactivation occurred above

200 °C and the formation of CO_2 was not observed until 225 °C. The loss in activity was attributed to strongly chemisorbed CO which was thought to be an intermediate in the formation of carbon dioxide.

Gentry et al.[5] studied the oxidation of methanol at atmospheric pressure over platinum wire at temperatures between 37 and 387 °C with P_{O2}/P_{CH3OH} from 2 to 100. Two experimental techniques were used to derive the kinetic parameters in the rate equation. The first method measured the gas-phase concentrations from a conventional flow reactor with methanol conversions below 25%. The second method was similar to Firth[3], where the kinetic parameters were derived from rates of heat generation at the catalyst surface using a micro-calorimeter. The methanol conversions in the micro-calorimeter experiments were less than 6%. Under the experimental conditions used in their study, the oxidation of methanol produced mainly carbon dioxide, formaldehyde and water, with trace amounts of methyl formate. Gentry et al.[5] proposed the general rate expression

$$-r_{CH_3OH} = kP^m_{CH_3OH}P^n_{O_2} \qquad (5.2\text{-}2)$$

with m = 1 and n = 0.5, for P_{O2}/P_{CH3OH} = 8-15 at T = 52-117 °C and m = 1, n = 0 for all pressure ratios at T>132 °C. The activation energy was calculated to be 33±5 kJ/mol in terms of methanol consumption and 33±10 kJ/mol in terms of carbon dioxide formation. The selectivity to methyl formate, defined as the ratio of the rate of formation of product to the total rate of consumption of methanol, did not exceed 1.4%. At temperatures above 157 °C the rate of reaction became almost independent of temperature. This is indicative of the rate of the reaction becoming controlled by the rate of diffusion of methanol to the catalyst surface. Gentry et al.[5] proposed the following mechanism for the oxidation of methanol over platinum which is consistent with their experimental results.

$$O_2(g) + 2\Diamond \rightleftharpoons 2O(a) \quad (5.2\text{-}3)$$

$$CH_3OH(g) + O(a) + \Diamond \rightarrow CH_3O(a) + OH(a) \quad (5.2\text{-}4)$$

$$CH_3O(a) + O(a) \rightarrow H_2CO(a) + OH(a) \quad (5.2\text{-}5)$$

$$H_2CO(a) \rightarrow H_2CO(g) + \Diamond \quad (5.2\text{-}6)$$

$$H_2CO(a) + O(a) \text{ etc.} \rightarrow CO_2(g) + H_2O(g) + \Diamond \quad (5.2\text{-}7)$$

$$2OH(a) \rightarrow H_2O(g) + O(a) + \Diamond \quad (5.2\text{-}8)$$

The symbol "◊" denotes an adsorption site. In the above mechanism, Step 5.2-5, the abstraction of hydrogen from the adsorbed methoxy species to form adsorbed formaldehyde, was taken to be the rate limiting step. Gentry et al.[5] found identical kinetics for methanol consumption and carbon dioxide formation which led them to postulate a common rate limiting step. They thought the successive hydrogen abstraction from $CH_3O(a)$ to be unlikely since the formation of CO(a) is expected to inhibit the reaction which did not occur in their work. They suggest that the most likely mechanism for CO_2 formation is oxygen insertion into a CHO(a) species to form COOH(a) which then decomposes to carbon dioxide.

Another kinetic study of methanol oxidation over platinum wire was conducted by McCabe and McCready.[6] The methanol oxidation rates were examined in a flow reactor at a maximum pressure of 133 Pa with temperatures ranging from 77 to 527 °C. In feeds containing excess oxygen, the only gaseous products were carbon dioxide, formaldehyde and water. In feeds containing excess methanol, carbon monoxide and hydrogen were formed at temperatures above 327 °C in addition to the above mentioned products. No methyl formate was observed in this study which may be due to the detectability limit of methyl formate at the low partial pressures in the study. Oxidation experiments with $^{18}O_2$ showed that methanol is oxidized to CO_2 principally by a pathway which leaves the C-^{16}O bond intact. McCabe and McCready[6] proposed that methanol is oxidized on Pt via a

major pathway involving a CO(a) intermediate and a minor pathway involving a C(a) intermediate. They suggest that the sharp transition in methanol conversion results from inhibition of O_2 adsorption by a CO(a) intermediate. McCabe and McCready[6] proposed the following mechanism for the oxidation of methanol.

$$O_2(g) + 2\lozenge \rightleftharpoons 2O(a) \qquad (5.2\text{-}9)$$

$$CH_3OH(g) + \lozenge \rightleftharpoons CH_3OH(a) \qquad (5.2\text{-}10)$$

$$CH_3OH(a) + \lozenge \rightarrow CH_3O(a) + H(a) \qquad (5.2\text{-}11)$$

$$CH_3O(a) + O(a) \rightarrow H_2CO(a) + OH(a) \qquad (5.2\text{-}12)$$

$$H_2CO(a) \rightleftharpoons H_2CO(g) + \lozenge \qquad (5.2\text{-}13)$$

$$H_2CO(a) + O(a) \rightarrow CHO(a) + OH(a) \qquad (5.2\text{-}14)$$

$$CHO(a) + O(a) \rightarrow CO(a) + OH(a) \qquad (5.2\text{-}15)$$

$$CO(a) \rightleftharpoons CO(g) \qquad (5.2\text{-}16)$$

$$CO(a) + O(a) \rightarrow CO_2(g) + 2\lozenge \qquad (5.2\text{-}17)$$

The close agreement between the apparent activation energies for methanol, formaldehyde and carbon monoxide oxidation under low temperature conditions observed by McCabe and McCready, suggests that oxidation of CO(a) is the rate limiting step in all three reactions studied. The apparent activation energies of 30±5 kJ/mol for overall methanol oxidation and 42±5 kJ/mol for CO_2 production were evaluated under differential operating conditions with less than 10% conversion.

5.3 COMPARISON OF THE PROPOSED MECHANISMS

Two types of methanol oxidation mechanisms have been proposed. Both types share the same initial steps but they differ in the way in which CO_2 is formed. The initial formation of a $CH_3O(a)$ (methoxide) intermediate has been well established.[7,8] The

production of formaldehyde in the gas phase indicates that the $CH_3O(a)$ is decomposed to some extent through an adsorbed formaldehyde intermediate. Hodges and Roselaar[4] and McCabe and McCready[6] proposed mechanisms based on the dissociation of the $CH_3O(a)$ to CO(a) and H(a) followed by oxidation with adsorbed atomic oxygen to CO_2 and H_2O. The intermediate species between $CH_3O(a)$ and CO(a), however, are unknown. McCabe and McCready[6] suggest that species having the H_2CO stoichiometry but lacking the double-bond character of formaldehyde are the main intermediates in the formation of CO_2 because of the absence of large formaldehyde yields in their study. Experiments presented in Chapter 7 show that formaldehyde is a significant product which suggests that adsorbed formaldehyde is an intermediate in the oxidation of methanol. Gentry et al.[5] proposed a different mechanism for the formation of CO_2. They suggest that the most likely mechanism for CO_2 formation is oxygen insertion into a CHO(a) species to form COOH(a) which then decomposes to CO_2 and H(a). However, a study by Abbas and Madix[8] on the Pt(111) surface, showed the formation of CO_2 to be caused by the oxidation of adsorbed carbon monoxide. Abbas and Madix[8] showed that an absorbed oxygen atom interacts with the CO already present on the surface to form carbon dioxide. The formation of CO_2 was reported to be instantaneous and occurred via a pseudo-first order process.

Gentry et al.[5] were the first to observe methyl formate as a gas phase product in the oxidation of methanol over *unsupported* platinum but they do not discuss its formation. McCabe and Mitchell[9] observed methyl formate as a major product in the oxidation of methanol over platinum supported on alumina at temperatures below 150 °C. Abbas and Madix[8] demonstrated the presence of methyl formate both on the Pt(111) catalyst surface and in the gas phase as a product. These authors observed methyl formate formation only upon dosing the Pt(111) surface with formaldehyde. They proposed two possible mechanisms for the formation of methyl formate.

(A) $CH_3O(a) + H_2CO(a) \rightarrow H_2COOCH_3(a) + \Diamond \rightarrow HCOOCH_3(a) + H(a)$

$HCOOCH_3(a) \rightarrow HCOOCH_3(g) + \Diamond$

(B) $2H_2CO(a) \rightarrow HCOOCH_3(a) \rightarrow HCOOCH_3(g) + \Diamond$

Abbas and Madix[8] consider the formation of methyl formate through the intermolecular hydrogen transfer between adjacent H_2CO molecules (Mechanism B) the more favorable mechanism because they did not observe any methyl formate when methanol was the reactant. Under conditions of high coverage, (i.e. insufficient number of sites available for formaldehyde dissociation) the presence of undissociated formaldehyde molecules located at adjacent sites is likely. Therefore, the formation of methyl formate could result from the interaction between adsorbed formaldehyde molecules. At low coverage the adsorbed formaldehyde dissociates using adjacent active sites. Experiments using the Pt/FC and the Pt/Al_2O_3 catalysts described earlier show methyl formate as the major product at low temperatures similar to that observed by McCabe and Mitchell.[9]

5.4 MODIFIED MECHANISM FOR THE OXIDATION OF METHANOL

Based on the above literature, the proposed mechanism for the oxidation of methanol has been modified and is shown in Figure 5.1. The following steps are assumed:

$O_2(g) + 2\Diamond \leftrightharpoons 2O(a)$ (5.4-1)

$CH_3OH(g) + O(a) + \Diamond \rightarrow CH_3O(a) + OH(a)$ (5.4-2)

$CH_3O(a) + O(a) \rightarrow H_2CO(a) + OH(a)$ (5.4-3)

$H_2CO(a) + 2O(a) \rightarrow CO(a) + 2OH(a)$ (5.4-4)

$CO(a) + O(a) \rightarrow CO_2(a) + \Diamond$ (5.4-5)

$2H_2CO(a) \rightarrow HCOOCH_3(a) + \Diamond$ (5.4-6)

$2OH(a) \leftrightharpoons H_2O(g) + O(a) + \Diamond$ (5.4-7)

Figure 5.1 Modified Mechanism for the Oxidation of Methanol

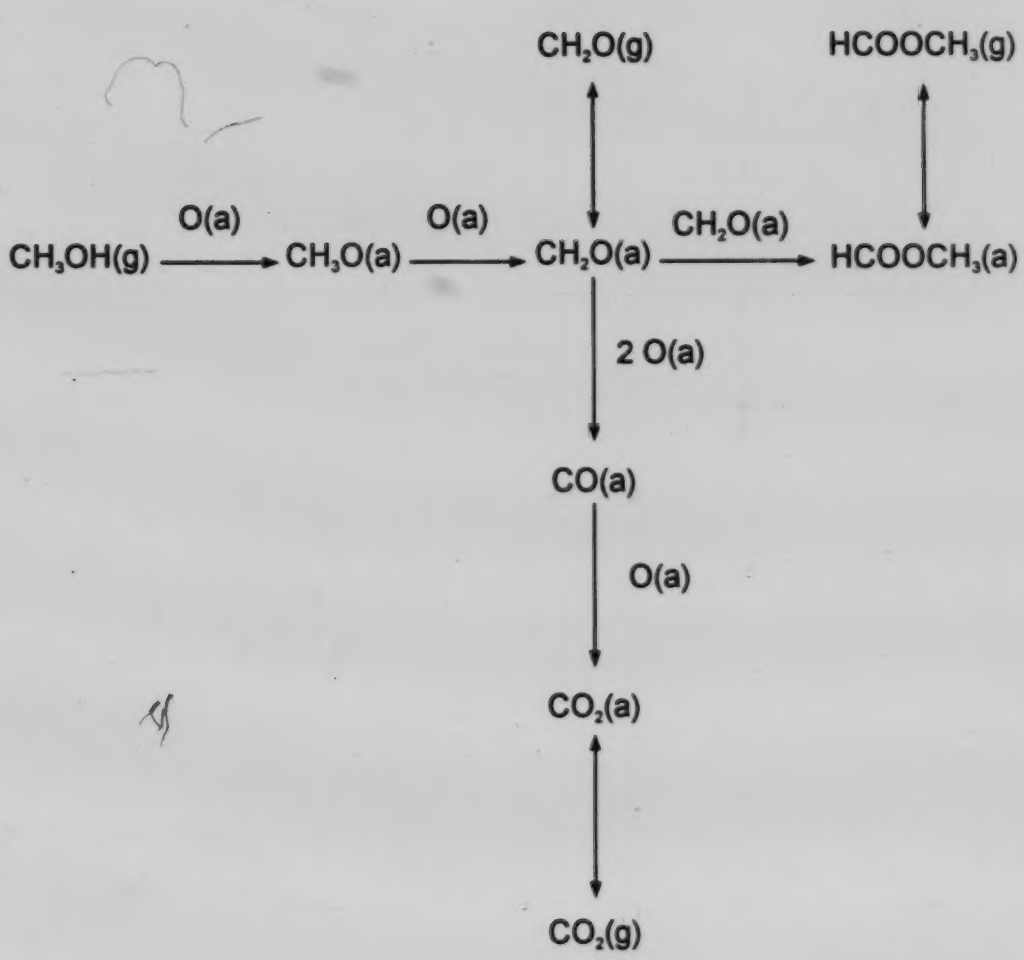

$$H_2CO(a) \rightleftharpoons H_2CO(g) + \Diamond \qquad (5.4\text{-}8)$$

$$HCOOCH_3(a) \rightleftharpoons HCOOCH_3(g) + \Diamond \qquad (5.4\text{-}9)$$

$$CO_2(a) \rightleftharpoons CO_2(g) + \Diamond \qquad (5.4\text{-}10)$$

The above mechanism follows the Langmuir-Hinshelwood kinetics and can be used to develop a mathematical model for the oxidation of methanol. It is proposed that the rate determining step is the oxidation of the adsorbed formaldehyde to carbon monoxide (Step 5.4-4). This assumption is based on the findings of McCabe and McCready[6] and Abbas and Madix.[8] The rate determining step chosen is validated in Chapter 7 with the experimental observations of the product distribution and catalyst deactivation for the methanol oxidation reaction.

Appendix C shows the derivation of the rate equations shown below. In dry feed conditions, the following rate equation was derived using the assumptions listed in Appendix C.

$$-r_{CH_3OH} = kP_{CH_3OH} \qquad (5.4\text{-}11)$$

where $-r_{CH_3OH}$ = the rate of disappearance of methanol

k = the rate constant which is a function of temperature

P_{CH_3OH} = partial pressure of methanol in the bulk gas phase

In wet feed conditions, the amount of water in the gas phase is no longer negligible and the rate equation, as shown in Appendix C, becomes:

$$-r_{CH_3OH} = \frac{kP_{CH_3OH}}{\left[1 + bP_{H_2O}^{1/2}\right]^2} \qquad (5.4\text{-}12)$$

where P_{H_2O} = the partial pressure of water in the bulk gas phase

b = a constant defined in Appendix C

The kinetic parameters for the rate equation are evaluated in Chapter 7 for dry feed conditions. An in-depth discussion of the proposed mechanism is presented in Chapter 7 based on the experimental observations.

5.5 EFFECT OF WATER ON THE CATALYTIC OXIDATION OF HYDROCARBONS

The effect of water vapor on the catalytic oxidation of hydrocarbons has been investigated by several authors covering a variety of catalysts.[9-25] Since this study focuses on Pt-supported catalysts, the effect of water on metal oxide catalysts is not considered. In the literature dealing with the oxidation of hydrocarbons, the effect of water is variable. Each reaction is unique and depending on the reaction mechanism, the effect of water can be dramatically different. Some authors have shown that water can enhance the activity and selectivity of certain oxidation reactions.[10-12] The oxidation of CO is enhanced by the presence of water over Pt-supported catalysts. This has been attributed to the weakening of self-poisoning by CO.[11,12] Yaparpalvi and Chuang[12] found an increase in the activity of a hydrophobic catalyst in wet conditions for the oxidation of CO, but observed a decrease in the activity of a hydrophilic catalyst under the same conditions. The decrease in activity for the hydrophilic catalyst was attributed to the accumulation of capillary condensed water in the catalyst pores. The condensation results in increased diffusional resistance for the reactants across the liquid film covering the catalyst active sites. Van de Beld et al.[13] found that the oxidation of propene over a Pt/Al_2O_3 catalyst was enhanced by the addition of small amounts of water up to 1.0 vol%. Marécot et al.[14] found that water inhibits the activity of a Pt/Al_2O_3 catalyst for the oxidation of propane while the oxidation of propene is slightly affected. These results were for catalysts prepared using non-chlorinated

precursor salts. On chloride containing Pt/Al_2O_3 catalysts, water was found to have a beneficial effect both on propane and propene oxidations. The authors concluded that the increase in activity for the chloride containing catalysts was a result of the water removing the chloride from the metal surface, thereby, regenerating the active sites for hydrocarbon oxidation. The inhibition of water on the non-chloride containing catalysts was explained by the adsorption of water on the platinum sites. The water decreases the catalytic activity as a result of the conversion of the surface platinum oxide to the corresponding hydroxide. Simon and Vortmeyer[15] found a strong influence of water vapor on the oxidation of ethane over a Pd catalyst. Similar results were obtained by Mezaki and Watson[16], Cullis et al.[17] and Ribeiro et al.[18] for the oxidation of methane. These researchers attributed the inhibition by water to the formation of $Pd(OH)_2$ on the PdO surface. The oxidation of methane is effectively suppressed because only the surface PdO is active.

The literature data on the influence of water vapor on the oxidation of methanol are in contradiction. Yao[19] studied the oxidation of methanol over Pt-alumina catalysts with methanol feed concentrations below 0.2% in excess oxygen and found the reaction was inhibited by water. McCabe and Mitchell[9], however, found that the introduction of water vapor in the feed had little affect on the methanol oxidation activity over a Pt-alumina catalyst. The discrepancy between these two studies is unclear because Yao[19] did not give details of the experimental conditions. McCabe and Mitchell[9] used a water concentration of 0.1% at temperatures between 60 and 300°C. Observations made during the experiments presented in Chapter 8 of this thesis, suggest that there is no significant effect on activity with water concentrations as low as 0.1%. Brewer et al.[20] found a dramatic decrease in the conversion of methanol over a Pd-supported catalyst at temperatures between 30 and 80°C with a water concentration of 1%. They observed a sharp increase in conversion near 80°C and complete conversion at 100°C.

There are several ways in which water can affect an oxidation reaction. The following is a list of possible mechanisms to explain the effect of water.

1. Water chemisorbs on the active sites of the catalyst inhibiting the reactant molecules (competitive adsorption).
2. Water physically blocks the active sites by capillary condensation effects.
3. Water adsorbs on the catalyst support and sterically hinders the reactant molecules making it difficult for adsorption.
4. The presence of water changes the adsorption characteristics of reactants or products.
5. Water removes contaminants on the catalyst surface which were present from the preparation process.

Another mechanism describing the inhibition effect of water has been proposed by Sperber.[25] It is suggested that there is an increase in the thermal capacity of the gas mixture when water is introduced. This decreases the reactor temperature and, therefore, the activity. This thermal effect, as pointed out by Lefferts et al.[10], is possible in an industrial adiabatically operated reactor but has no significant effect on the majority of the experiments reported in the literature.

The deactivation of conventional hydrophilic catalysts in the presence of water may occur by any of the above mechanisms or a combination of them. Adsorption of water on the active sites of the catalyst has been the explanation used by most research groups studying the effects of water on the oxidation of hydrocarbons. However, the adsorption of water on the catalyst support cannot be overlooked, especially, for catalysts supported on alumina. Alumina, the most widely used support material, and the one used for comparison in this study, is a well known drying agent. The structure of alumina interacts with water in several ways including both reversible and irreversible adsorption. Desai et al.[26] clearly points out four types of water-alumina interactions; (i) chemisorption on defects in the alumina structure, (ii) quasichemisorption which involves molecular water that is hydrogen bonded to hydroxyl groups on the activated alumina surface, (iii)

physically adsorbed water molecules on top of the quasichemisorbed water and, (iv) capillary condensation within the smaller pores depending on the pore size and water partial pressure. The three types of water interactions that are of interest in the present study are the quasichemisorbed, physically adsorbed and capillary condensed water because they can sterically affect the catalytic process. With small platinum crystallites present on the surface of the alumina, quasichemisorbed and physically adsorbed water have the potential to block a significant number of active sites resulting in deactivation of the catalyst. The water can come either from the feed mixture or from the products of the reaction. As water accumulates on the surface of the support, the catalyst becomes deactivated. The use of a fluorinated carbon support can circumvent the accumulation of water and, therefore, reduce the amount of deactivation.

Studying the kinetics of both Pt-alumina and Pt-fluorinated carbon catalysts in dry and wet conditions can add insight into the mechanism of the methanol oxidation reaction and the role water plays. Chapter 6 describes, in detail, the experimental equipment used to study the methanol oxidation reaction.

5.6 REFERENCES

1. Sohrabi, M., B. Dabir, F. Mozaffari, *Chem. Eng. Technol.*, **1991**, 14, 96.

2. Tronconi, E., A. S. Elmi, N. Ferlazzo, P. Forzatti, G. Busca, P. Tittarelli, *Ind. Eng. Chem. Res.*, **1987**, 26, 1269.

3. Firth, J.G., *J. Chem. Soc. Faraday Trans. I*, **1971**, 67, 212.

4. Hodges, C.N., and L.C. Roselaar, *J. Appl. Chem. Biotechnol.*, **1975**, 25, 609.

5. Gentry, S. J., A. Jones, P. T. Walsh, *J.C.S. Faraday I*, **1980**, 76, 2084.

6. McCabe, R. W., and D. F. McCready, *J. Phys. Chem.*, **1986**, 90, 1428.

7. Sexton, B. A., *Surf. Sci.*, **1981**, 102, 271.

8. Abbas, N. M., and R. J. Madix, *Appl. Surf. Sci.*, **1981**, 7, 241.

9. McCabe, R. W., and P. J. Mitchell, *Appl. Cat.*, **1986**, 27, 83.

10. Lefferts, L., J. G. van Ommen, J. R. H. Ross, *J. Chem. Soc. Faraday Trans. I*, **1988**, 84, 1491.

11. Muraki, H., S. Matunaga, H. Shinjoh, M. S. Wainwright, D. L. Trimm, *J. Chem. Tech. Biotechnol.*, **1991**, 52, 415.

12. Yaparpalvi, R., and K. T. Chuang, *Ind. Eng. Chem. Res.*, **1991**, 30, 2219.

13. Van de Beld, L., M. P. G. Bijl, A. Reinders, B. Van der Werf, K. R. Westerterp, *Chem. Eng. Sci.*, **1994**, 49, (24), 4361.

14. Marécot, P., A. Fakche, B. Kellali, G. Mabilon, M. Prigent, J. Barbier, *Appl. Cat. B*, **1994**, 3, 283.

15. Simon, B. and D. Vortmeyer, *Chem. Eng. Sci.*, **1978**, 33, 109.

16. Mezaki, R., and C. C. Watson, *I.E.C. Proc. Des. Dev.*, **1966**, 5, 62.

17. Cullis, C. F., T. G. Nevell, D. L. Trimm, *J. Chem. Soc. Faraday Trans. I*, **1972**, 68, 1406.

18. Ribeiro, F. H., M. Chow, R. A. Dalla Betta, *J. Catal.*, **1994**, 146, 537.

19. Yao Y. F. Y., *183rd A.C.S. Nat'l Meet. Las Vegas*, **1982**, Mar.28-Apr.2, Coll 89.

20. Brewer, T. F., M. A. Abraham, R. G. Silver, *Ind. Eng. Chem. Res.*, **1994**, 33, 526.

21. Zhu, J. and S. L. T. Andersson, *Appl. Catal.*, **1989**, 53, 251.

22. Arnold, E. W. and S. Sundaresan, *Appl. Catal.*, **1988**, 41, 225.

23. Chang, C. C. and H. S. Weng, *Ind. Eng. Chem. Res.*, **1993**, 32, 2930.

24. Germain, J. E. and Peuch, *Bull. Soc. Chim. Fr.*, **1969**, 6, 1844.

25. Sperber, H., *Chem.-Ing.-Techn.*, **1969**, 41, 962.

26. Desai, R., M. Hussain, D. M. Ruthven, *Can. J. Chem. Eng.*, **1992**, 70, 699.

CHAPTER 6

EXPERIMENTAL EQUIPMENT AND OPERATION

6.1 EXPERIMENTAL EQUIPMENT

A schematic diagram of the apparatus used to study the catalytic oxidation of methanol is shown in Figure 6.1. For the purpose of discussion the experimental set-up is broken into three sections; the feed section, the reaction section and the feed and product analysis section.

6.1.1 Feed Section

The feed system was designed to supply the reactor with a gas stream of reactants at a constant composition and flowrate for long operating periods. It was desirable to change the feed composition to the reactor while still maintaining a constant total feed flowrate.

Extra dry air was obtained in 2500 psig cylinders from the Linde Division of Union Carbide. The flow of air from the single cylinder was split into three lines with mass flow controllers to adjust the flowrate through each of the lines. One feed line was passed through a series of two methanol saturators; another feed line was passed through a series of two water saturators and the third feed line was used to maintain the total flowrate to the reactor. The three feed lines were necessary to enable quick and easy adjustment of the feed composition.

The flowrate through the methanol saturators was controlled by a Matheson model 8272-0421 mass flow controller with a range of 0-20 mL/min. The exit stream from the flow controller was passed through two 500 mL saturators in series. The methanol used in this study was reagent grade methanol (99.8%) from Fisher Scientific. The first methanol saturator was kept at room temperature (~ 23 °C) while the second saturator was held at -8 °C using a circulating cooling bath. This set-up ensured that the stream leaving the second saturator was completely saturated. The low temperature of the second saturator also allowed for higher flowrates of air through the methanol line while

Figure 6.1 Schematic Diagram of Reaction Apparatus

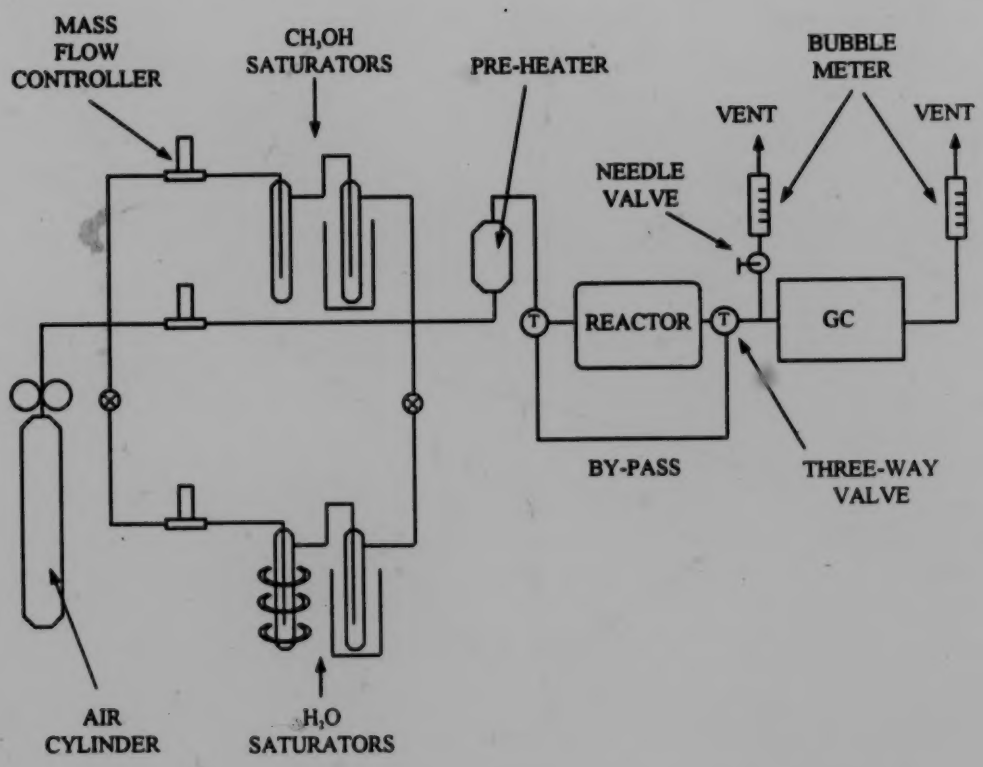

still maintaining a low overall methanol concentration. The higher flowrate enabled the flow controller to operate at a level of stability acceptable for the experiments. Initially, only a single saturator was used for the introduction of methanol to the feed stream. Figure 6.2 shows the variation of the methanol concentration as a function of time for both the single saturator and dual saturator systems. The concentration of the methanol shown in Figure 6.2 is approximately 1000 ppm which is the lowest inlet feed concentration used in this study. The dual saturators give a ±0.7% standard error in concentration over a 20 hour period where as the single saturator gives a ±2.0% standard error over a period of 11.5 hours. A ±0.7% error in the analysis of the feed gas is well within the experimental error of the gas chromatographic (GC) analysis at the concentration range used in this study (1000-3000 ppm). The dual saturator system was required in order to attain a steady inlet concentration in the feed.

The second feed line was controlled using a Matheson Model 8272-0432 mass flow controller with a range of 0-300 mL/min. This stream merged with the exit stream of the second methanol saturator. Together these two streams formed the feed to the reactor when the experiments required "dry feed". The total flowrate and methanol concentration was controlled by adjusting the relative flowrates of these two streams.

The third feed line was used during experiments which required a "wet feed". The flowrate of the third line was controlled with a Unit Instruments Model UFC-1100 mass flow controller with a range of 0-500 mL/min. The exit of the mass flow controller was passed through two 1000 mL water saturators in series. De-ionized water was used in the saturators. The temperature of the first water saturator (50 °C) was controlled using a Staco model 3PN-1010 variable auto transformer and electrical heating tape. The temperature of the second saturator was maintained at 30 °C using a 58 L circulating bath. Similar to the methanol system, the water system gives a steady water concentration in the feed stream over long periods of time. Figure 6.3 shows the concentration of water as

Figure 6.2 Inlet Methanol Concentration versus Time

(a) Single Saturator System

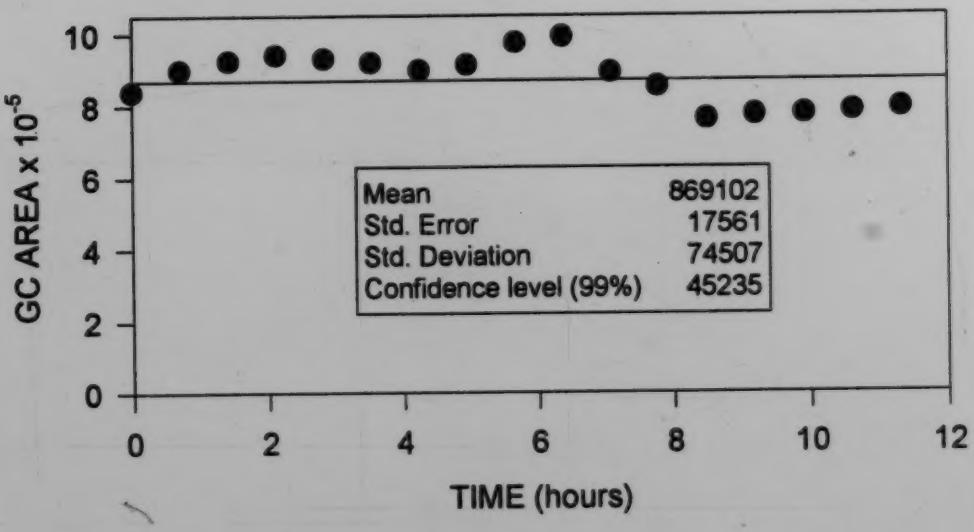

(b) Dual Saturator System

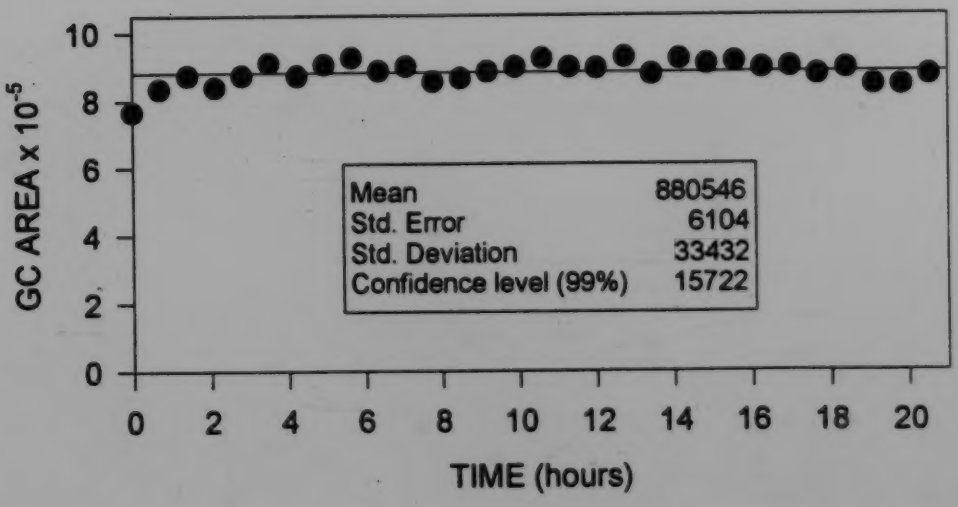

Figure 6.3 Inlet Water Concentration versus Time

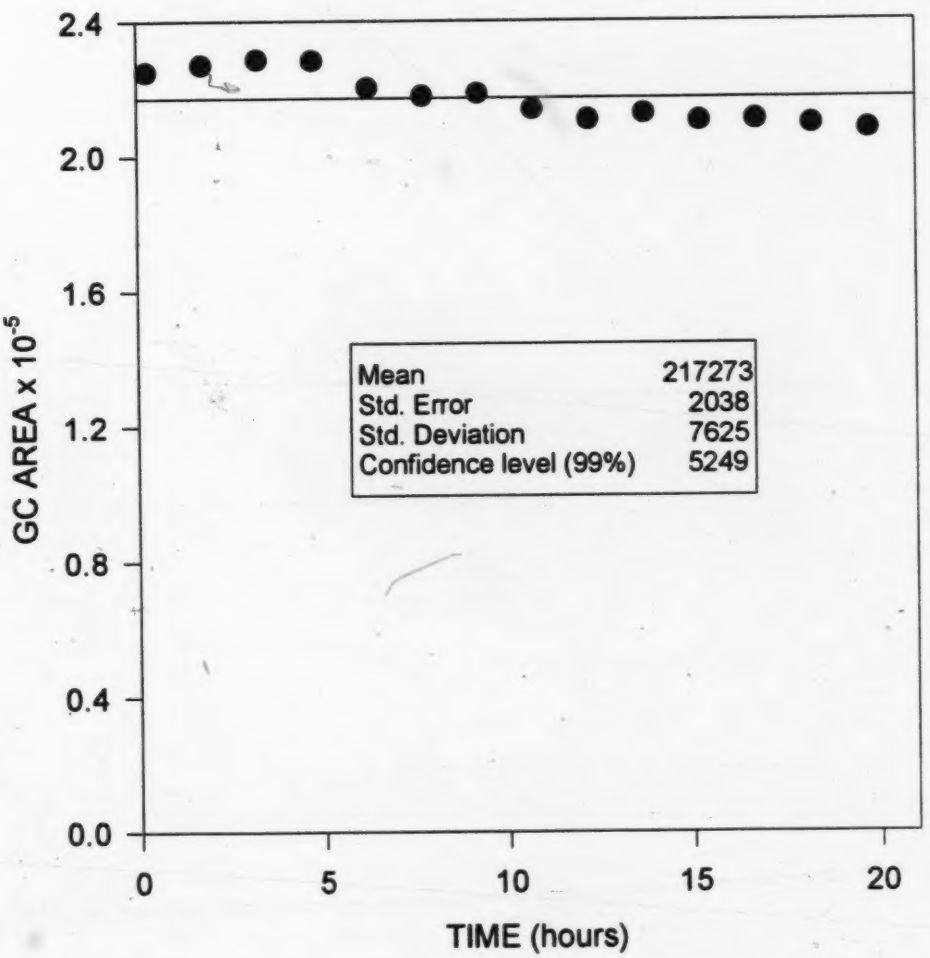

a function of time. The water saturators give a ±0.9% standard error in concentration at a water partial pressure of approximately 2.5 kPa.

The exit of the second water saturator is merged with the combined flow from the methanol saturators and the main line. Under "wet feed" conditions the concentration of both methanol and water can be controlled, as well as the total flowrate, by adjusting the flowrates of the individual streams. The feed system, set-up in this way, allows for great flexibility, easy operation, a constant inlet flowrate and a stable inlet composition.

All the lines down stream of the saturators are heat traced to prevent condensation of the feed components. The inlet stream is completely mixed by passing the feed through a 200 mL pre-heater filled with inert ceramic spheres. The stream exiting the pre-heater can be passed to the reactor or directly to the GC using two 3-way valves. The flowrate of each feed line, as well as the total flowrate, is measured using on-line bubble meters placed at the exit of the GC and at the vent upstream of the GC. A needle valve on the vent upstream of the GC is used to set the flowrate through the GC sample loop so as to avoid the upstream pressure build-up that would occur if the entire flow was passed through the small diameter loop. During each experiment, the flow rates were measured directly using the bubble meters. In this way, the flowrates are measured accurately and there is no need to calibrate the mass flow controllers.

6.1.2 Reaction Section

Oxidation reactions generally produce a large amount of heat. This makes it difficult to investigate the kinetics of these type of reactions in conventional packed bed reactors because the catalyst bed is not at a uniform temperature. The temperature gradient produced in the catalyst bed greatly affects the interpretation of the reaction data obtained with packed bed reactors because the conversion is a strong function of temperature. For this reason, a Berty-type reactor, similar to the one seen in Figure 6.4,

Figure 6.4 Schematic Diagram of the Berty Reactor

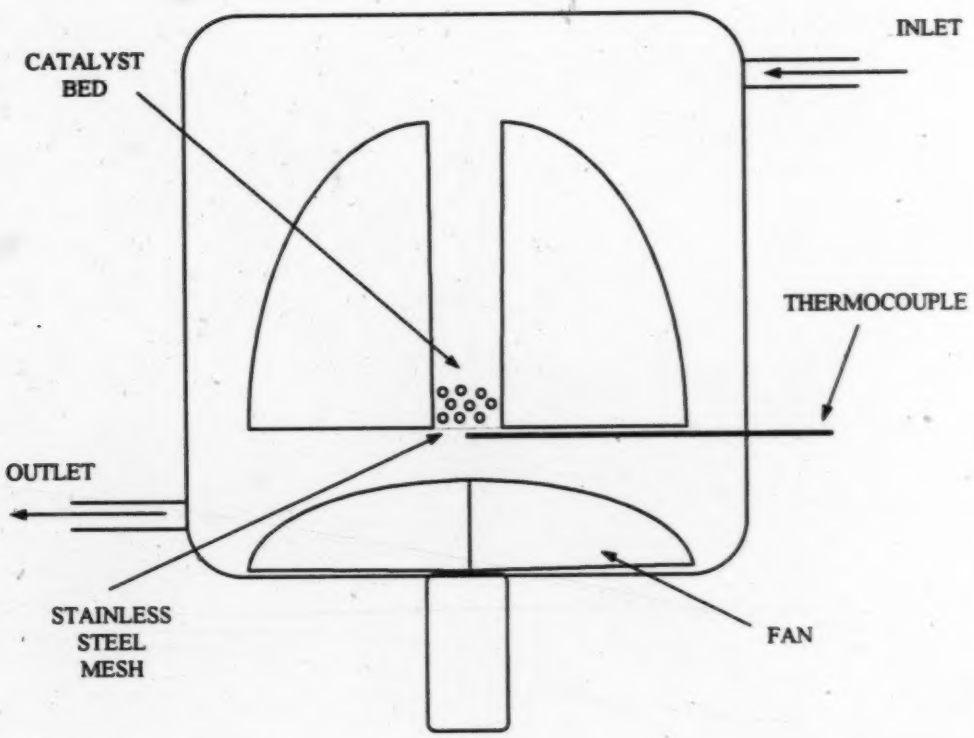

was used for this study. The Berty reactor is an isothermal reactor which eliminates heat transfer effects.

The reactor is a 21 cm diameter x 19 cm height internal circulating reactor identical to the one described by Tong.[1] The reactor inside volume is approximately 800 mL with a catalyst bed size of 3.8 cm (i.d.) x 8.9 cm (height). The internal circulation of the gas phase is provided by a sealed MagneDrive, belt-driven by a variable V*S Reliance Motor. The rotation speed is measured using an optical tachometer. A high temperature furnace surrounds the Berty reactor, and both the furnace and the bottom of the reactor are insulated to provide better temperature control. The furnace temperature is monitored by three thermocouples located in different sections of the furnace. The top and side temperature of the furnace are regulated independently. The catalyst is placed on a stainless steel mesh and the catalyst bed temperature is measured using a thermocouple directly underneath the catalyst bed.

6.1.3 Feed and Product Analysis

Both the feed and product streams were analyzed using a Hewlett-Packard 5890 on-line gas chromatograph equipped with a thermal conductivity detector (TCD) and a flame ionization detector (FID). A single column (0.32 cm diameter by 3 m length) containing Porapak T was employed. The gas chromatographic separations were carried out isothermally at 145 °C. The TCD was used to analyze for carbon dioxide, water and formaldehyde while the FID was used to analyze for methanol and methyl formate. A 1 mL sample loop was used to enable better accuracy of the GC analysis over the concentration range used in this study. The sample loop was housed in a heated oven at 150 °C to prevent any condensation of the gas sample.

The calibration of the components present in the feed and product streams was done using several different methods. A cylinder of 100% CO_2 was used to calibrate the carbon dioxide response peak. A stream of 100% CO_2 was diluted with a stream of extra

dry air to obtain the desired concentrations of carbon dioxide. Both the CO_2 and air flowrates were accurately measured using bubble meters. A liquid phase calibration method was used to determine the methanol, methyl formate and formaldehyde calibration factors. Reagent grade methanol (99.8%) was diluted with high grade ethanol (USP dehydrated 200 proof) as was the methyl formate (99.0%). The formaldehyde (37%) was diluted with de-ionized water. All of the chemicals were obtained from Fisher Scientific, with the exception of the ethanol, which was obtained from Quantum Chemical Corporation. Each of the components calibrated with the liquid phase method were diluted with solvents that had longer retention times in the column so that the solvent peak did not interfere with the calibration peak. The water was calibrated using the dual saturator system described above. The water concentrations were varied by changing the relative flowrates though the water saturator and a diluent air stream.

Figure 6.5 shows the calibration response peaks plotted against the concentrations together with the linear regression analysis. The regression line was not forced through the origin. In the analysis of the experimental data, small peak areas for methyl formate and formaldehyde were considered negligible based on detectability limits from the calibration. All the components calibrated showed a linear relationship between the concentration and the GC peak area as seen by the R squared values. The calibration procedure was repeated periodically over the course of the experiments with very little change in the calibration factors.

6.2 OPERATING OF EQUIPMENT AND EXPERIMENTAL PROCEDURES

Prior to starting the methanol oxidation experiments, a blank test of the reactor system was performed. The reactor was loaded with 10 g of the ceramic spheres used as

Figure 6.5 Component GC Peak Area versus Concentration

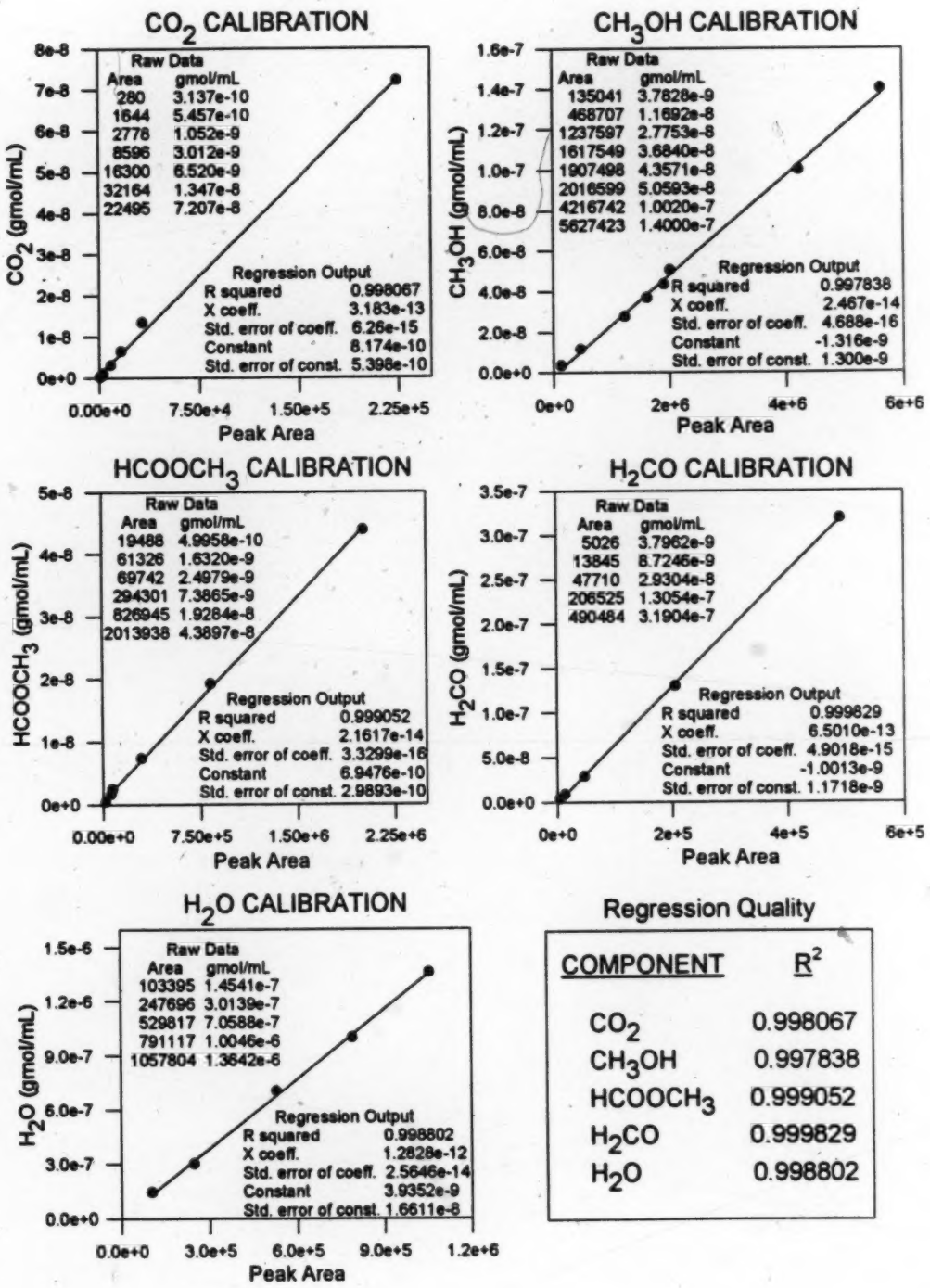

Regression Quality

COMPONENT	R^2
CO_2	0.998067
CH_3OH	0.997838
$HCOOCH_3$	0.999052
H_2CO	0.999829
H_2O	0.998802

the support for the catalysts described in Chapter 2. A feed stream containing 3000 ppm methanol was passed through the reactor at 250 °C. The difference between the inlet and outlet concentrations of methanol was found to be negligible and there were no other peaks present in the product stream that would suggest any reaction occurred. This showed that the ceramic spheres, the stainless steel mesh and the walls of the reactor had no catalytic activity towards the oxidation of methanol.

The Berty reactor is an internal circulating reactor. The internal circulation allows the reactor to be modeled as a continuous stirred tank reactor which means that the gas phase in the reactor is homogeneous. The stirring speed has a direct effect on the homogeneity of the gas phase and on the external mass transfer in the reactor. The gas phase must be passed through the catalyst bed with a velocity such that the stagnant layer of gas around the catalyst surface is minimized. With a thin stagnant layer, the diffusion rate of reactants and products to and from the bulk gas phase is greater, thereby reducing external diffusion effects. Figure 6.6 shows the effect of the stirring speed on the methanol conversion. The maximum in the curve at 100 rpm, which was reproducible, is thought to be caused by an increase in the catalyst surface temperature. At the low stirring speed, the bulk gas phase is unable to remove the reaction heat from the surface of the catalyst. This increase in catalyst surface temperature increases the methanol conversion. As the stirring speed is reduced, the conversion decreases because the diffusion rate of the reactant molecules to the surface of the catalyst becomes lower than the specific rate of reaction. The reaction becomes externally mass transfer controlled. At stirring speeds greater than 1000 rpm, the conversion is constant which suggests that the external mass transfer limitation and the heat transfer effect is eliminated. All of the experiments in this study were performed with a stirring speed of 1300 rpm.

A standard general operating procedure was developed to obtain reproducible results for the reaction experiments. After loading a fresh batch of catalyst, the reactor was pressure tested with helium up to 40 psig. A small helium flow was passed through

Figure 6.6 Methanol Conversion versus Rotation Speed

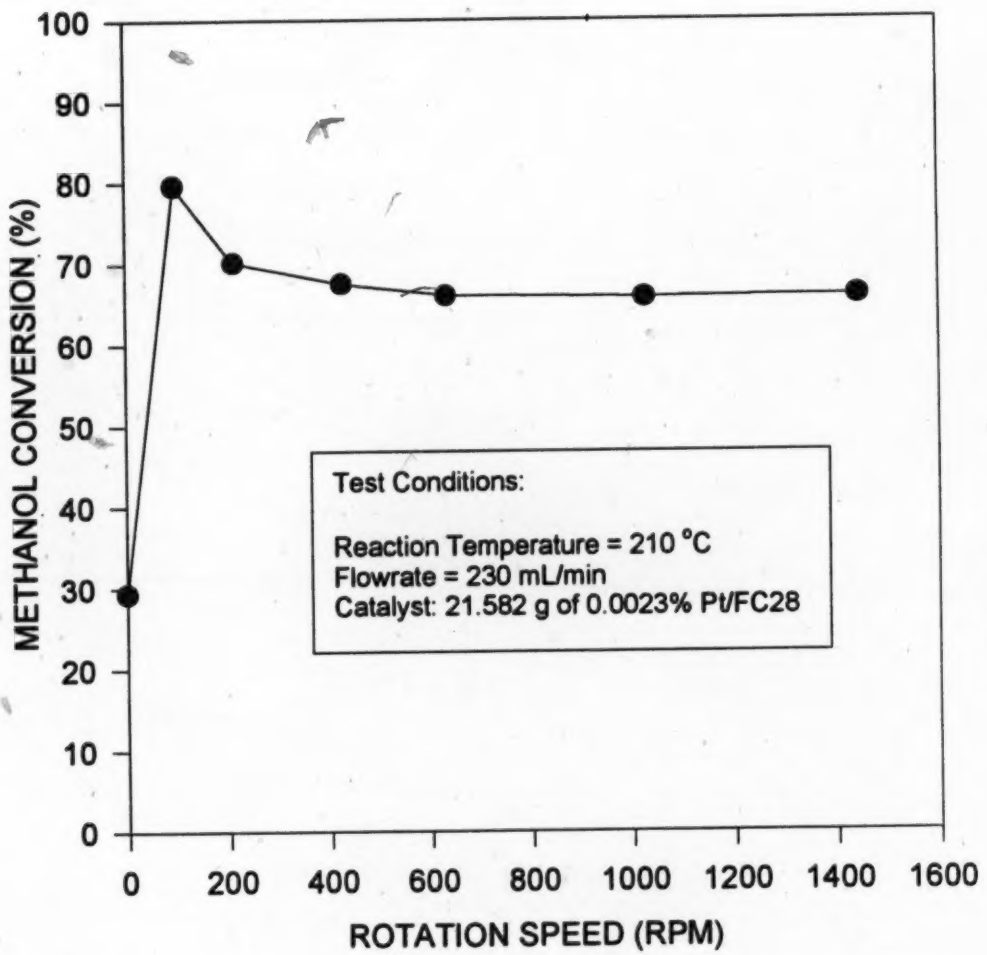

the reactor as the reactor temperature was raised to the set point for the specific experiment. To ensure a uniform reactor temperature the reactor system was left for at least 15 hours. The catalyst surface was then exposed to the feed flow and the reaction was allowed to stabilize. A total of 4-6 samples were taken for each experimental point and the average value of the conversion and reaction rate were reported. The standard deviation of the samples was below 1%. At the end of the experiment a small helium flow was passed through the reactor while it was hot. This helium flow was continued until the reactor reached room temperature so that no condensation occurred in the reactor system.

6.3 REFERENCES

1. Tong, S., Ph. D. Thesis, Dept. of Chem. Eng., University of Alberta, 1992.

CHARTER 7

EVALUATING THE KINETICS FOR THE OXIDATION OF METHANOL

7.1 INTRODUCTION

In Chapter 5, the rate equation for the oxidation of methanol was developed using the Langmuir-Hinselwood model. This chapter presents the results of the kinetic experiments which determine the parameters in the rate equation. The experiments discussed in this chapter are concerned only with dry feed conditions to enable a clear representation of the mechanism discussed in Chapter 5. The reaction rate and selectivity for each catalyst is presented, compared and discussed. The effect of water in the feed stream is examined in Chapter 8.

To elicit the true kinetic parameters of the methanol oxidation reaction on the catalysts of interest, it is important to ensure that the reaction is in the kinetic regime when the data are collected. In Chapter 6, both the external mass transfer effect and the heat transfer effect were eliminated by evaluating the necessary stirring speed of the Berty reactor. Two more factors that can prejudice the experimental data are the internal mass transfer effect and the stability of the catalyst.

7.2 CATALYST STABILITY IN DRY CONDITIONS

To accurately determine the kinetic parameters for the rate equation, it is important to know if the catalyst under investigation is deactivating during the kinetic study. If catalyst deactivation occurs, the interpretation of the data is more complex. It is possible to extract the kinetic parameters if deactivation occurs, however, the dynamics of the deactivation process must be fully understood. It is desirable to run the kinetic experiments under conditions and time frames where the catalyst is stable. For this reason, a stability test was run for each of the catalysts tested to determine if the catalysts are stable in the operating range of the kinetic study.

7.2.1 Hydrophobic Catalysts

Figures 7.1 to 7.3 show the methanol conversion versus time for the different platinum/fluorinated carbon catalysts. The test conditions are shown on the graphs and the data are tabulated in Appendix D. Each catalyst deactivated to some degree in the first 15 hours of operation. There was little change in the conversion after the initial 15 hour period. The most dramatic deactivation occurred on the highly fluorinated carbon catalysts. To gain insight into the mechanism of the deactivation process, the Pt/FC28 catalyst was purged with helium for 12 hours at the reaction temperature (163 °C) in an attempt to regain the initial activity. The helium purge did not affect the activity of the catalyst. The Pt/FC28 was then purged with air for 12 hours at 205 °C. The reaction was run again at 163 °C with no significant change in activity. Purging the catalysts with helium at 300 °C also showed no change in the activity at 163 °C. The initial activity of the Pt/FC28 catalyst was regained only after purging in air at 300 °C for 3 hours. The air purge was identical to the calcination step performed when the catalyst was prepared. The regenerated catalyst deactivated in the same fashion as the fresh catalyst. These tests show that the deactivation in dry conditions is reversible upon heating the catalyst in an oxidizing atmosphere. This suggests several possible deactivation mechanisms.

Figure 7.4 shows the product yield for the Pt/FC28 catalyst during the deactivation process in dry conditions. The amount of formaldehyde produced increases slightly as the deactivation occurs. Since the desorption of formaldehyde is dependent on the amount of $CH_2O(a)$, Figure 7.4 suggests that there is a small increase in the amount of $CH_2O(a)$ during the deactivation. The amount of CO_2 produced decreases following the same trend shown for the decrease in methanol conversion. The deactivation of the catalysts is caused by a decrease in the rate of CO_2 production. This reinforces the assumption that the oxidation of the adsorbed formaldehyde to CO_2 is the rate limiting step as proposed in Chapter 5. It is possible that there is a build up of an adsorbed species on the surface of the platinum. The eventual stabilization of the catalyst indicates that the adsorbed species

Figure 7.1 Methanol Conversion vs Time for Pt/FC10 Catalyst in Dry Conditions

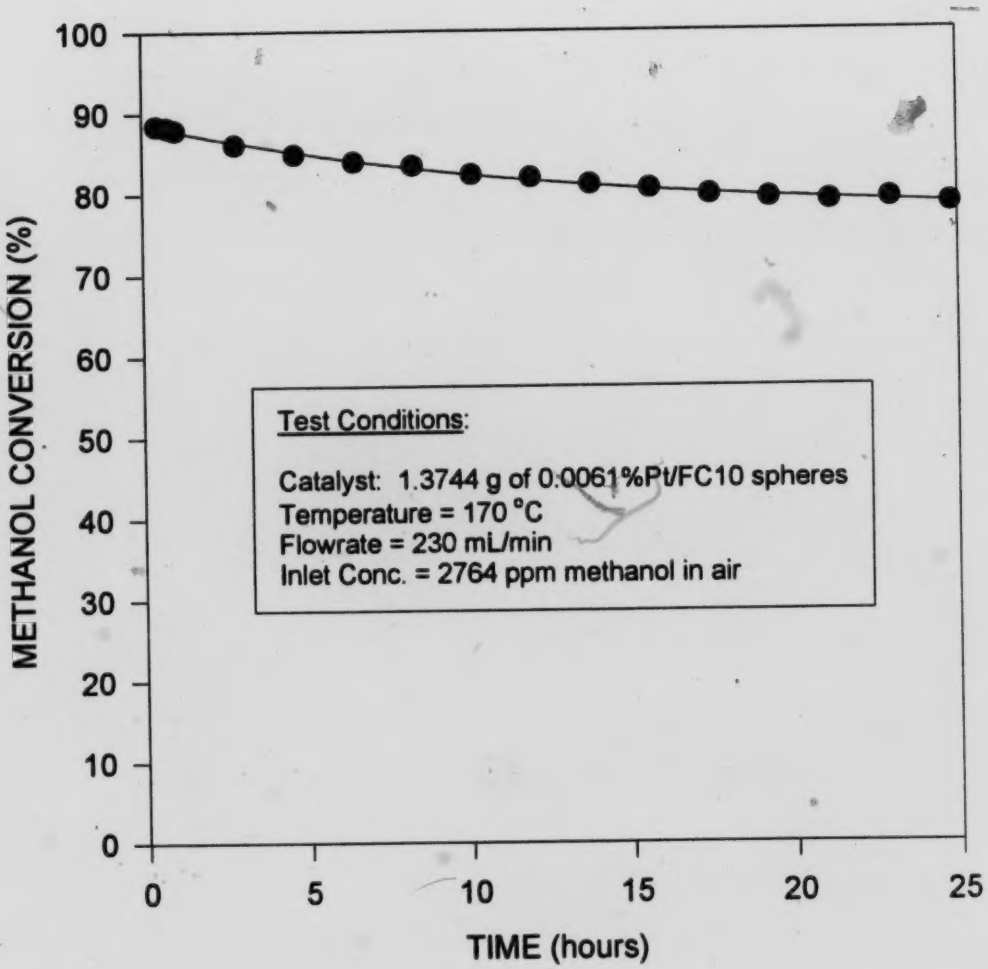

Figure 7.2 Methanol Conversion vs Time for Pt/FC28 Catalyst in Dry Conditions

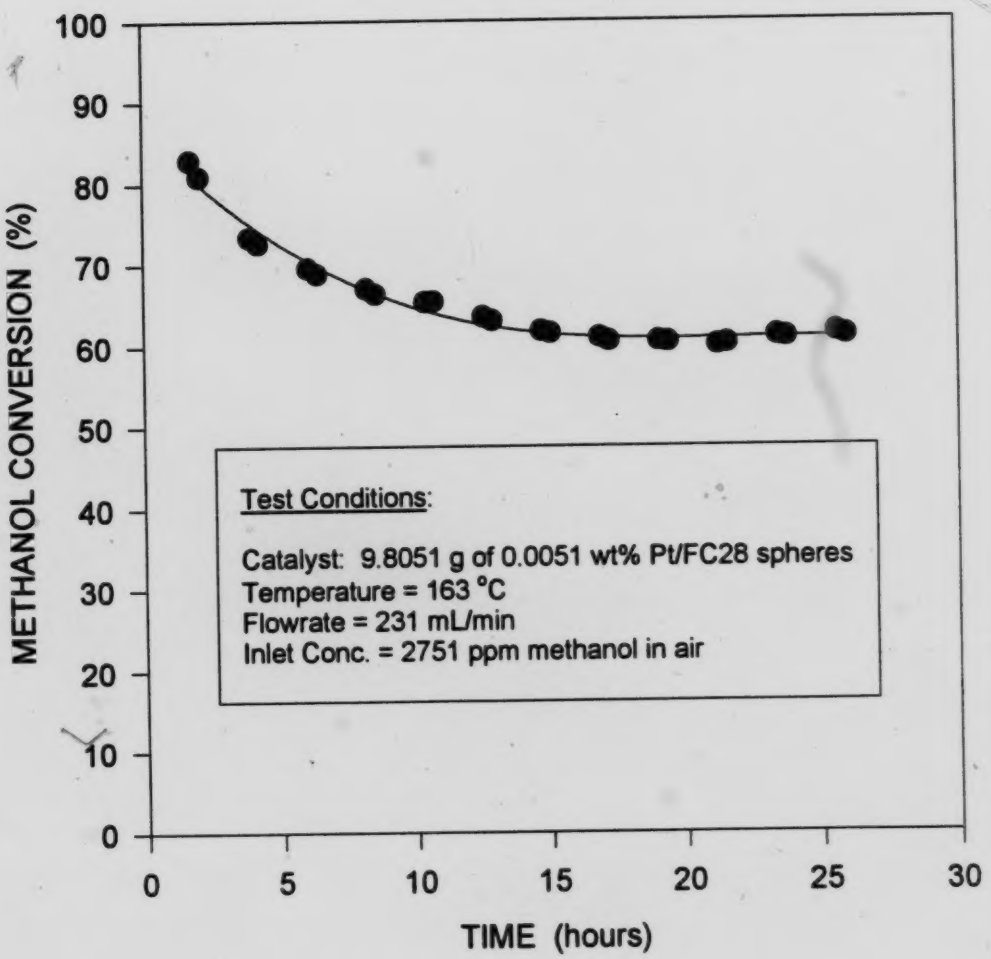

Figure 7.3 Methanol Conversion vs Time for Pt/FC65 Catalyst in Dry Conditions

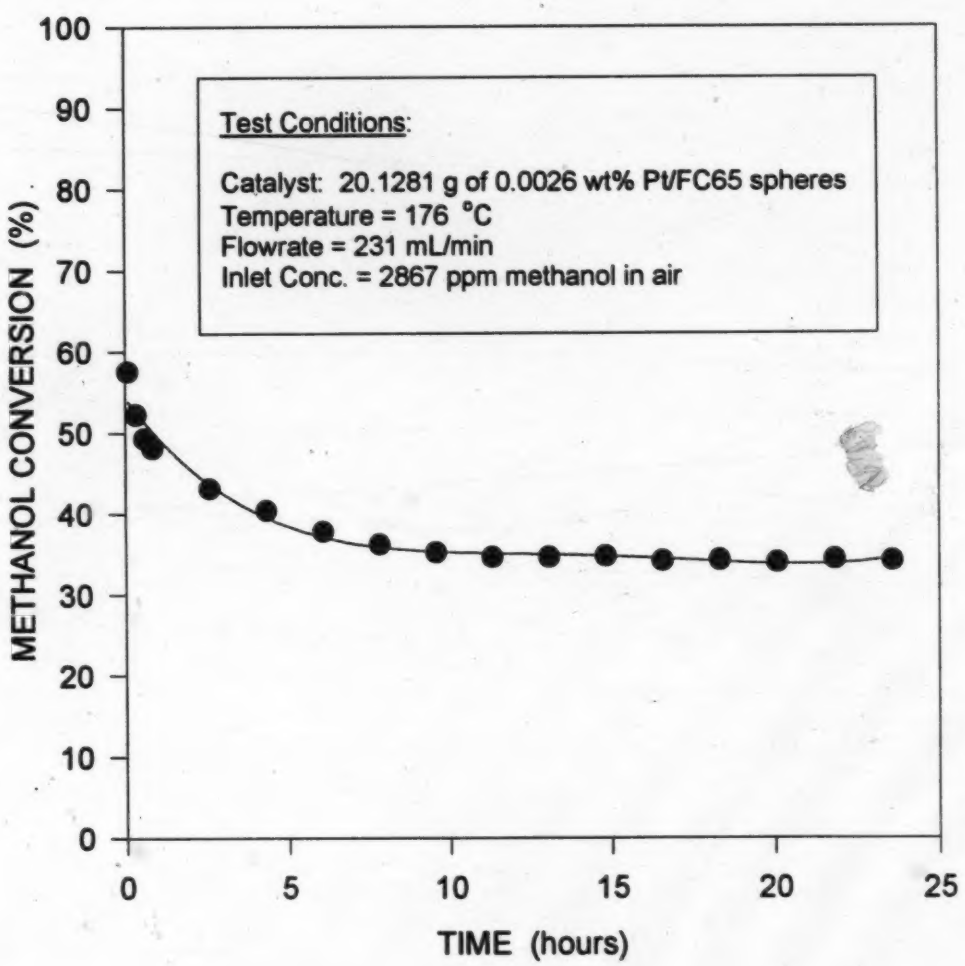

Figure 7.4 Product Yield vs Time for Pt/FC28 Catalyst in Dry Conditions

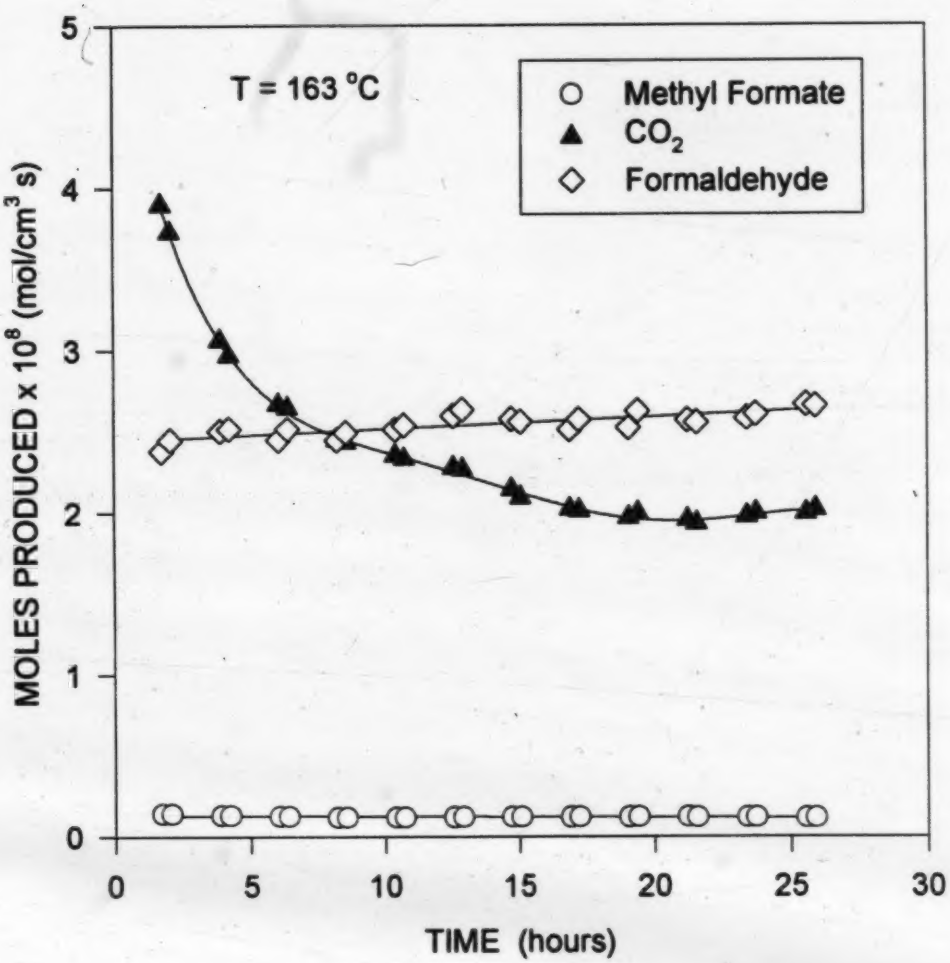

only affects certain active sites. McCabe and McCready[1] showed that the oxidation of methanol to carbon dioxide goes through a minor pathway involving an adsorbed carbon. Hodges and Roselaar[2] reported a loss in activity at temperatures below 200 °C for the oxidation of methanol over a platinum gauze catalyst. They attributed the poisoning to the adsorbed carbon monoxide intermediate. Thermal gravimetric analysis (TGA) of the Pt/FC28 catalyst after reaction showed no significant loss of mass as the catalyst was heated from room temperature to 300 °C in flowing air. The small platinum dispersion of this catalysts (7.5%) makes it difficult to observe a change in mass caused by the oxidation of an absorbed species. These results are considered inconclusive because of the small platinum surface area. Lefferts et al.[3] observed the suppression of the total oxidation of methanol to carbon dioxide over a silver catalyst in the presence of water without a decrease in the formation of formaldehyde. They suggest that the CO_2 is formed in conjunction with a weakly adsorbed atomic oxygen species.[4,5] It is probable that such species are deactivated by the presence of water, as has also been suggested by Kurina et al.[6] In the dry deactivation experiments shown in Figures 7.1-7.3, water is produced as a by-product of the oxidation reaction. It is possible that this water can interact with weakly adsorbed atomic oxygen on the surface of the platinum. The weakly adsorbed oxygen is required in the formation of CO_2 but is not a site that is used by the adsorbed formaldehyde. This would explain the results shown in Figure 7.4 and also the eventual stabilization of the catalyst. The experiments show that the catalysts eventually stabilize which indicates the possibility of different active sites on the platinum for the formation of formaldehyde and carbon dioxide. The interaction between the water and weakly adsorbed oxygen is expected to be eliminated upon heating in helium to 300 °C. The high temperature purge in helium proved to be ineffective in regenerating the catalyst. It is skeptical that the process described by Lefferts et al.[3] is operating in this situation despite the similarities in the product yield behavior.

The data in Figure 7.4 suggest that there is no loss of active sites for the formation of formaldehyde and methyl formate but rather a decrease in the number of sites for the complete oxidation to carbon dioxide. It is possible that there is a change in the oxidation state of the platinum. The reduced platinum may not be as active towards the complete oxidation of adsorbed formaldehyde as the oxidized platinum. X-ray photoelectron spectroscopy (XPS) experiments run at AECL were unable to determine if a change in the oxidation state of platinum occurred. The platinum peak intensities were too weak because of the small surface area of platinum on the catalyst samples.

It must be noted that the main focus of the stability experiments was to establish when the catalysts are stable so that accurate kinetic data can be obtained. It has been seen that the hydrophobic catalysts must be operated under reaction conditions for at least 15 hours before the kinetic experiments can commence.

7.2.2 Hydrophilic Catalyst

Figure 7.5 shows the methanol conversion versus time for the Pt/Al_2O_3 catalyst at three different temperatures. The data shown in Figure 7.5 was obtained with a flowrate of 230 mL/min and an inlet concentration of 2670 ppm methanol in air. To achieve similar conversions for the experiments, the mass of catalyst used in each run was different. For the 72, 161 and 206 °C runs, the amount of 0.0028%Pt/Al_2O_3 catalyst was 6.7369, 5.1137, and 2.3860 g respectively. At temperatures above 160 °C the catalyst deactivates continuously. However, at 72 °C the catalyst is much more stable. Figure 7.6 shows that the product yields, during the deactivation process, for the Pt/Al_2O_3 catalyst behave similar to that observed for the Pt/FC28 catalyst. The formation of CO_2 decreases while the formation of the other products stays relatively constant. The stability of the catalyst at lower temperatures is difficult to explain. At lower temperatures there is a shift in the reaction mechanism to the production of formaldehyde and methyl formate as will be

Figure 7.5 Methanol Conversion vs Time for Pt/Al_2O_3 Catalyst in Dry Conditions

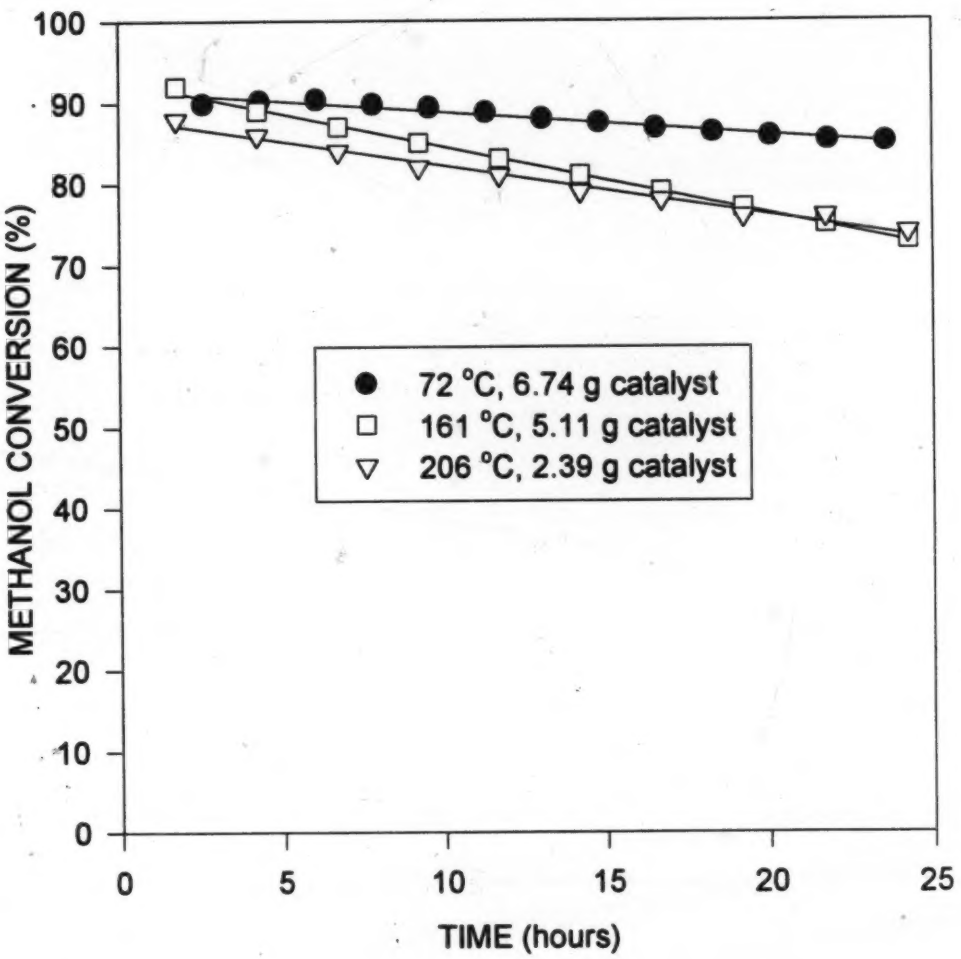

Figure 7.6 Product Yield vs Time for Pt/Al_2O_3 Catalyst in Dry Conditions

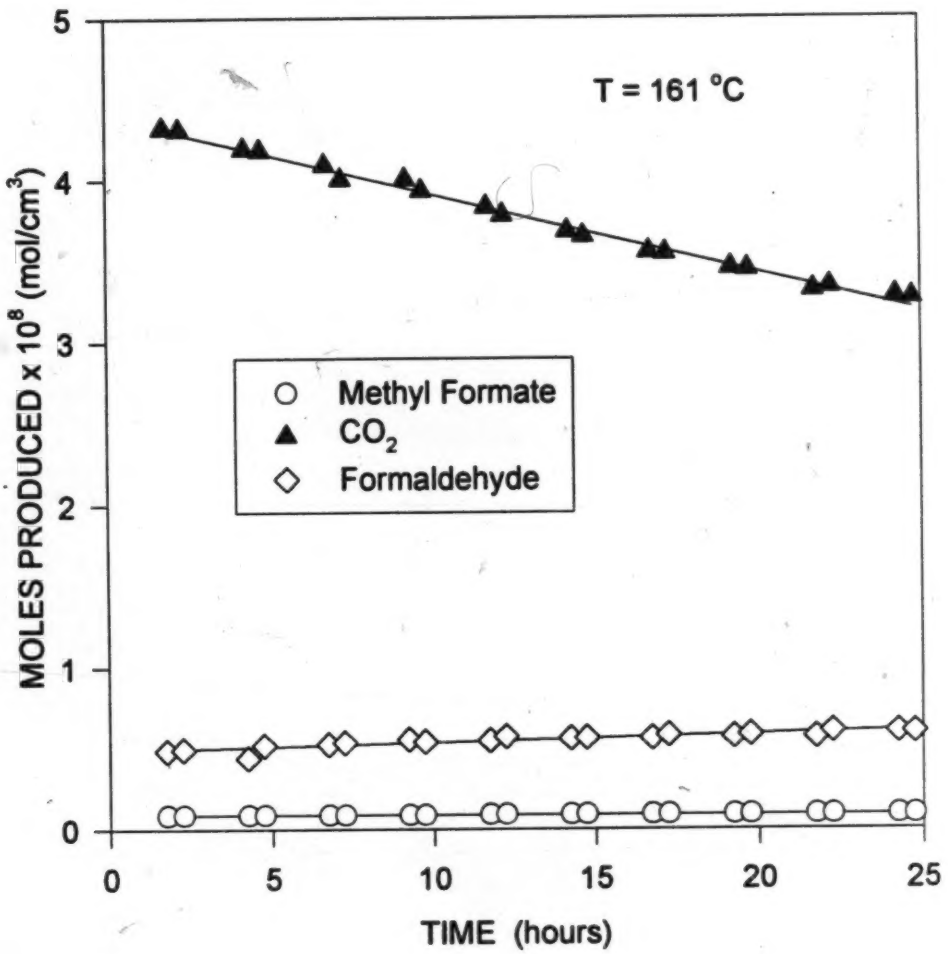

shown later in this chapter. These two mechanisms are not affected by the water produced by the reaction. Also, the formation of methyl formate and formaldehyde produce less water than the complete oxidation to carbon dioxide. The combination of lower water partial pressure and a shift in the reaction mechanism could explain the decrease in the deactivation rate at lower temperatures. The kinetic study of the Pt/Al_2O_3 catalysts was restricted to temperatures below 85 °C to reduce the effects of deactivation.

Another factor that can greatly affect the interpretation of the results from a kinetic study is the internal mass transfer of reactants or products to and from the catalyst sites. The next section investigates the presence of internal mass transfer effects in order to establish the maximum active phase layer thickness and the operating conditions required to eliminate all mass transfer limitations.

7.3 INTERNAL MASS TRANSFER EFFECT

Internal mass transfer can affect the reaction data in a similar way as external mass transfer limitations. The difference between the two is the location of the mass transfer inhibition. Internal mass transfer is used to describe the movement of molecules within the structure of the catalyst, whereas external mass transfer describes the movement of molecules between the bulk fluid and the external surface of the catalyst. To collect meaningful kinetic data, it is necessary to eliminate all mass transfer limitations. Internal mass transfer, for the catalysts used in this study, refers to the movement of a molecule from the outer surface of the catalyst to the active sites within the structure of the active phase layer. This means that the thickness of the active phase layer is an important parameter which can affect the overall reaction rate. If the internal mass transfer of a species is the rate limiting step under the operating conditions of the experiment, then the results of the kinetic study do not represent the true reaction kinetics. Two important parameters which are used to theoretically estimate if a reaction is in the mass transfer regime is the Thiele modulus (ϕ) and the effectiveness factor (η). The Thiele modulus is a

dimensionless parameter consisting of a group of variables which result from the mathematical manipulation of the mass balance on the active phase layer. The effectiveness factor is defined as the ratio between the rate of reaction observed and the rate of reaction that would occur if no mass transfer limitations were present. In the theoretical approach to determining the effectiveness factor, it is necessary to obtain the concentration profile within the catalyst. The equation for the Thiele modulus and the effectiveness factor for a first-order reaction with a flat plate geometry, as given by Satterfield,[7] is shown below.

$$\phi = L\sqrt{(k_v / D_{eff})} \qquad (7.3\text{-}1)$$

$$\eta = \frac{\tanh \phi}{\phi} \qquad (7.3\text{-}2)$$

where L = the thickness of the flat plate

k_v = the intrinsic rate constant per unit volume of catalyst

D_{eff} = the effective diffusion coefficient within the catalyst

It should be noted that the Thiele modulus and, hence, the effectiveness factor is a function of temperature. In general, the larger the temperature the greater the reaction rate. The rate of reaction is an exponential function of temperature, whereas the rate of diffusion in fine pores is proportional to the square root of the absolute temperature. This leads to a decrease in the effectiveness factor as the temperature increases. Therefore, the most severe mass transfer limitations occur at the highest reaction temperature.

The internal mass transfer effect was investigated using three different thicknesses of 10%Pt/FC28 powder on the ceramic sphere support. The three catalysts were prepared using the procedure described in Chapter 2. For the purpose of discussion, the catalyst with the thickest active phase layer will be designated as Catalyst X. Catalyst Y has the active phase with the intermediate thickness and Catalyst Z has the thinnest active phase

layer. The calculation of the thickness of the active phase layer, the Thiele modulus, and the effectiveness factor for each catalyst is shown in Appendix E. A flat plate geometry was used to calculate the effectiveness factor because the thickness of the active phase layer for the three catalysts is small compared to the radius of curvature of the ceramic sphere. Table 7.1 shows the results obtained in Appendix E. From Table 7.1, the effectiveness factor for Catalyst X is 0.876. Theory predicts that there will be an internal mass transfer limitation for this catalyst. Catalyst Y and Z have effectiveness factors of 0.989 and 1.000 respectively. It is expected that these catalysts will be free of any internal mass transfer limitations.

The presence of internal mass transfer limitations can affect the value of the activation energy determined from experiments. Satterfield[7] discusses the effect of mass transfer limitations on the observed kinetics of reactions. In the mass transfer controlled regime, the observed activation energy can be half that of the actual activation energy. Figure 7.7 shows the Arrhenius plot for Catalysts X, Y, and Z. Table 7.1 shows the activation energy determine from Figure 7.7. The method used to experimentally determine the activation energy is given in Section 7.4. Catalyst X has an activation energy of 22.2 kJ/mol where as Catalyst Y and Z have activation energies of 42.8 and 37.8 kJ/mol respectively. The error shown for the activation energy in Table 7.1 is from the error in the linear regression analysis of the Arrhenius plot. The activation energy for Catalysts Y and Z is similar; however, the activation energy for Catalyst X is approximately half that of the other two. This indicates that Catalyst X is in the internally mass transfer controlled regime. The theoretical calculations predicted that Catalyst X would be mass transfer limited.

Many studies have used the supported fluorinated carbon catalysts.[8-10] No study to date has investigated the effect of the active phase layer thickness. From the above experiments, it is seen that a thickness of the active phase layer has a great effect on the overall kinetics of the reaction. To maximize the effective use of platinum on these type

Table 7.1 Effect of Active Layer Thickness

Catalyst	Platinum Loading (wt%)	Active Phase Thickness (cm)	Effectiveness Factor (η)	Activation Energy (kJ/mol)
X	0.0340	0.01018	0.876	22.2±1.6
Y	0.0094	0.00284	0.989	42.8±1.1
Z	0.0023	0.00070	1.000	37.8±2.1

Figure 7.7 Arrhenius Plot for Various Thicknesses of the Active Phase Layer

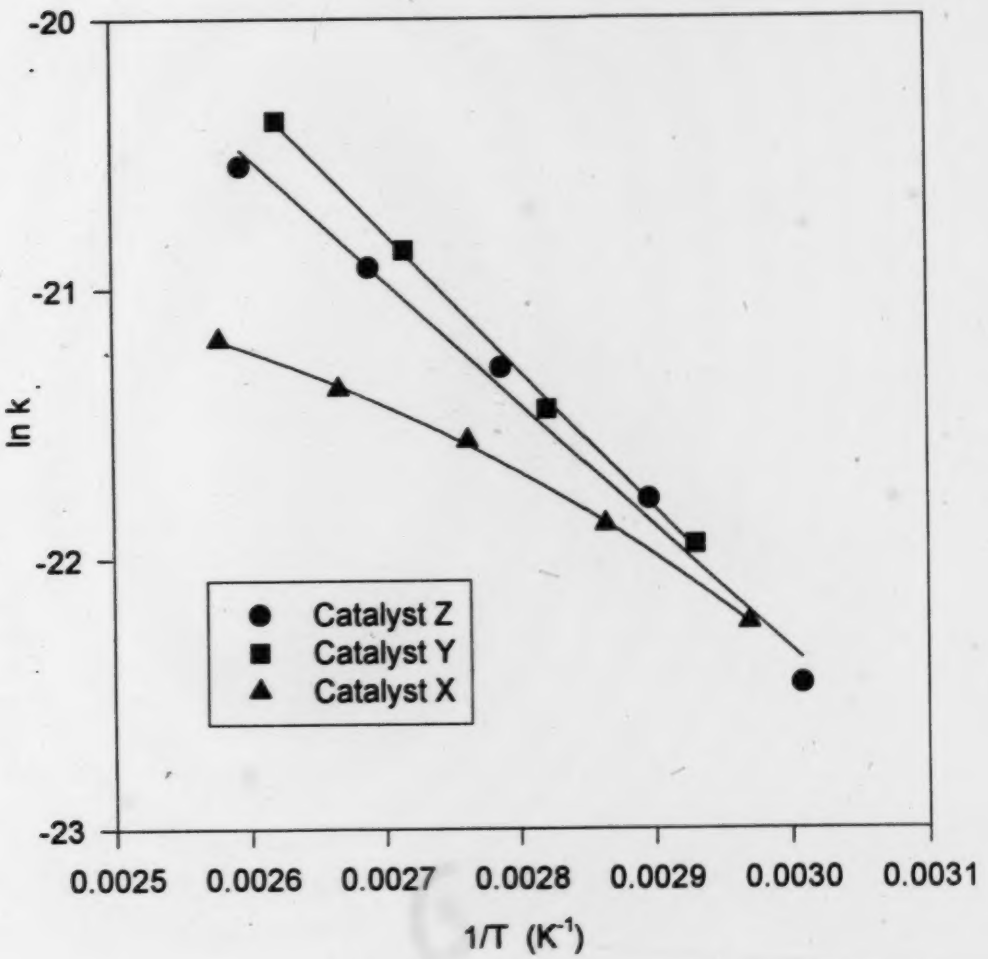

of catalysts, it is important to consider the internal mass transfer effect. The theoretical determination of the effectiveness factor gave a good estimate of the mass transfer effects in this study. It is recommended that the theory be used to estimate the maximum thickness of the active phase layer for future studies on different reactions.

7.4 EVALUATION OF THE KINETIC PARAMETERS

The method used to evaluate the kinetic parameters of a rate equation depends on the form of the equation. For the rate equation developed in Chapter 5, in dry feed conditions, the following method was used to evaluate the order of reaction and the activation energy.

$$-r_{CH_3OH} = kP_{CH_3OH}^{\alpha} \qquad (7.4\text{-}1)$$

Taking the logarithm of both sides,

$$\ln\left(-r_{CH_3OH}\right) = \ln k + \alpha \ln P_{CH_3OH} \qquad (7.4\text{-}2)$$

The order of reaction (α) can be evaluated from the slope of a plot of $\ln r$ versus $\ln P$. The rate constant k is a function of temperature and can be represented by the Arrhenius equation.

$$k = Ae^{\left(\frac{-E}{RT}\right)} \qquad (7.4\text{-}3)$$

Taking the logarithm of both sides,

$$\ln k = \frac{-E}{RT} + \ln A \qquad (7.4\text{-}4)$$

The activation energy (E) and the pre-exponential factor (A) can be evaluated from an Arrhenius plot of $\ln k$ versus $1/T$.

Three different concentrations of methanol were used at each different temperature to evaluate the order of reaction and the $\ln k$ value of the rate equation. Temperatures between 33 °C and 112 °C were used to evaluate the activation energy and the pre-

exponential factor. The kinetic experiments were performed on the catalysts after they were deemed stable by the experiments shown in Section 7.2.

The Berty reactor is modeled similar to a continuous stirred tank reactor. The methanol concentration at the catalyst surface is the same as the exit concentration of methanol because the gas phase in the reactor is homogeneous. The rate of disappearance of methanol ($-r_{CH_3OH}$) is calculated using Equation 7.4-5.

$$-r_{CH_3OH} = \frac{\left[\left(C_{CH_3OH}\right)_{in} - \left(C_{CH_3OH}\right)_{out}\right]}{\left(W \times A_s\right)} \times F_T \qquad (7.4\text{-}5)$$

where C_{CH_3OH} = the concentration of methanol (mol/cm^3)

F_T = the total flowrate through the reactor (cm^3/s)

W = the mass of catalyst in the reactor (g)

A_s = the surface area of Pt per mass of catalyst (cm^2 Pt /g)

Figures 7.8 to 7.10 show the Arrhenius plot for the Pt /FC10, Pt/FC65 and Pt/Al_2O_3 catalysts respectively. Table 7.2 summarizes the pre-exponential factor, the activation energy, and the order of reaction for the four types of catalysts tested. The Pt/Al_2O_3 catalyst has an activation energy of 28.3 kJ/mol which is similar to the activation energy found over a platinum wire catalyst by McCabe and McCready[1] (30±5 kJ/mol) and Gentry et al.[11] (33±5 kJ/mol). This indicates that the platinum active sites on the alumina catalyst are the same as that found on the platinum wire. The activation energy of the three fluorinated carbon catalysts increases with increasing degree of fluorination. The Pt/FC10, Pt/FC28, and Pt/FC65 catalysts have activation energies of 19.0, 37.8, and 50.8 kJ/mol respectively. The Pt/FC10 catalyst has an activation energy much lower than the rest of the catalysts. Low activation energies are an indication of mass transfer limitations. The lower activation energy does not of itself prove that a mass transfer limitation exists. As seen from the Pt/FC28 and Pt/FC65 catalysts, the amount of fluoride on the support

Figure 7.8 Arrhenius Plot for Pt/FC10 Catalyst

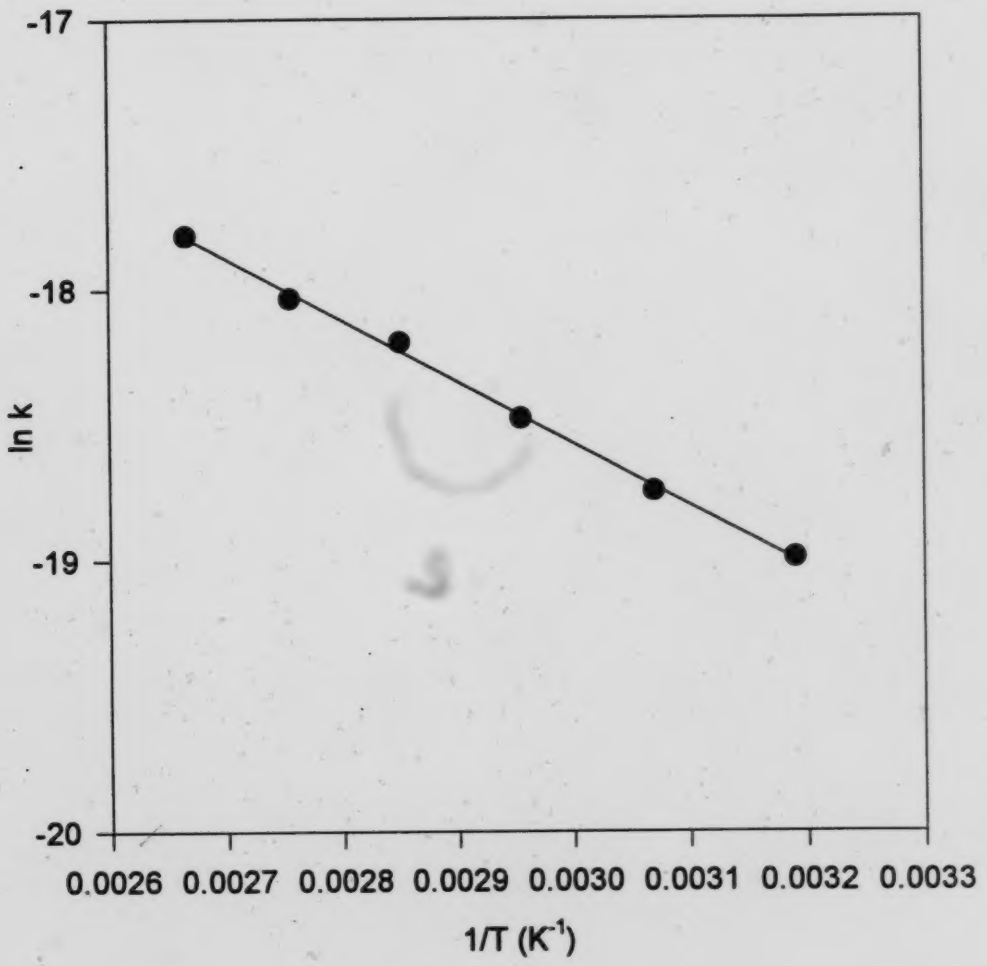

Figure 7.9 Arrhenius Plot for Pt/FC65 Catalyst

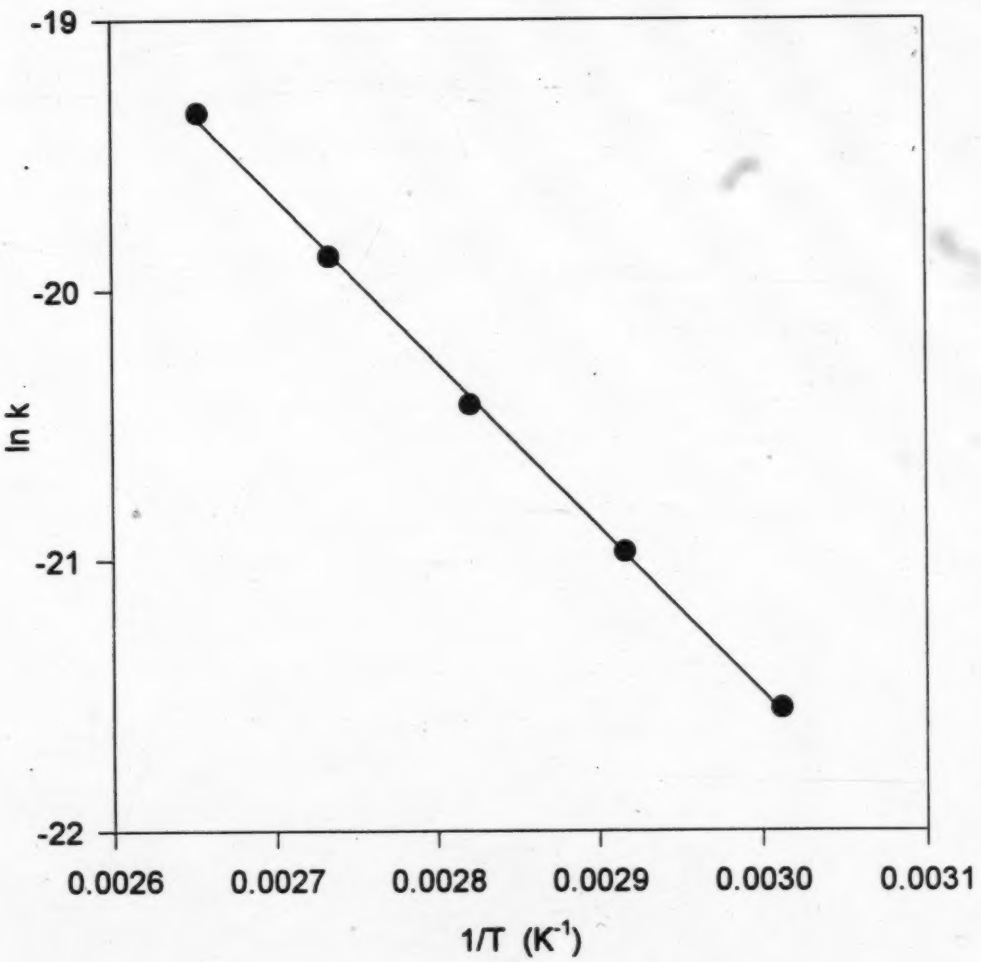

Figure 7.10 Arrhenius Plot for Pt/Al_2O_3 Catalyst

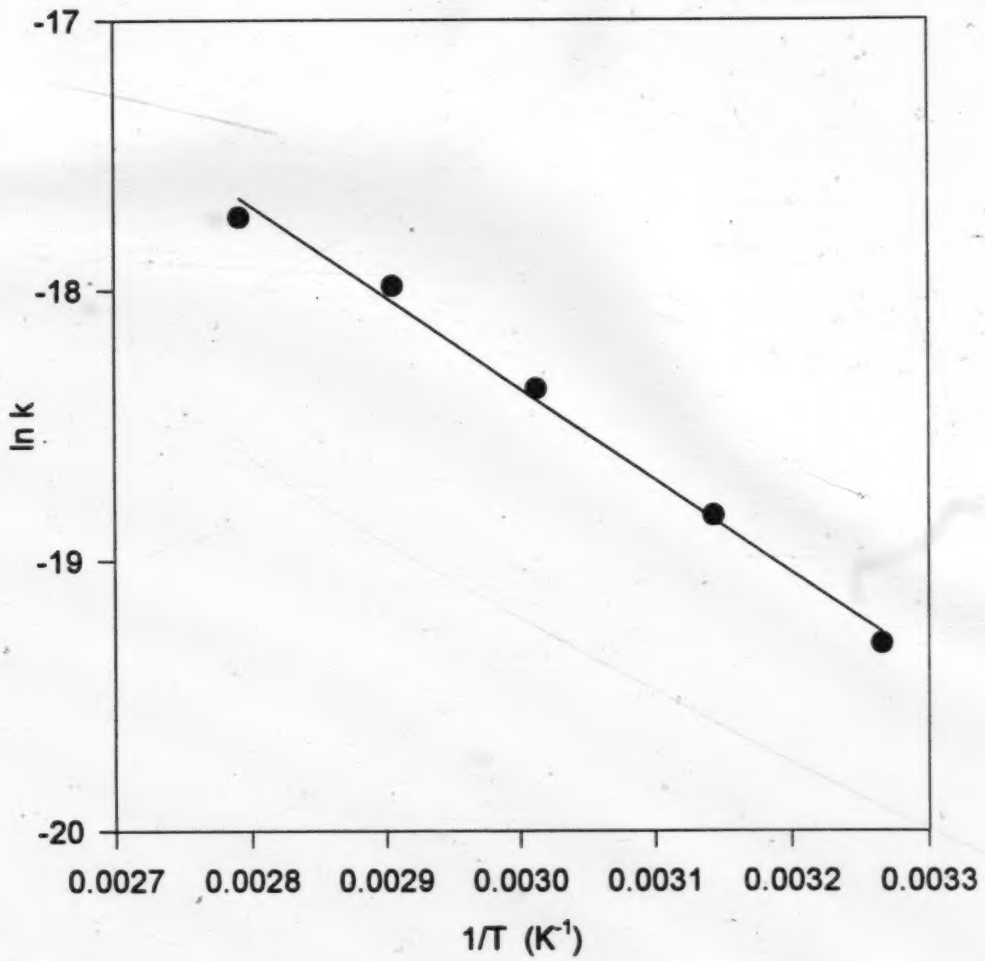

Table 7.2 Results of the Kinetic Study on Various Catalysts

Catalyst	Platinum Loading (wt%)	Pre-exponential Factor (A) (mol/cm² Pt·s·mmHg)	Activation Energy (E) (kJ/mol)	Average Order of Reaction (α)
Pt/Al_2O_3	0.0028	2.830×10^{-4}	28.3±1.4	0.82
Pt/FC10	0.0061	8.216×10^{-6}	19.0±0.4	0.83
Pt/FC28	0.0023	1.697×10^{-4}	37.8±2.1	0.94
Pt/FC65	0.0026	4.325×10^{-2}	50.8±0.7	0.81

affects the activation energy of the catalyst significantly. It is possible the true activation energy for Pt/FC10 is 19.0 kJ/mol. However, the reaction rate for the Pt/FC10 catalyst is an order of magnitude larger than the Pt/FC28 and Pt/FC65 catalysts. A comparison of the rates is discussed latter in this section. The higher reaction rate on the Pt/FC10 catalyst can cause a decrease in the effectiveness factor, shifting the reaction into the transition region between the kinetically controlled and mass transfer controlled regimes. Calculation of the effectiveness factor, for the Pt/FC10 catalyst, resulted in a value of 0.9. Satterfield[7] shows that a reaction is influenced by mass transfer at this point. The nature of the support and the influence of mass transfer is, therefore, considered to be the reason for the low activation energy for the Pt/FC10 catalyst.

The order of reaction (α) with respect to methanol was calculated at each temperature in the kinetic study. Appendix F shows the values of α for each catalyst. In all cases, α was found to be a function of temperature. The order of reaction shown in Table 7.2 is the averaged value obtained over the temperature range of the kinetic study. The reaction order is similar for all four catalysts. The reason for the temperature dependence of α is that the mechanism for the oxidation of methanol is changing over the temperature range of the kinetic study. Table 7.3 shows the order of reaction as a function of temperature for the Pt/FC28 catalyst over the entire range of temperatures tested. At temperatures above 112 °C, the order of reaction is stable at approximately 1.2. This can be explained by looking at the selectivity of the reaction as a function of temperature. Figures for the selectivity versus temperature are shown in the next section. At this point, it is sufficient to say that at temperatures below 112 °C the reaction mechanism shifts causing a dramatic change in selectivity. At temperatures above 112 °C the change in selectivity is less dramatic. The average order of reaction for Pt/FC28 over the entire temperature range studied (60-210 °C) is 1.07 (i.e. first order reaction).

Table 7.3 Reaction Order as a Function of Temperature for Pt/FC28

Temperature (°C)	Reaction Order (α)
59.2	0.68
72.1	0.87
85.5	0.93
98.6	1.04
112.2	1.18
124.0	1.18
136.6	1.22
162.0	1.24
187.1	1.20
210.7	1.20

As mentioned above, the reaction rate for the Pt/FC10 catalyst is an order of magnitude greater than that of the Pt/FC28 and Pt/FC65 catalysts. The Pt/Al_2O_3 catalyst has a reaction rate on the same order of magnitude as that of the Pt/FC10 catalyst. Figure 7.11 shows the rate of reaction versus temperature for the three fluorinated carbon catalysts. The pre-exponential factor (A) shown in Table 7.2 is somewhat misleading. Since the Pt/FC10 catalyst has a much higher rate of reaction, the pre-exponential factor for the Pt/FC10 catalyst is expected to be larger than that for the Pt/FC28 and Pt/FC65 catalysts. This, however, is not the case because of the differences in the activation energy of the three catalysts. As the Arrhenius plot is extrapolated to higher temperatures, in order to obtain the value of the pre-exponential factor, the curves for the individual catalysts cross because of the differences in the slope (i.e. the activation energies).

The rate of reaction for the overall methanol conversion is given by,

$$-r_{CH_3OH} = Ae^{(-E/RT)}P^{a}_{CH_3OH}$$

The rate, as defined in this study, has the units of mol/cm² Pt·s. The kinetic study was performed over the same range of temperatures and methanol concentrations for each catalyst. Yet, the rate of reaction for the Pt/FC10 and Pt/Al_2O_3 catalysts is an order of magnitude greater than that for the Pt/FC28 and Pt/FC65 catalysts. Recall that the platinum surface area used to calculate the rate of reaction was found using the dispersion results from the XRD data. The XRD data showed that the platinum dispersion was similar for each of the catalysts. However, the chemisorption tests showed that the Pt/FC28 and Pt/FC65 catalysts had a much lower hydrogen adsorption capacity than that of the Pt/FC10 and Pt/Al_2O_3 catalysts (see Table 3.2). This was attributed to platinum-

Figure 7.11 Reaction Rate vs Temperature for the Fluorinated Carbon Catalysts

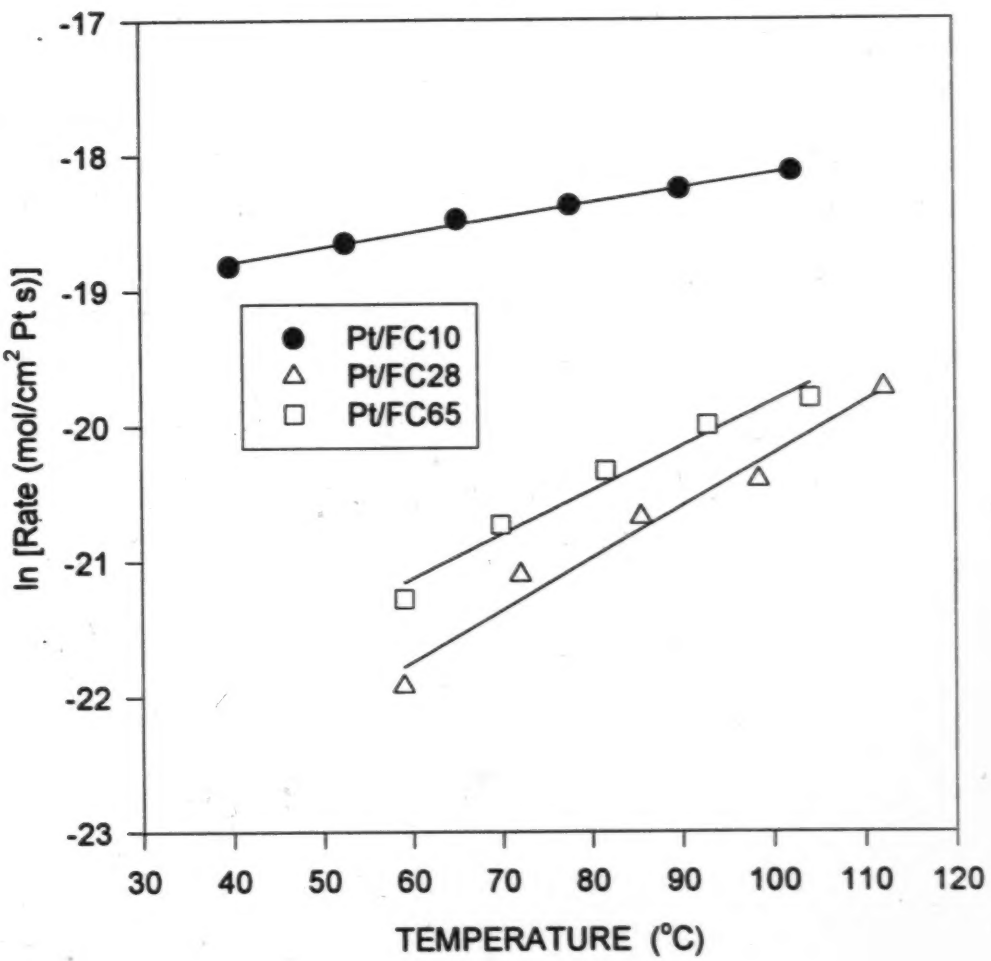

fluoride interactions in Chapter 3. The connection between the lower hydrogen adsorption capacity and the lower reaction rate, suggests that the increased fluorination of the support does cause an increase in the metal-support interaction. It is postulated that the fluoride on the catalyst support blocks or distorts the surface electronic properties of the platinum leading to poor hydrogen adsorption and low activity. The results reported by Simone et al.[12] strongly suggest that localized site blockage and/or inductive effects are responsible for poor performance of chloride containing palladium/alumina catalysts for the oxidation of methane. Simone et al.[12] verified that Pd/Al_2O_3 catalysts prepared from $PdCl_2$ were considerably less active for the oxidation of methane than catalysts prepared from $Pd(NO_3)_2$. These authors observed a significant improvement in the activity of the catalysts prepared from $PdCl_2$ after long term aging at 600 °C in air. The aging process removed 96% of the chloride from the catalyst. Simone et al.[12] concluded that the chloride has a strong negative effect on the activity. Marécot et al.[13] also describe similar halogen-metal interactions on platinum/alumina catalysts used for the oxidation of propane and propene. These authors also show that the removal of chloride from the catalyst increase the activity. In Chapter 3, it was shown that heating the Pt/FC28 catalyst to 500 °C in nitrogen removes fluoride. To observe the effect of fluoride on the methanol oxidation rate, the Pt/FC28 catalyst was heated to 500 °C for 3 hours in 100 mL/min flowing nitrogen. The catalysts was then calcined at 300 °C for 3 hours in 100 mL/min flowing air similar to the calcination step described in Chapter 2. XRD experiments showed that there was no change in the platinum dispersion after the heat treatment. Figure 7.12 shows the effect of fluoride removal on the Pt/FC28 catalysts. The activity of the Pt/FC28 catalyst after heat treatment is increased by an order of magnitude. The rate of reaction is similar to that of the Pt/FC10 catalyst. The results of the present work emphasize the strong negative effect of fluoride on the activity of these highly fluorinated carbon catalysts.

Figure 7.12 Comparison of Heat Treated Pt/FC28 to Pt/FC10 and Regular Pt/FC28

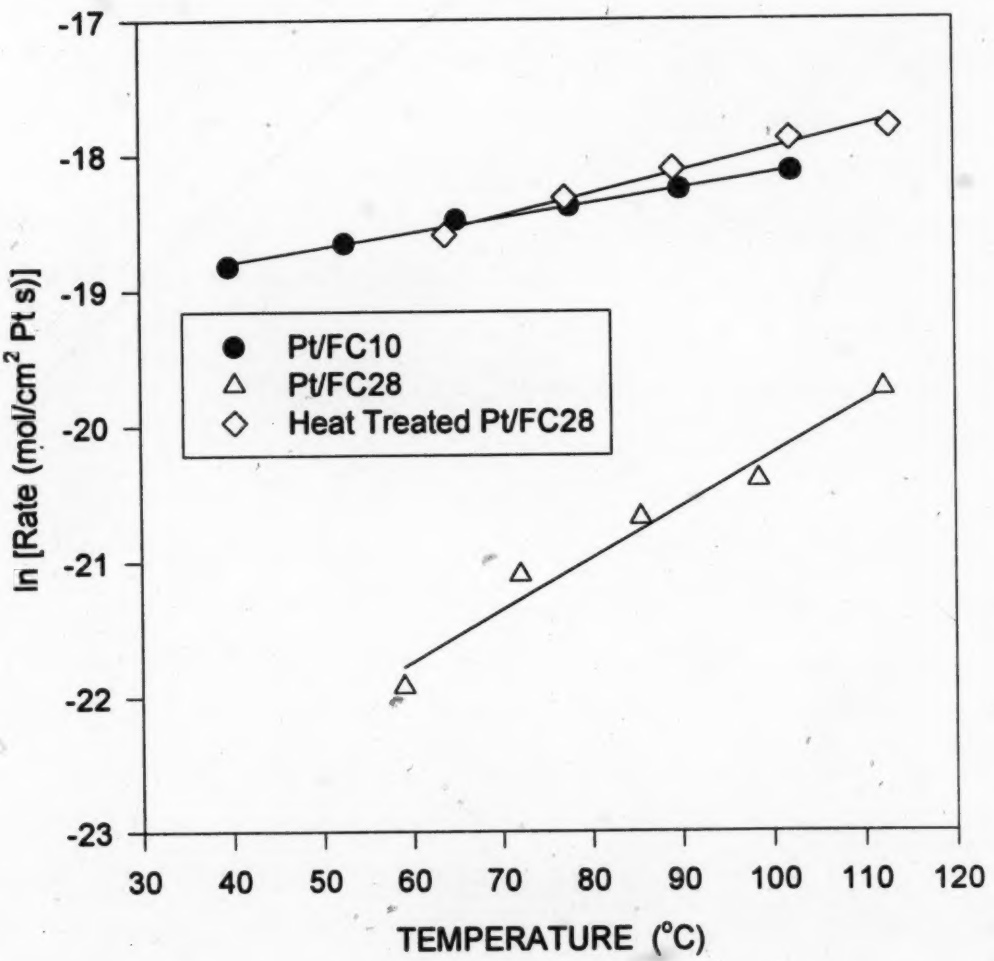

7.5 SELECTIVITY OF THE METHANOL OXIDATION REACTION

The only carbon containing products of methanol oxidation under the reaction conditions tested (i.e. excess oxygen) were carbon dioxide, methyl formate, and formaldehyde. Figures 7.13 to 7.16 show the product selectivity for the Pt/FC10, Pt/FC28, Pt/FC65, and Pt/Al_2O_3 catalysts respectively. For each catalyst there is an increase in the selectivity towards methyl formate as the temperature decreases. Based on the mechanism proposed in Chapter 5, this suggests a higher amount of adsorbed formaldehyde species on the surface of the platinum. As the temperature increases, the desorption rate of formaldehyde increases, as well as, the oxidation rate of adsorbed formaldehyde to carbon dioxide. The increase in the rate of these two mechanisms dramatically reduces the formation of methyl formate. With higher rates of formaldehyde desorption and oxidation, there is a decrease in the amount of adsorbed formaldehyde on the catalyst surface. Since the formation of methyl formate is dependent on the interaction of the two adsorbed formaldehyde species, there is a decrease in the amount of methyl formate produced as the temperature is increased. The production of formaldehyde goes through a maximum as the temperature is increased. This is caused by the competing effects of the formaldehyde desorption and oxidation processes. The rate of oxidation may increase more rapidly with temperature than the rate of desorption. Eventually, the oxidation rate surpasses the desorption rate and the formaldehyde selectivity decreases. The maximum in the formaldehyde selectivity occurs between 80 and 115 °C for all the catalysts tested. McCabe and McCready[1], Hodges and Roselaar[2] and Gentry et al.[11] reported a maximum in the formaldehyde yield at 192, 210 and 92 °C respectively, over platinum wire catalysts. All three studies report formaldehyde selectivity at less than 10%. Yao[14] observed a maximum in the formaldehyde yield at a temperature of 115 °C over a Pt/Al_2O_3 catalyst. The maximum selectivity of formaldehyde in his study was 23%. This agrees well with the Pt/Al_2O_3 results shown in Figure 7.16, in which, the maximum formaldehyde selectivity is 23% at a temperature of 106 °C. The maximum formaldehyde

Figure 7.13 Selectivity versus Temperature for Pt/FC10 Catalyst

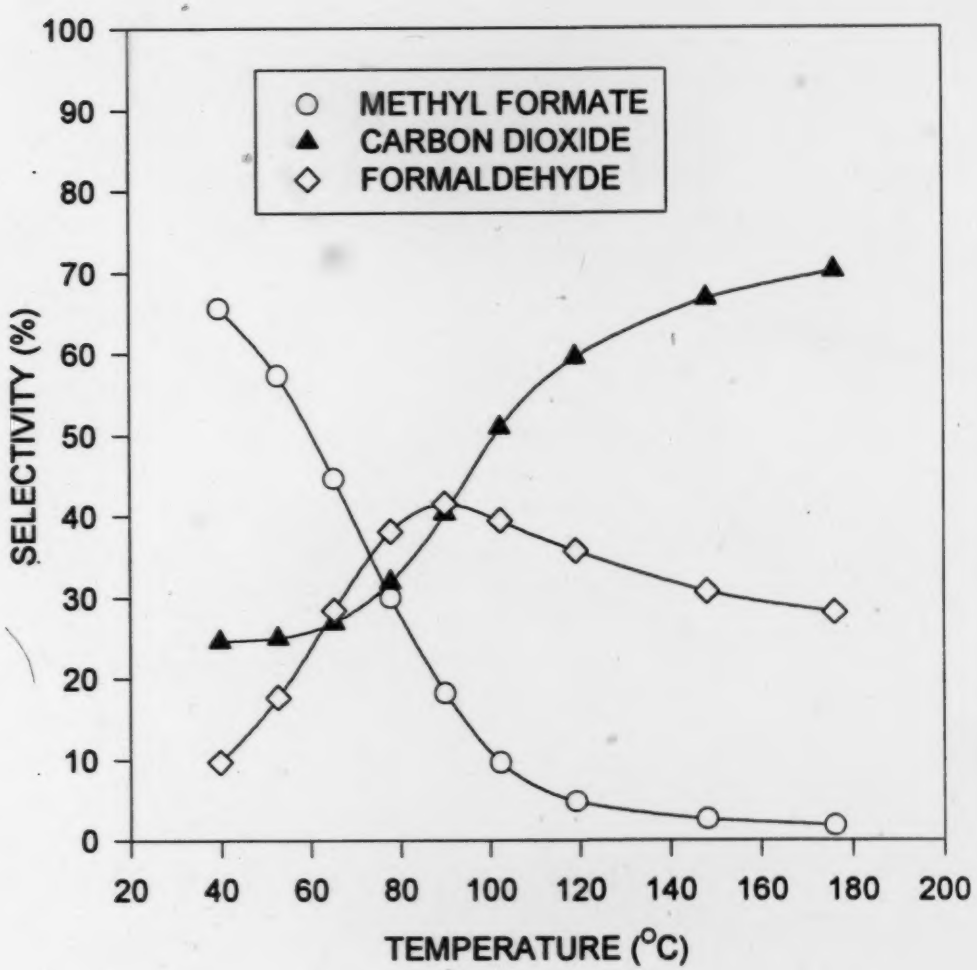

Figure 7.14 Selectivity versus Temperature for Pt/FC28 Catalyst

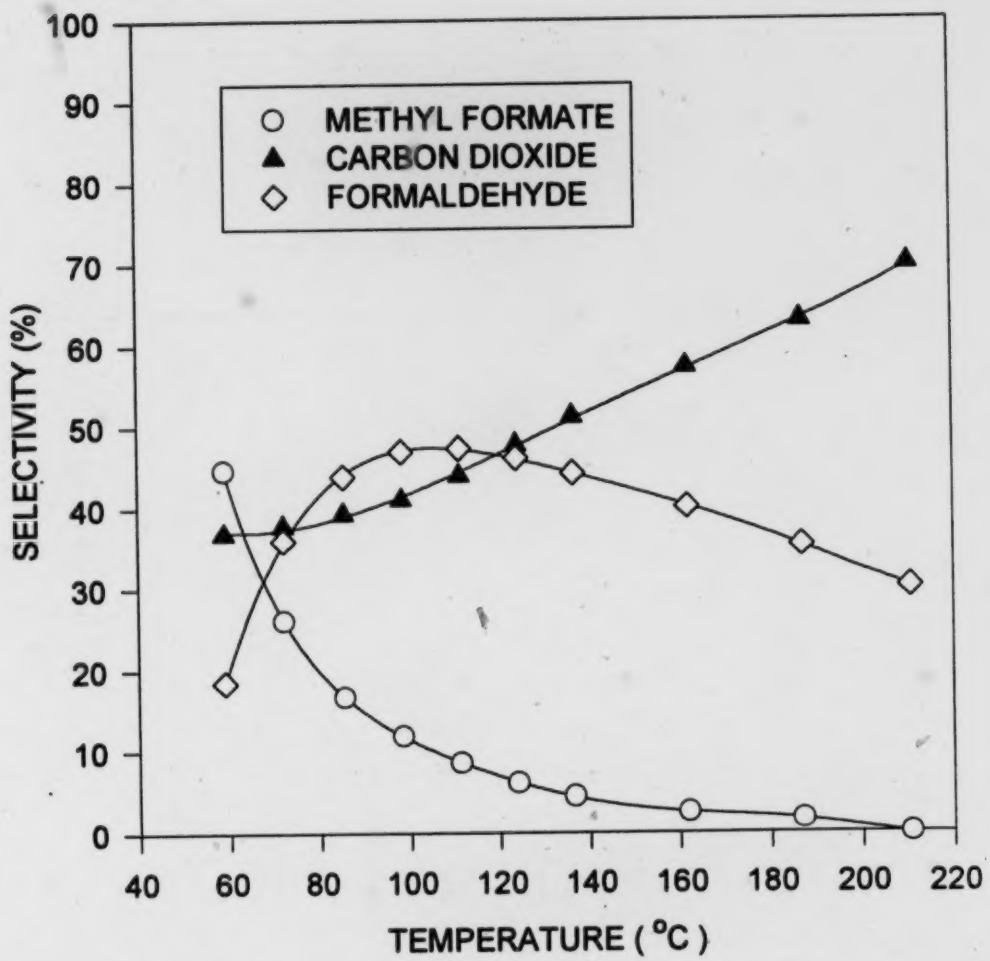

Figure 7.15 Selectivity versus Temperature for Pt/FC65 Catalyst

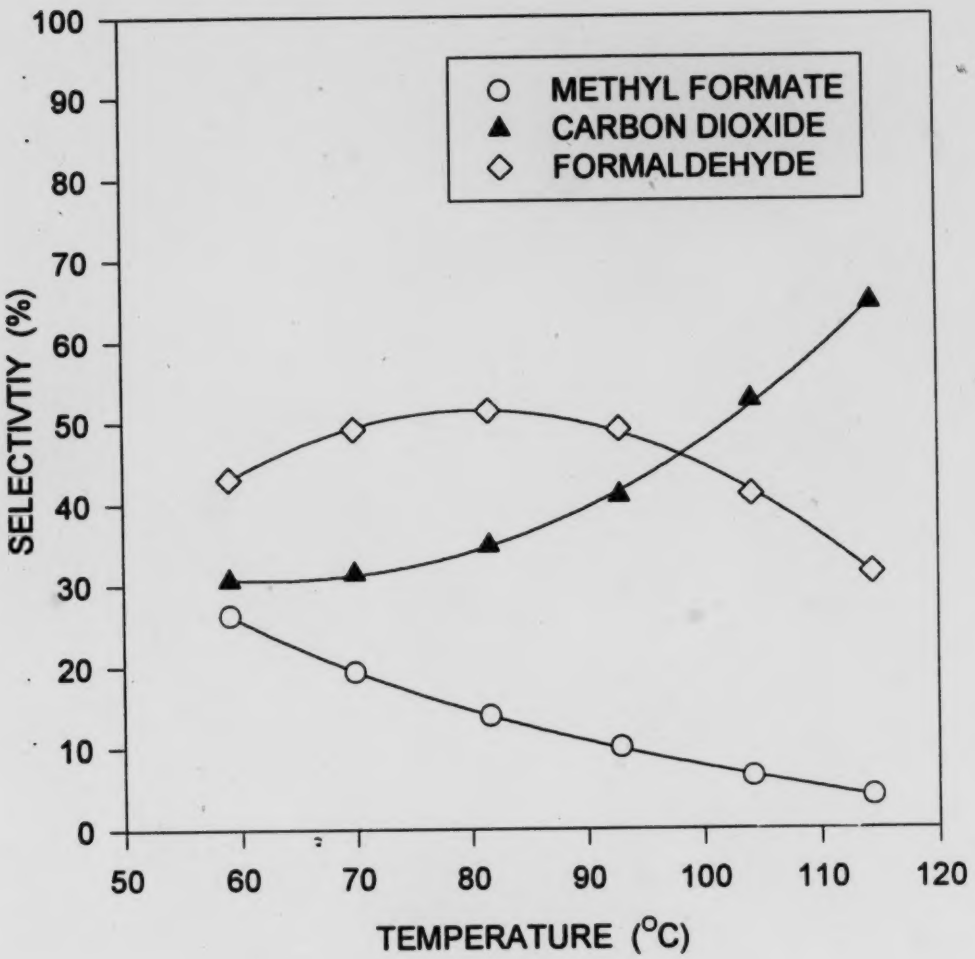

Figure 7.16 Selectivity versus Temperature for Pt/Al_2O_3 Catalyst

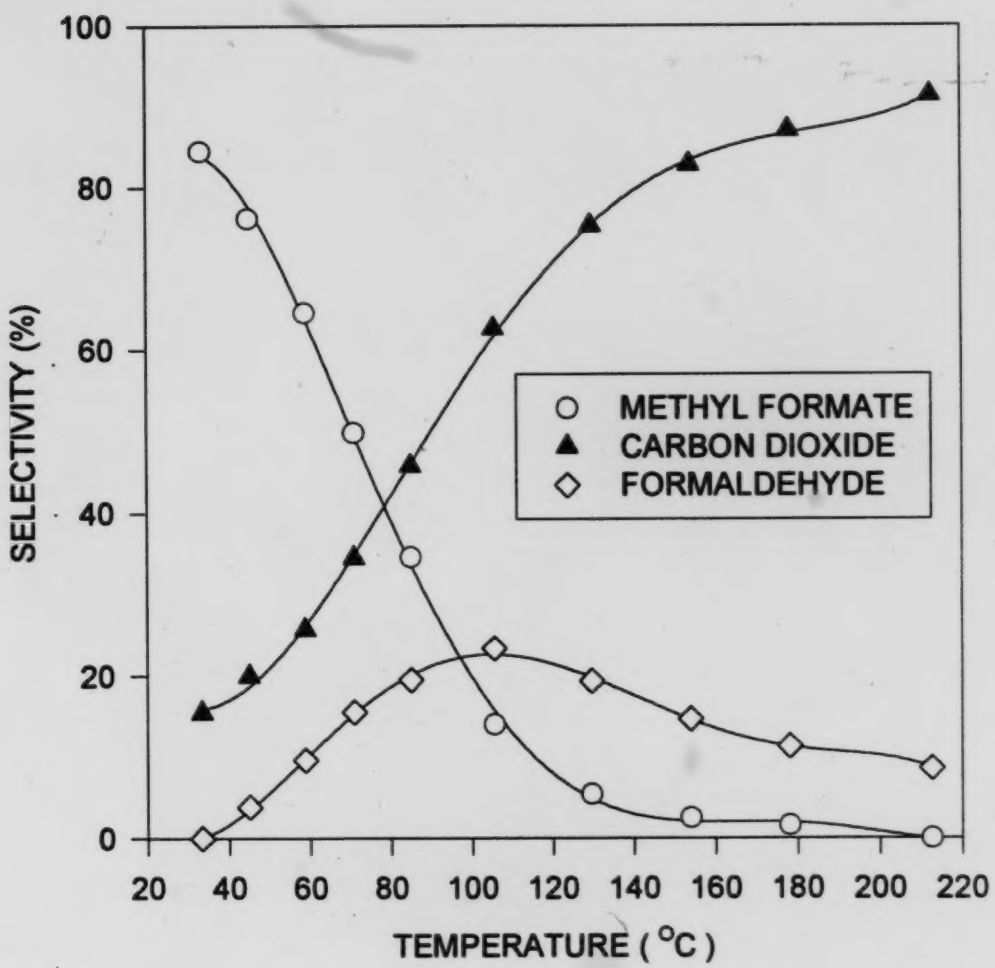

selectivity over the Pt/FC10, Pt/FC28, and Pt/FC65 catalysts is 42, 47, and 51% respectively. The selectivity towards formaldehyde is much lower on the Pt/Al_2O_3 catalyst than on the Pt/FC catalysts. This indicates that the formaldehyde is more tightly bound to the platinum on the Pt/Al_2O_3 catalyst than on the hydrophobic catalysts. The Pt/Al_2O_3 catalyst also has the largest selectivity for methyl formate at low temperatures. With the low desorption rate of formaldehyde, there is more opportunity to form methyl formate. Figures 7.13 to 7.16 show that the amount of fluoride on the catalyst support affect the maximum selectivity of formaldehyde. The presence of fluoride appears to weaken the formaldehyde-platinum bond which is another indication of possible fluoride-platinum interactions. As the temperature is increased above 115 °C, the selectivity towards formaldehyde decreases. This indicates that the oxidation rate of adsorbed formaldehyde increases more rapidly than the desorption rate. As the temperature is increased further, carbon dioxide becomes the main product of the oxidation reaction. From Figure 7.16, it appears that the Pt/Al_2O_3 catalyst must be operated at above 250 °C in order to achieve complete oxidation of methanol at the levels required for an emissions catalyst. The hydrophobic catalysts, in most probability, would have to be operated at temperatures above 300 °C in order to achieve greater than 95% selectivity to carbon dioxide. These temperatures are estimates based on the data shown in Figures 7.13 to 7.16. No experimental data were obtained at temperatures above 220 °C in this study. The next chapter investigates the effect of water vapor in the feed stream on the activity of the catalysts.

7.6 REFERENCES

1. McCabe, R. W., and D. F. McCready, *J. Phys. Chem.*, **1986**, 90, 1428.
2. Hodges, C.N., and L.C. Roselaar, *J. Appl. Chem. Biotechnol.*, **1975**, 25, 609.
3. Lefferts, L., J. G. van Ommen, J. R. H. Ross, *J. Chem. Soc. Faraday Trans. 1.*, **1988**, 84, (5), 1491.
4. Lefferts, L., J. G. van Ommen, J. R. H. Ross, *Appl. Catal.*, **1986**, 23, 385.
5. Lefferts, L., J. G. van Ommen, J. R. H. Ross, *Appl. Catal.*, **1987**, 31, 291.
6. Kurina, L. N., L. I. Novozhenova, L. P. Orlova, L. M. Koval, T. D. Dobrynina, *Russ. J. Phys. Chem.*, **1978**, 52, 867.
7. Satterfield, C. N., "Mass Transfer in Heterogeneous Catalysis, The Colonial Press Inc., 1977.
8. Chuang, K. T., S. Chen, S. Tong, *Ind. Eng. Chem. Res.*, **1992**, 31, (11), 2466.
9. Chuang, K. T., B. Zhou, S. Tong, *Ind. Eng. Chem. Res.*, **1994**, 33, (7), 1680.
10. Cheng, S., and K. T. Chuang, *Can. J. Chem. Eng.*, **1992**, 70, (Aug.), 727.
11. Gentry, S. J., A. Jones, P. T. Walsh, *J.C.S. Faraday I*, **1980**, 76, 2084.
12. Simone, D. O., T. Kennelly, N. L. Brungard, R. J. Farrauto, *Appl. Catal.* **1991**, 70, 87.
13. Marécot, P., A. Fakche, B. Kellali, G. Mabilon, M. Prigent, J. Barbier, *Appl. Catal. B* **1994**, 3, 283.
14. Yao, Y. F., United States Patent No. 4,304,761, December 8, **1981**.

CHAPTER 8

EFFECT OF WATER ON THE METHANOL OXIDATION REACTION

8.1 INTRODUCTION

The introduction of water vapor in the feed stream to a catalytic reactor has been shown to affect the activity of catalysts in various ways as discussed in Chapter 5. The effect of water depends on the type of catalyst and the nature of the reaction under investigation. Chapter 5 describes the contradictions found in the literature on the effect of water for the oxidation of methanol over platinum catalysts. This chapter focuses on the effect of water and the mechanism for the deactivation which occurs.

8.2 CATALYST STABILITY IN WET FEED CONDITIONS

To determine the stability of the catalysts in wet feed conditions, the catalysts were first stabilized in dry conditions as shown in Chapter 7. Once the catalyst was stable, water was introduced in the feed stream and the conversion was measured as a function of time.

8.2.1 Hydrophobic Catalysts

Figures 8.1 to 8.3 show the methanol conversion versus time for both the wet and dry feed conditions over the Pt/FC10, Pt/FC28, and Pt/FC65 catalysts, respectively. The partial pressure of water for each experiment was between 1.3 and 1.7 kPa. The test conditions are shown in Appendix H along with the tabulated stability data. The presence of water vapor decreased the activity of each hydrophobic catalyst. The catalysts eventually stabilize indicating that there is no build up of water on the support as is expected for a hydrophilic catalyst. The Pt/FC10 catalyst dropped from 79% conversion in dry conditions to 57.5% conversion in wet conditions. This represents a 27.2% loss in activity. The Pt/FC28 and Pt/FC65 catalysts were affected more by the presence of water with a 56.6% and 57.8% loss in activity respectively. The larger effect of water on the highly fluorinated carbon catalysts shows that the hydrophobicity of the support is not the

Figure 8.1 Methanol Conversion vs Time for Pt/FC10 Catalyst in Wet Conditions

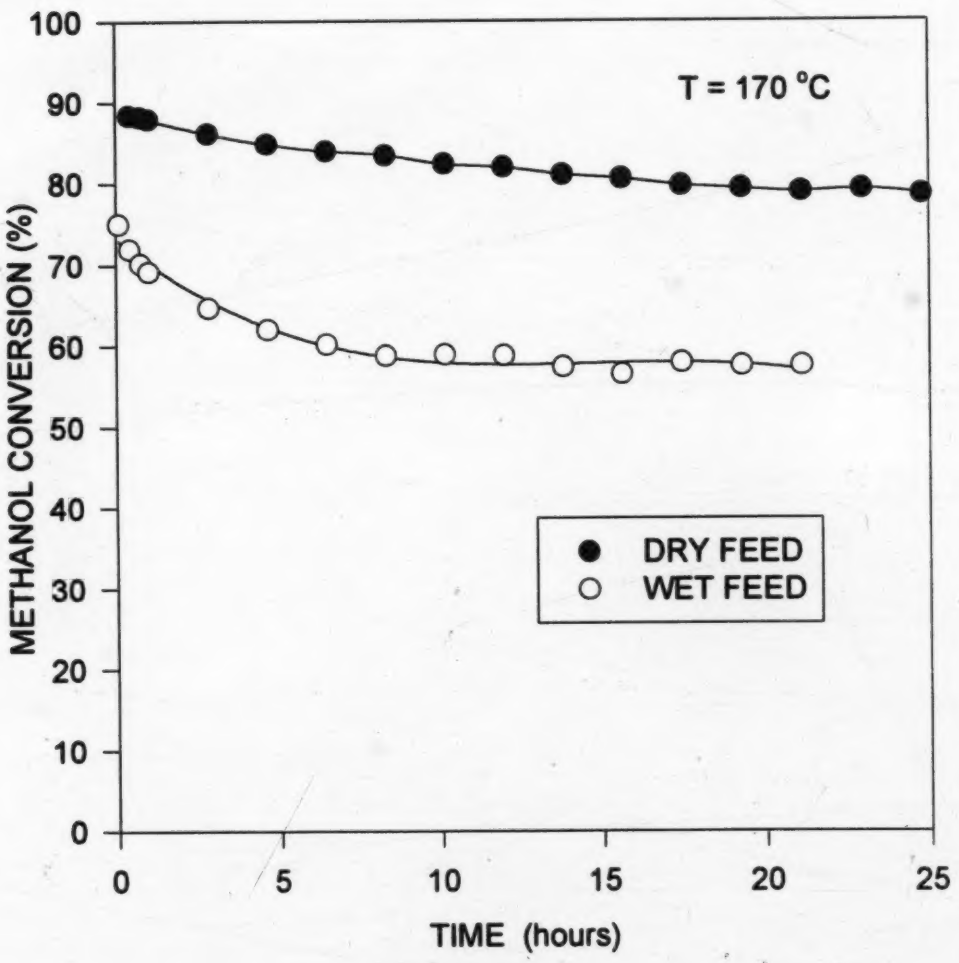

Figure 8.2 Methanol Conversion vs Time for Pt/FC28 Catalyst in Wet Conditions

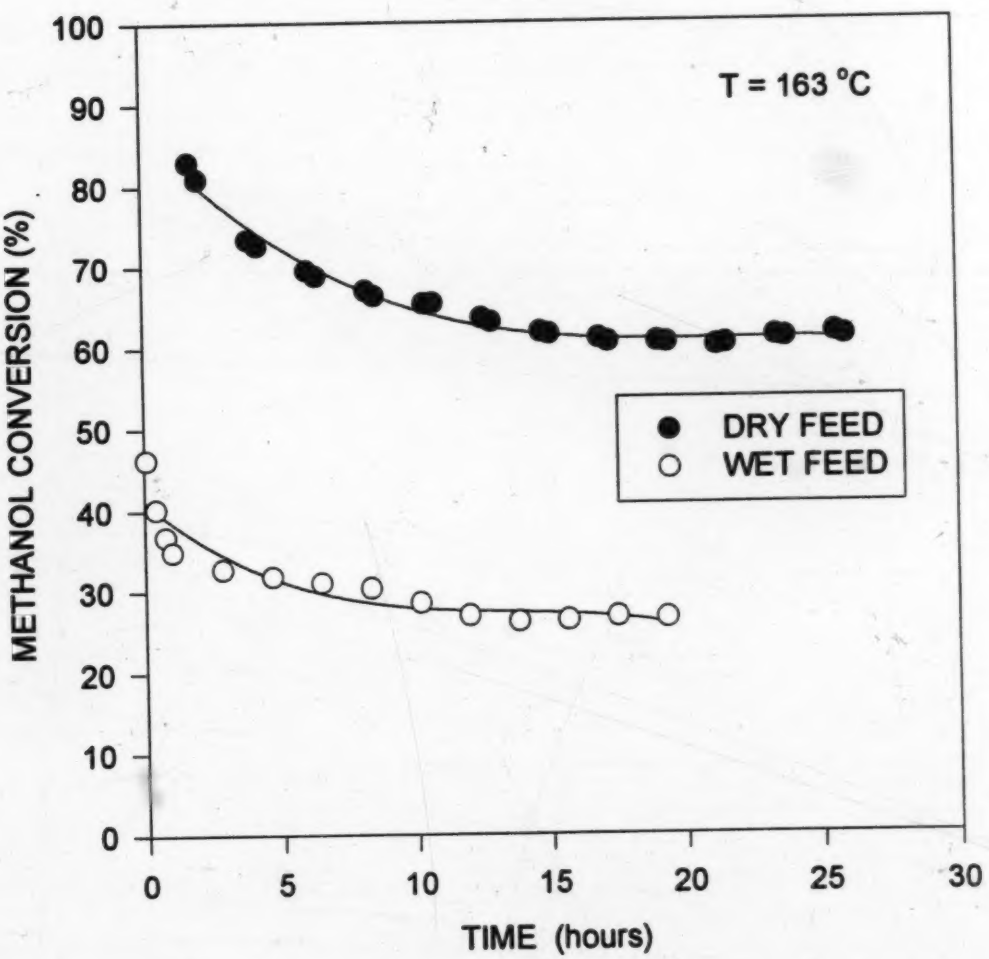

Figure 8.3 Methanol Conversion vs Time for Pt/FC65 Catalyst in Wet Conditions

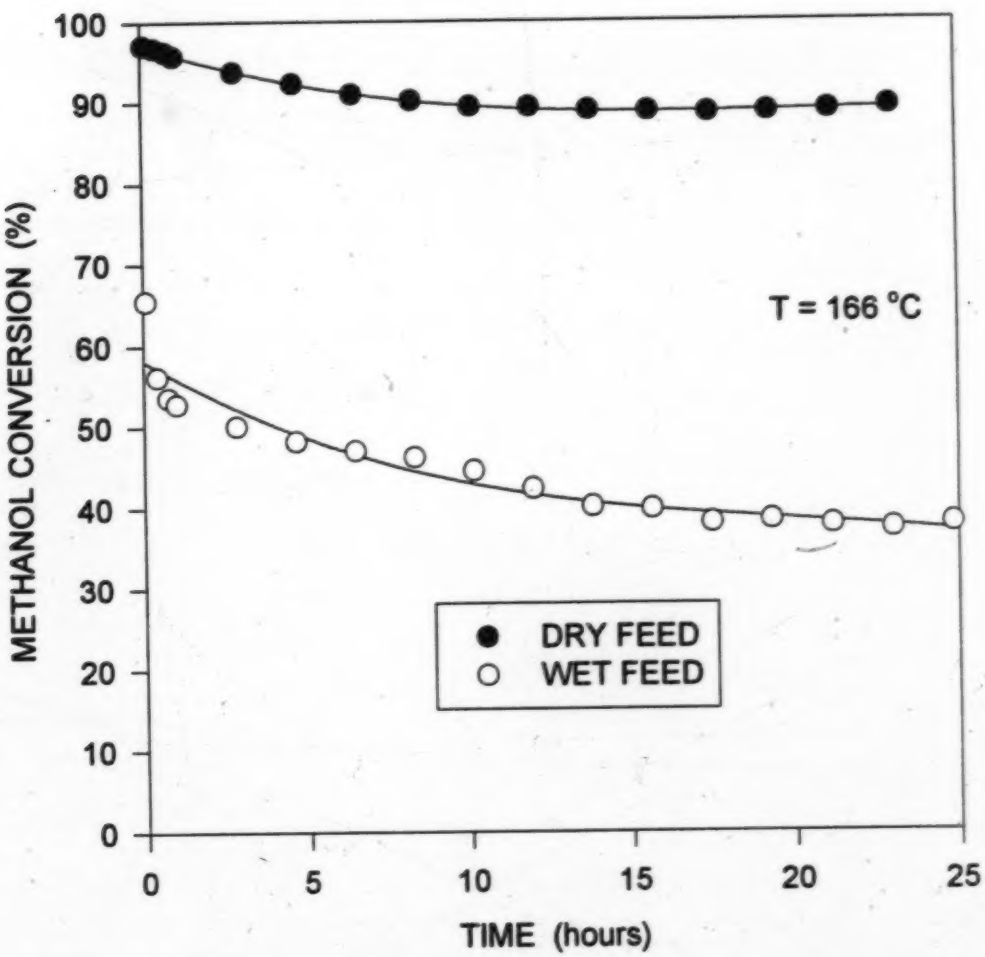

cause of the deactivation for the hydrophobic catalysts. The effect of water is caused by the interaction of water with the active sites. Recall, that the fluoride present on the Pt/FC28 and Pt/FC65 catalysts affects the platinum active sites. It appears that active sites on the highly fluorinated carbon catalysts are more susceptible to water than the active sites on the Pt/FC10 catalyst. Figure 8.4 shows the conversion of the Pt/FC10 catalyst when the feed stream is cycled between dry and wet conditions. When the feed is switched back to dry conditions, almost all of the original activity is regained. This shows that the deactivation on the Pt/FC10 catalyst, caused by the presence of water, is reversible. Figure 8.5 shows a similar plot for the Pt/FC28 catalyst in which the feed stream is cycled between dry and wet conditions. When the feed is switched back to dry conditions, the conversion increases and stabilizes. However, the conversion does not return to that found in dry conditions before the catalyst was exposed to water. This indicates that there are two mechanisms responsible for the deactivation on the highly fluorinated carbon catalysts. One mechanism of the deactivation is reversible, and assumed to be similar to the Pt/FC10 catalyst, and the other is irreversible. The reversible deactivation accounts for 30.3% of the loss in activity which is close to that observed for the Pt/FC10 catalyst (27.2%). This indicates that if the irreversible deactivation did not occur, the effect of water would be similar on all three hydrophobic catalysts. To gain some understanding of the irreversible deactivation that is occurring on the highly fluorinated carbon catalysts, experiments were performed in an attempt to regain the activity of the catalyst. The solid triangles in Figure 8.5 show that there is no significant change in activity when the catalyst is purged with air at the reaction temperature of 163 °C. The solid squares show that the catalyst can be regenerated to the level of the stabilized catalyst by purging with air at 205 °C, which is slightly higher than the temperature at which the deactivation occurred. No increase in activity was observed when helium was purged at any temperature. This indicates that the irreversible deactivation of the catalyst, caused by the presence of water vapor, is due to an adsorbed

Figure 8.4 Cyclic Behavior of the Pt/FC10 Catalyst

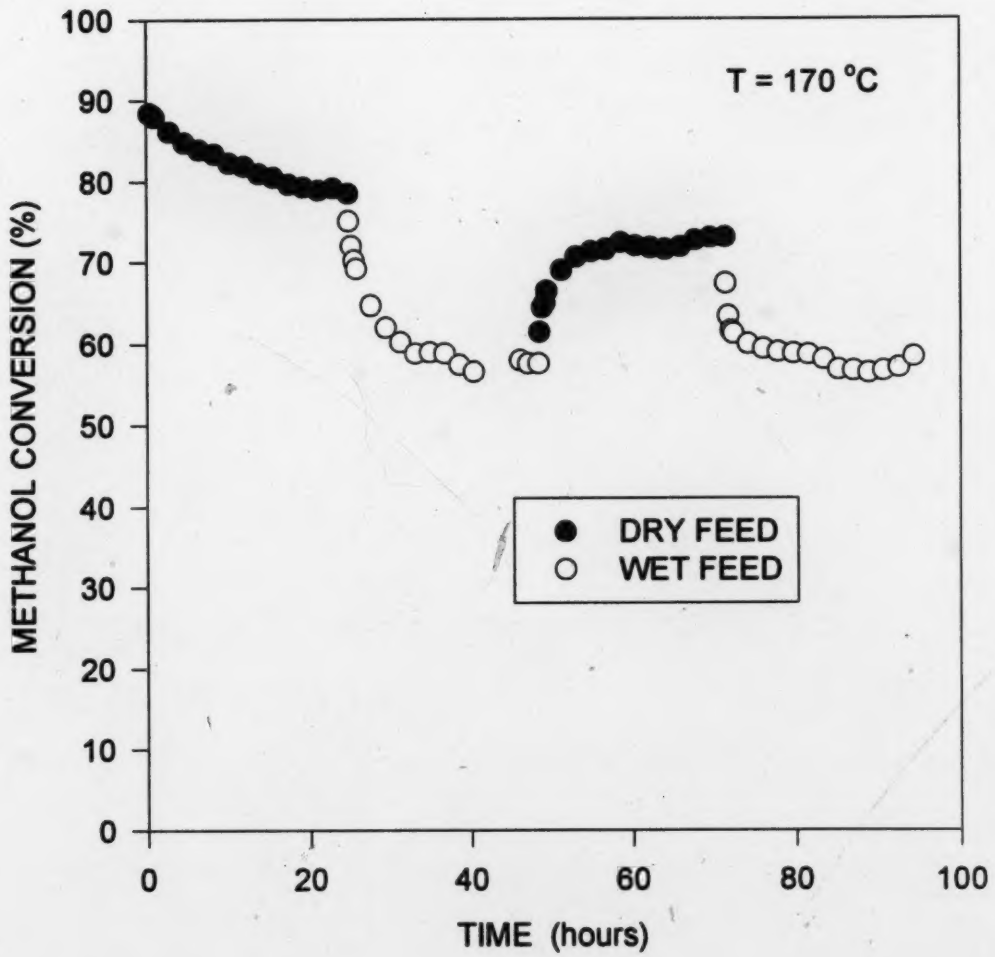

Figure 8.5 Cyclic Behavior of the Pt/FC28 Catalyst

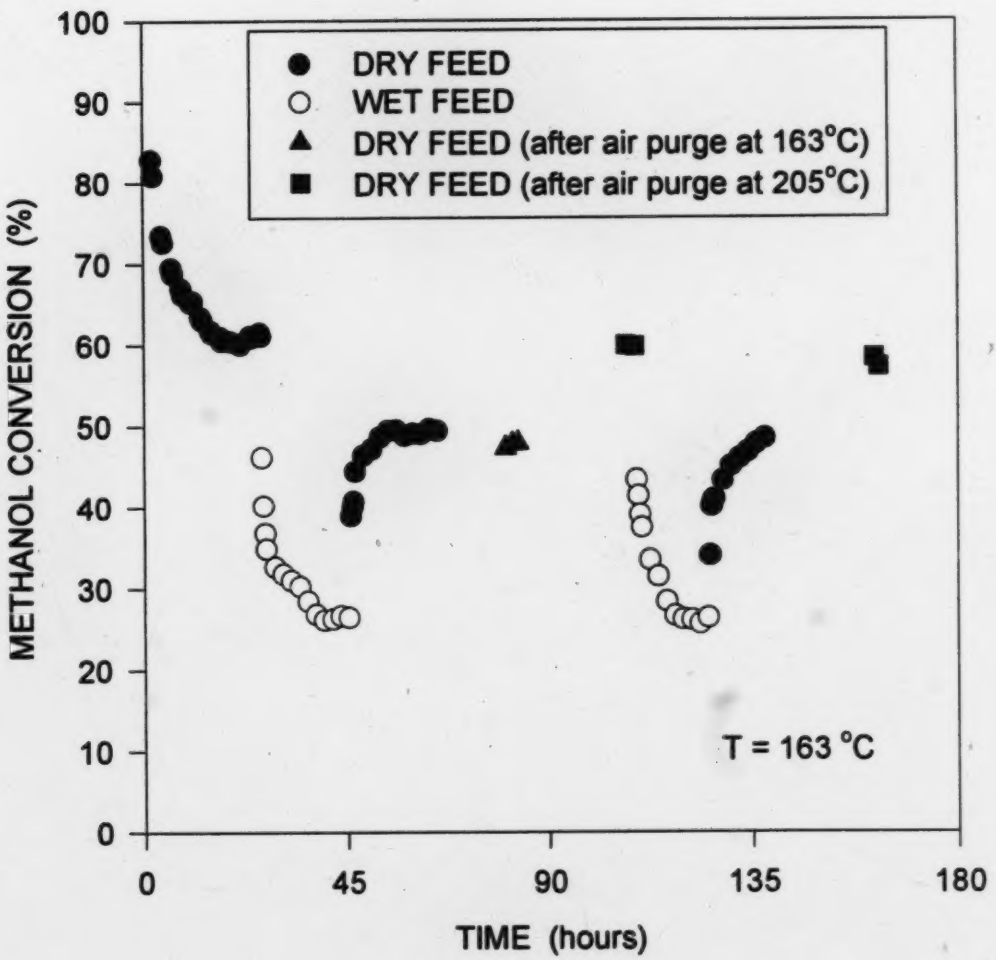

species that can be oxidized off the active sites at temperatures slightly greater than the reaction temperature. This adsorbed species must be stabilized on the active sites that are present on the highly fluorinated carbon catalysts and not on the Pt/FC10 catalyst. The fluoride-platinum interaction that exists in the Pt/FC28 and Pt/FC65 catalysts must stabilize the adsorbed species.

A new catalyst was prepared to differentiate between the effects of hydrophobicity and the presence of fluoride on the catalysts. Platinum was supported on Porapak Q which is a hydrophobic polymer material (SDB). The Porapak Q has a contact angle with water similar to the FC65. This catalyst was prepared using the methods described in Chapter 2. Figure 8.6 shows the methanol conversion versus time for the Pt/SDB catalyst when exposed to dry and wet feed conditions. The behavior of the Pt/SDB catalyst is similar to the Pt/FC10 catalyst in that the deactivation is reversible. This shows that the irreversible nature of the Pt/FC28 and Pt/FC65 catalysts is caused by the presence of fluoride.

To explain the reversible deactivation observed in wet conditions, it is useful to compare the product yields during the deactivation process in dry conditions to that observed in wet conditions. Recall, the product yields shown in Figure 7.3 for the deactivation of Pt/FC28 in dry conditions. During the deactivation process, only the production of carbon dioxide dropped. The production of formaldehyde and methyl formate stayed constant. This suggests that the number of adsorbed formaldehyde species is constant during the deactivation process. Figure 8.7 shows the product yield for the Pt/FC28 catalyst during the deactivation process in wet conditions. The production of both carbon dioxide and formaldehyde decrease during the deactivation. The amount of methyl formate produced in wet conditions was below the calibration limits, however, there was some indication that methyl formate was produced in trace amounts. The decrease in yield of both products indicates that the deactivation is caused by a decrease in the number of adsorbed formaldehyde species (i.e. a loss of active sites) which is not the

Figure 8.6 Cyclic Behaviour of the Pt/SDB Catalyst

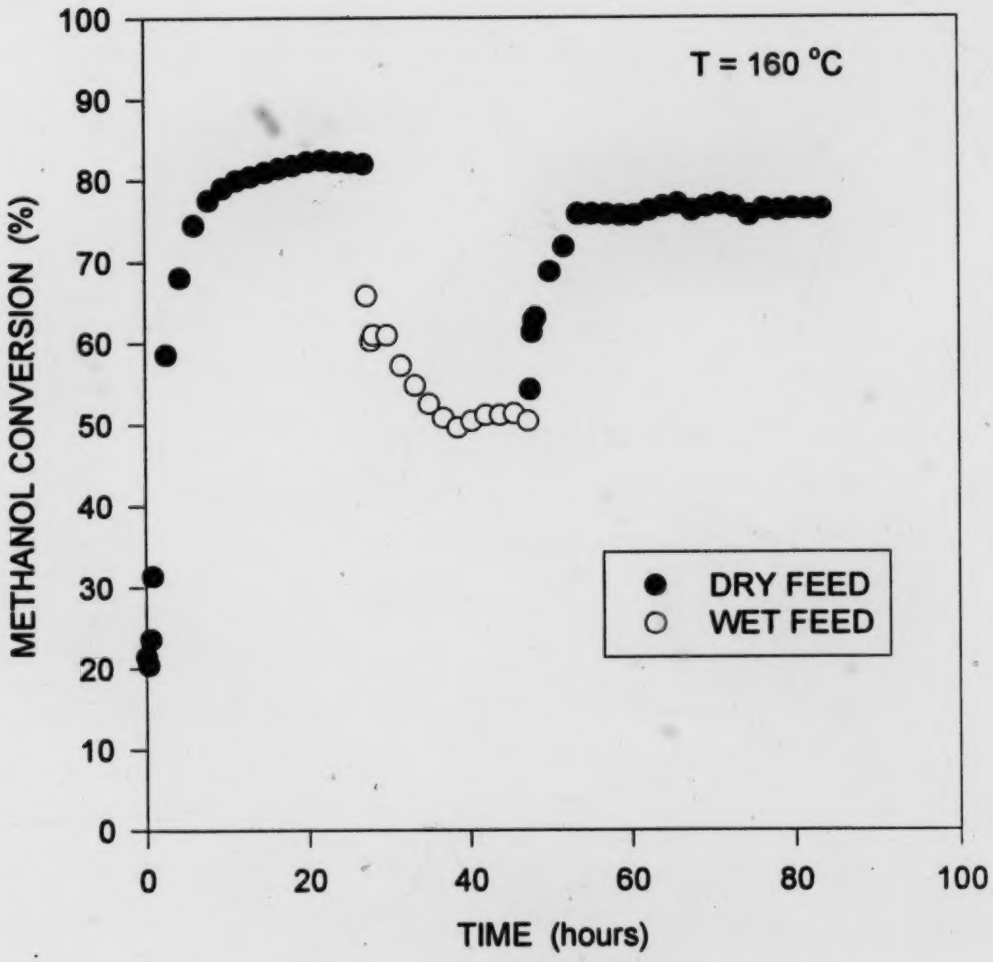

Figure 8.7 Product Yield vs Time for Pt/FC28 Catalyst in Wet Conditions

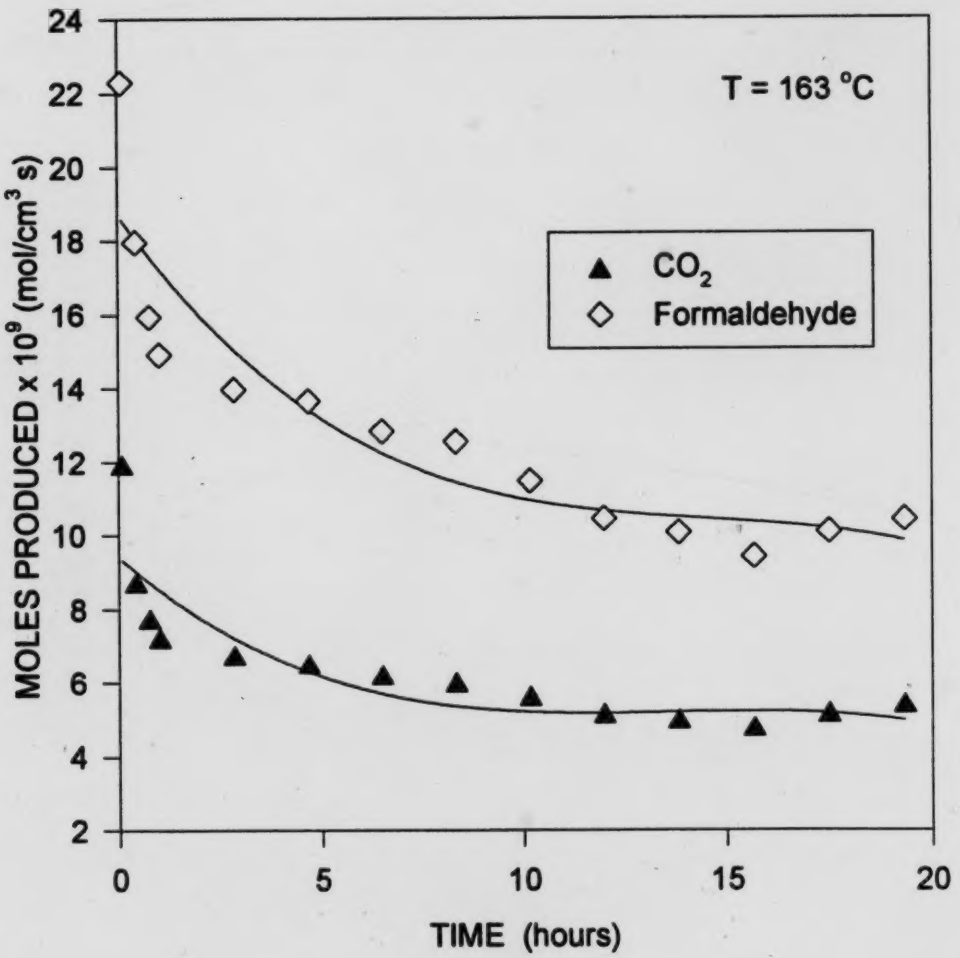

case for the deactivation of the fresh catalyst in dry conditions. The effect of water can be explained by competitive adsorption of water on the active sites. Chapter 5 lists the proposed elementary steps involved in the oxidation of methanol. The two steps that are involved in the competitive adsorption theory are given below.

$$CH_3OH(g) + O(a) + \Diamond \rightarrow CH_3O(a) + OH(a) \qquad (5.4\text{-}2)$$

$$2OH(a) \leftrightharpoons H_2O(g) + O(a) + \Diamond \qquad (5.4\text{-}7)$$

The water vapor shown in Equation 5.4-7 competes with methanol in Equation 5.4-2 for the platinum sites required for the formation of the methoxide species. The methoxide species is the precursor to the adsorbed formaldehyde species from which all the observed products are derived (see Figure 5.1). Therefore, the presence of water decreases the number of active sites for the adsorption of methanol resulting in a decrease in the yield of all product species. When the water is removed from the feed stream, the active sites responsible for the reversible deactivation are once again open to interact with the methanol.

8.2.2 Hydrophilic Catalyst

Figure 8.8 shows the deactivation of the Pt/Al_2O_3 catalyst as a function of time in wet feed conditions. The partial pressure of water was 1.4 kPa. The alumina catalyst did not stabilize in the presence of water vapor. The linear deactivation shown in Figure 8.8 suggests that there is an accumulation of water on the catalyst support which blocks the active sites. Figure 8.9 shows the product yields for the Pt/Al_2O_3 catalyst during the deactivation process in wet conditions. The deactivation is similar to the hydrophobic catalysts with respect to the decrease in yield of each product. The deactivation mechanism for the Pt/Al_2O_3 catalyst is a combination of the accumulation of water on the support and the competitive adsorption of water on the active sites. The competitive

Figure 8.8 Methanol Conversion vs Time for Pt/Al_2O_3 Catalyst in Wet Conditions

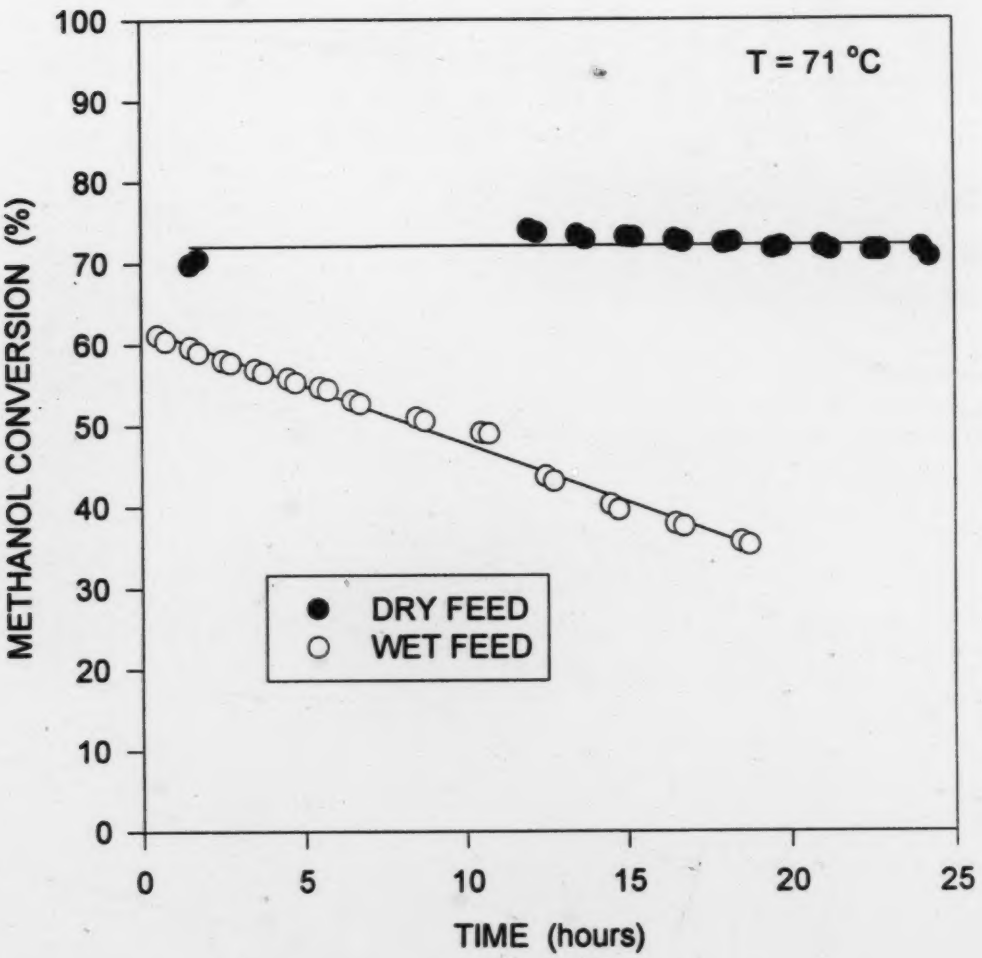

Figure 8.9 Product Yield vs Time for Pt/Al_2O_3 Catalyst in Wet Conditions

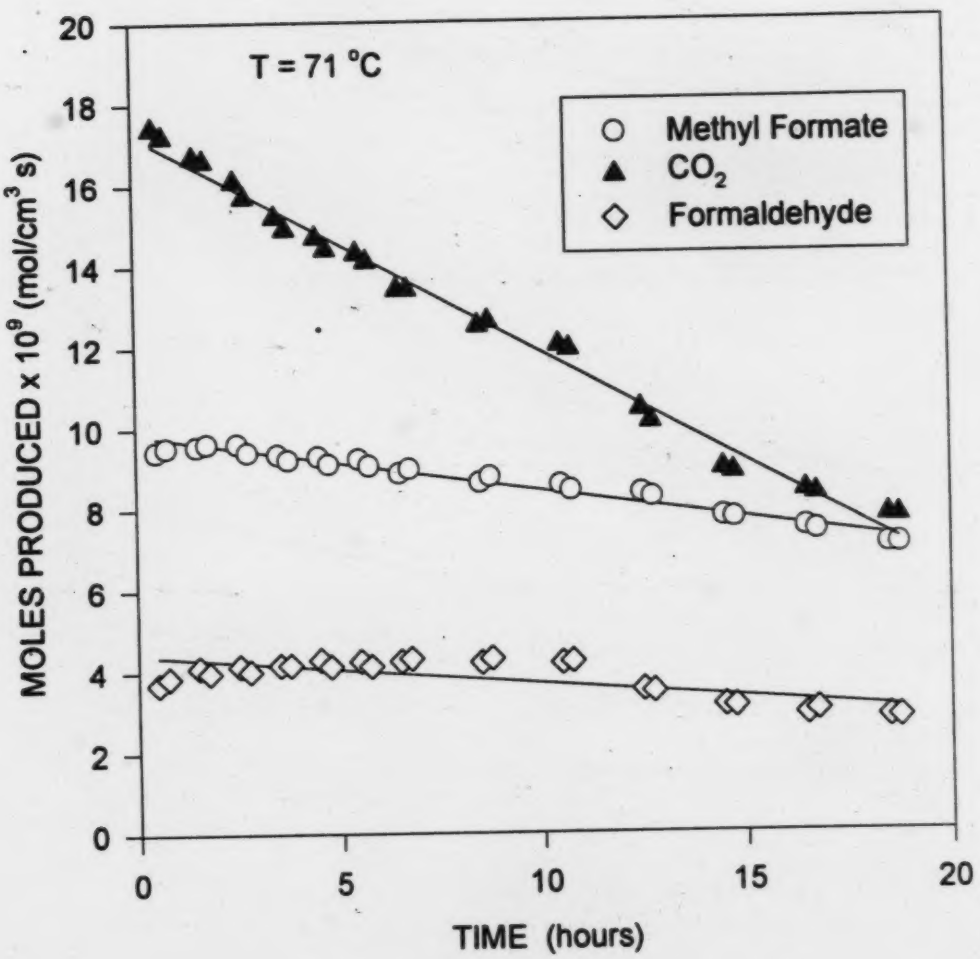

adsorption mechanisms is expected to reach an equilibrium condition as seen from the stabilization of the hydrophobic catalysts. The continual drop in conversion seen in Figure 8.8 is caused by the accumulation of water on the alumina support. The hydrophobic catalysts studied in this work show an advantage over the conventional platinum alumina catalyst when water is present in the feed stream because they eventually stabilize.

8.3 EFFECT OF WATER ON FLUORINATED CARBON CATALYSTS

Section 8.2.1 shows that water does reduce the activity of the fluorinated carbon catalysts for the oxidation of methanol. Figure 8.10 shows the reaction rate versus temperature for a Pt/FC10 catalyst in wet and dry feed conditions. The points on the graph are values obtained after the catalyst has stabilized. Figure 8.11 shows the activity of the Pt/FC28 catalyst as a function of temperature for different water concentrations. The solid circles in Figure 8.11 represent a catalyst that has never been exposed to water. The solid squares represent a catalyst operating in dry conditions after being exposed to water. These two curves show the irreversible nature of the deactivation caused by water. The reversible deactivation caused by the competitive adsorption of water on the active sites is apparent from the decrease in activity with increasing water concentration. Comparing Figures 8.10 and 8.11, the Pt/FC10 catalyst is much more active in the presence of water than the more hydrophobic Pt/FC28. In the past, research efforts have been placed on the Pt/FC28 catalyst solely because of its higher hydrophobicity. The experiments performed in this study clearly show the superiority of the Pt/FC10 catalyst. The hydrophobicity of the FC10 support is sufficient to prevent the accumulation of water and the lack of significant Pt-fluoride interactions on this catalyst result in higher activity.

Figure 8.10 Reaction Rate vs Temperature for Pt/FC10 Catalyst in Wet Conditions

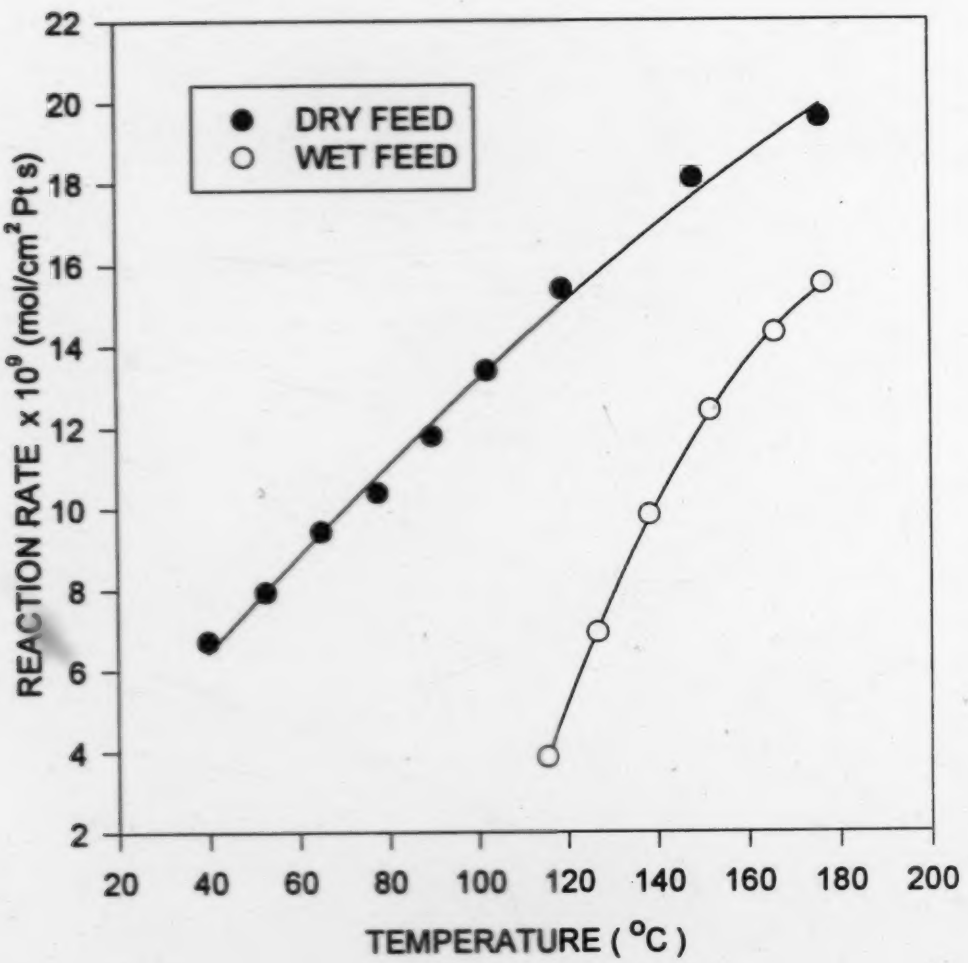

Figure 8.11 Reaction Rate vs Temperature for Pt/FC28 Catalyst in Wet Conditions

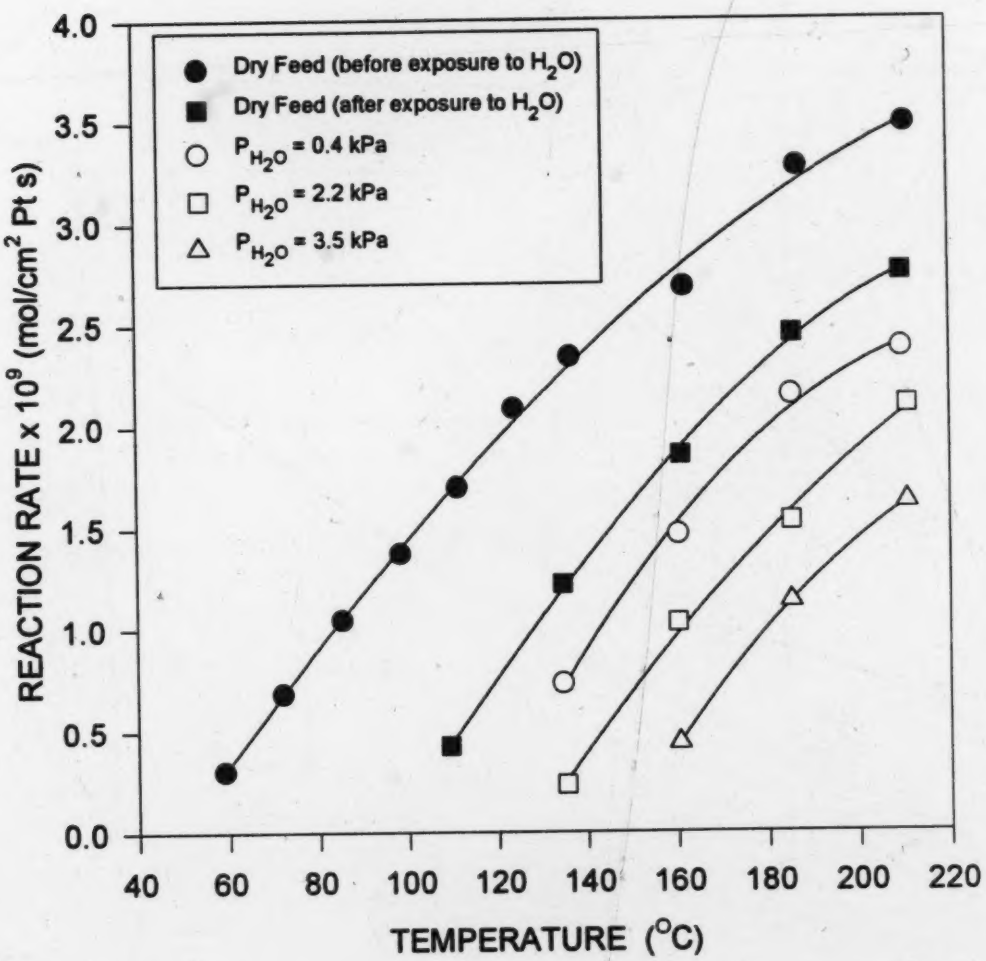

CHAPTER 9

CONCLUSIONS AND RECOMMENDATIONS

9.1 CONCLUSIONS

The study of the catalytic oxidation of methanol in air using hydrophobic platinum/fluorinated carbon catalysts has lead to the development and discovery of many interesting and useful concepts in the area of surface science and catalysis.

1. An equation that relates the contact angle and the heat of immersion has been developed which enables the calculation of the contact angle from heat of immersion data for hydrophobic powders. The heat of immersion method has many advantages over the conventional methods for measuring contact angle. However, it is limited for use with large contact angle systems because of the assumptions made in the derivation of Equation 4.2-8.

2. The platinum supported on the highly fluorinated carbon material (FC28 and FC65) has lower hydrogen adsorption capacity than the platinum supported on the lower fluorinated carbon support (FC10) and the alumina powder. The low hydrogen adsorption capacity of platinum has been related to fluoride-platinum interactions. The fluoride on the catalyst support blocks or distorts the surface electronic properties of the platinum leading to poor hydrogen adsorption.

3. A mechanism for the methanol oxidation reaction has been proposed which can explain the various products and the temperature dependence of the product distribution experimentally observed. A first order rate equation developed using the Langmuir-Hinselwood kinetics has been used to successfully describe the overall methanol conversion at temperatures below 112 °C. At higher temperatures, the reaction becomes mass transfer limited.

4. The thickness of the active phase layer affects the mass transfer of reactants to the active sites within the catalyst structure. Minimizing the active phase layer increases the effectiveness of the platinum by minimizing the internal mass transfer limitations for the type of catalyst tested in this study.

5. The Pt/Al_2O_3 catalyst has similar activity as the Pt/FC10 catalyst for the oxidation of methanol in air for dry feed conditions. These two catalysts have an activity an order of magnitude larger than the Pt/FC28 and Pt/FC65 catalysts. Platinum-fluoride interactions are responsible for the low activity of the highly fluorinated carbon catalyst. Removing the fluoride by heat treatment improves the activity of the Pt/FC28 catalyst. The selectivity of the oxidation reaction is also affected by the presence of fluoride. It is suggested that the fluoride influences the bonding strength of the intermediate species in the oxidation reaction which affects the product distribution of the various catalysts tested.

6. All three hydrophobic catalysts were stable in wet feed conditions. The presence of water vapor decreased the activity of each catalyst. The water competitively adsorbs on the active sites required for the methanol oxidation reaction. The Pt/FC10 catalyst is least affected by the water vapor and the deactivation is reversible. The Pt/FC28 catalyst showed both reversible and irreversible deactivation in the presence of water. The irreversible deactivation is attributed to the platinum-fluoride interactions on this catalyst. The Pt/Al_2O_3 catalyst is unstable in wet feed conditions because of an accumulation of water on the catalyst support.

9.2 RECOMMENDATIONS

From the results of this research the following recommendations are offered:

1. The hydrophobic catalysts show an advantage over conventional hydrophilic catalysts for low temperature reactions in the presence of water. Hydrophobic catalysts which do not contain halogens should be investigated for the oxidation of volatile organic compounds. Catalysts, such as platinum supported on styrene-divinylbenzene (SDB) or other high surface area, low energy materials is suggested. The elimination of metal-support interactions would enable a better comparison between the hydrophilic and hydrophobic nature of the catalysts.

2. An in-depth, infra-red (IR) spectroscopic study of the interaction between platinum and various adsorbed species, such as CO and CH_2O, on the fluorinated carbon catalysts would add insight into the nature of the fluoride-platinum interaction. An in-situ IR cell would be required to perform accurate analysis. Since the fluorinated carbon is black, reflective IR experiments are preferable.

APPENDICES

A. CALCULATIONS FOR THE CHARACTERIZATION OF CATALYSTS

A.1 Calculation of Platinum Particle Size from X-ray Diffraction Data

The following is the data obtained from the plots of the x-ray intensity peaks shown in Figure 3.1 . The Scherrer formula was used to calculate the platinum particle diameter (t) as shown in Table A-1.

Table A-1 Calculation of the Platinum Particle Diameter

Catalyst	θ_B	B (radians)	λ (Å)	t (Å)
10%Pt/Al_2O_3	19.89°	0.01065	1.54178	138.6
10%Pt/FC10	19.90°	0.00855	1.54178	172.6
10%Pt/FC28	19.90°	0.01028	1.54178	143.5
10%Pt/FC65	19.80°	0.00728	1.54178	202.5

A.2 Calculation of Platinum Dispersion from Platinum Particle Size

The platinum dispersion is given by[1]:

$$Dispersion = \left(\frac{N_S}{N_T}\right) = \left(\frac{A_P / A_A}{V_P / V_A}\right)$$

where N_S = number of surface atoms
N_T = number of total atoms
A_P = surface area of platinum particle
A_A = surface area of platinum atom (8.4 Å^2)
V_P = volume of platinum particle
V_A = volume of platinum atom (15.1 Å^3)

The particles of platinum on the surface of the support are assumed to be hemispheres. It follows that the surface area and the volume of the semi-spherical particle is given by:

$$A_P = 2\pi\left(\frac{t}{2}\right)^2$$

$$V_P = \frac{2}{3}\pi\left(\frac{t}{2}\right)^3$$

From the measurement of the particle size and the above equations, the percent dispersion for the catalysts is calculated in Table A-2.

Table A-2 Calculation of Dispersion from X-ray Data

Catalyst	A_P (Å^2)	V_P (Å^3)	Dispersion (%)
10%Pt/Al_2O_3	30180	697203	7.8
10%Pt/FC10	46795	1346142	6.2
10%Pt/FC28	32346	773614	7.5
10%Pt/FC65	64412	2173921	5.3

A.3 Sample Calculation of the Platinum Dispersion from Hydrogen Pulse Chemisorption Data

Experimental Results:

Sample weight = 0.5068 g
Platinum loading = 10 wt%
Total amount of hydrogen adsorbed = 400.3 μL

Physical property data:

MWt. Pt = 195.09
1 mol H_2 = 2.241×10^7 μL H_2
1 mol H_2 = 2 mol surface Pt

Calculation Steps:

1. Calculate the total moles of platinum present in the sample.

   Total moles (Pt) = $(0.1 \times 0.5068) \div 195.09 = 2.5978\times10^{-4}$

2. Calculate the total moles of hydrogen adsorbed.

   Total moles (H_2) = $400.3 \div 2.241\times10^7 = 1.7863\times10^{-5}$

3. Calculate the moles of surface platinum.

   Moles of surface Pt = $2 \times 1.7863\times10^{-5} = 3.5725\times10^{-5}$

4. Calculate the percent dispersion.

$$\text{Percent dispersion} = \left(\frac{3.5725 \times 10^{-5}}{2.5978 \times 10^{-4}}\right) \times 100\% = 13.8\%$$

REFERENCES

1. Anderson, J.R., and K.C. Pratt, *Introduction to Characterization and Testing of Catalysts*, Academic Press Inc., **1985**, 58.

B. HEAT OF IMMERSION DATA

B.1 FC10 Powder

Concentration n-propanol (wt%)	Enthalpy of Immersion (mJ/m^2)			
	Sample A	Sample B	Sample C	Average
0.0	-28.7645	-23.0595	-30.1693	-27.3311
2.5	-49.3557	-40.5071	-41.4806	-43.7811
5.0	-74.6499	-67.0955	-71.0264	-70.9239
7.5	-96.6861	-92.8243	-90.6881	-93.3995

B.2 FC28 Powder

Concentration n-propanol (wt%)	Enthalpy of Immersion (mJ/m^2)			
	Sample A	Sample B	Sample C	Average
10.0	-26.4310	-33.5808	-30.4526	-30.1548
12.5	-42.9342	-45.9358	-43.1654	-44.0118
15.0	-57.9666	-48.3108	-53.4386	-53.2387
17.5	-62.4847	-60.3486	-74.4153	-65.7495

B.3 FC65 Powder

Concentration n-propanol (wt%)	Enthalpy of Immersion (mJ/m^2)			
	Sample A	Sample B	Sample C	Average
12.5	-9.3711	-7.8736	-8.8817	-8.7088
15.0	-14.9624	-16.3473	-15.3549	-15.5549
17.5	-19.7368	-20.0028	-21.6645	-20.4680
20.0	-22.7192	-24.4262	-24.1095	-23.7516
25.0	-30.1671	-26.1414	-26.4008	-27.5698
35.0	-32.3751	-25.6271	-29.2678	-29.0900
45.0	-28.2989	-26.8985	-25.9488	-27.1487

C. DERIVATION OF THE RATE EQUATION FOR THE OXIDATION OF METHANOL

The steps, as shown in Chapter 5, are as follows:

$O_2(g) + 2\Diamond \xleftrightarrow{K_1} 2O(a)$ (C-1)

$CH_3OH(g) + O(a) + \Diamond \xrightarrow{k_2} CH_3O(a) + OH(a)$ (C-2)

$CH_3O(a) + O(a) \xrightarrow{k_3} H_2CO(a) + OH(a)$ (C-3)

$H_2CO(a) + 2O(a) \xrightarrow{k_4} CO(a) + 2OH(a)$ (C-4)

$CO(a) + O(a) \xrightarrow{k_5} CO_2(a) + \Diamond$ (C-5)

$2H_2CO(a) \xrightarrow{k_6} HCOOCH_3(a) + \Diamond$ (C-6)

$2OH(a) \xleftrightarrow{K_7} H_2O(g) + O(a) + \Diamond$ (C-7)

$H_2CO(a) \xleftrightarrow{K_8} H_2CO(g) + \Diamond$ (C-8)

$HCOOCH_3(a) \xleftrightarrow{K_9} HCOOCH_3(g) + \Diamond$ (C-9)

$CO_2(a) \xleftrightarrow{K_{10}} CO_2(g) + \Diamond$ (C-10)

The equilibrium rate constants are represented by

$$K_n = \frac{k_{-n}}{k_n} = \frac{k_{n(backward)}}{k_{n(forward)}}$$

The rate determining step for the disappearance of methanol is assumed to be the oxidation of adsorbed formaldehyde to carbon monoxide (Step C-4). Thus,

$$-r_{MeOH} = k_4 \theta_{H_2CO} \theta_O^2 \qquad \text{(C-11)}$$

Where θ represents the fraction of the total number of active sites occupied by an adsorbed species.

The steady state coverage of $H_2CO(a)$ is maintained by Reactions C-3, C-4 and C-6. Therefore,

$$\frac{d\theta_{H_2CO}}{dt} = k_3 \theta_{CH_3O} \theta_O - k_4 \theta_{H_2CO} \theta_O^2 - k_6 \theta_{H_2CO}^2 = 0 \qquad \text{(C-12)}$$

Rearranging C-12 and substituting into C-11 gives

$$-r_{CH_3OH} = k_3\theta_{CH_3O}\theta_O - k_6\theta^2_{H_2CO} \qquad \text{(C-13)}$$

The steady state coverage of $CH_3O(a)$ is maintained by Reactions C-2 and C-3.

Therefore,

$$\frac{d\theta_{CH_3O}}{dt} = k_2 P_{CH_3OH}\theta_O\theta_\phi - k_3\theta_{CH_3O}\theta_O = 0 \qquad \text{(C-14)}$$

Rearranging C-14 and substituting into C-13 gives

$$-r_{CH_3OH} = k_2 P_{CH_3OH}\theta_O\theta_\phi - k_6\theta^2_{H_2CO} \qquad \text{(C-15)}$$

At equilibrium, the fractional coverage of $H_2CO(a)$ and $O(a)$ are found from Reactions C- 8 and C-1, respectively.

$\theta_{H_2CO} = K_8 P_{H_2CO}\theta_\phi$ from (C-8)

$\theta_O = K_1^{1/2} P_{O_2}^{1/2}\theta_\phi$ from (C-1)

Substituting these into C-15 gives

$$-r_{CH_3OH} = \theta_\phi^2\left[k_2 K_1^{1/2} P_{O_2}^{1/2} P_{CH_3OH} - k_6 K_8 P^2_{H_2CO}\right] \qquad \text{(C-16)}$$

To evaluate the rate using terms that can be measured experimentally, an expression for the fraction of empty sites must be developed. The sum of the fractional coverage of all adsorbed species and empty sites must equal to one.

Therefore,

$$1 = \theta_\phi + \theta_O + \theta_{H_2CO} + \theta_{OH} + \theta_{CO} + \theta_{CH_2O} + \theta_{CO_2} + \theta_{HCOOCH_3} \qquad \text{(C-17)}$$

Abbas and Madix[1] showed that the formation of CO_2 and $HCOOCH_3$ on platinum (111) surfaces are not desorption limited. These authors also report that the oxidation of adsorbed CO is instantaneous if there is sufficient absorbed oxygen atoms. Therefore, the amount of adsorbed CO_2, $HCOOCH_3$ and CO is negligible. Since the oxidation of adsorbed formaldehyde is assumed to be the rate determining step, the amount of adsorbed CH_3O is also considered negligible.

Equation C-17 then becomes,

$$1 = \theta_\phi + \theta_O + \theta_{H_2CO} + \theta_{OH} \qquad \text{(C-18)}$$

From Equation C-7, the fractional coverage of OH(a) is given by

$$\theta_{OH} = K_7^{1/2} K_1^{-1/4} P_{O_2}^{1/4} P_{H_2O}^{1/2} \theta_0$$

Substituting the fractional coverage's of O(a), H_2CO(a) and OH(a) into Equation C-18 and rearranging gives

$$\theta_0 = \frac{1}{\left[1 + K_1^{-1/4} P_{O_2}^{1/4} + K_7^{1/2} K_1^{-1/4} P_{O_2}^{1/4} P_{H_2O}^{1/2} + K_8 P_{H_2CO}\right]} \qquad \text{(C-19)}$$

Substituting Equation C-19 into C-16, the rate equation becomes

$$-r_{CH_3OH} = \frac{\left[k_2 K_1^{1/2} P_{O_2}^{1/4} P_{CH_3OH} - k_6 K_8 P_{H_2CO}^2\right]}{\left[1 + K_1^{-1/4} P_{O_2}^{1/4} + K_7^{1/2} K_1^{-1/4} P_{O_2}^{1/4} P_{H_2O}^{1/2} + K_8 P_{H_2CO}\right]^2} \qquad \text{(C-20)}$$

Since the experiments in this study focus only on the oxidation of methanol in excess oxygen, (i.e. air) the partial pressure of oxygen can be considered constant. The effect of the partial pressure of formaldehyde in the above rate equation can be assumed negligible for this study. The low concentration range of methanol (<3000 ppm) results in very dilute mixtures of formaldehyde in the gas phase. The change in the formaldehyde partial pressure during the kinetic experiments is assumed to be negligible. Using these assumptions, equation (C-20) can be reduced to

$$-r_{CH_3OH} = \frac{k P_{CH_3OH}}{\left[1 + b P_{H_2O}^{1/2}\right]^2} \qquad \text{(C-21)}$$

where $k = \dfrac{k_2 K_1^{1/2} P_{O_2}^{1/4}}{\left[1 + K_1^{-1/4} P_{O_2}^{1/4}\right]}$

$$b = \frac{K_7^{1/2} K_1^{1/4} P_{O_2}^{1/4}}{\left[1 + K_1^{-1/4} P_{O_2}^{1/4}\right]}$$

For experiments in dry conditions, a similar argument for the partial pressure of water can be made as was used for the formaldehyde. With the use of dilute methanol

concentrations, the amount of water produced is very small. Changes in the partial pressure of water during the kinetic study can be considered negligible. Equation C-21 can be reduced to the following rate equation for the kinetic study in dry feed conditions.

$$-r_{CH_3OH} = kP_{CH_3OH} \qquad \text{(C-22)}$$

The form of the above rate equation is validated in Chapter 7 for the oxidation of methanol in air.

REFERENCES

1. Abbas, N. M., and R. J. Madix, *Appl. Surf. Sci.*, **1981**, 7, 241.

D. CATALYST STABILITY DATA

D.1 Data for Pt/FC10 catalyst (dry conditions)

Catalyst: 1.3744 g of 0.0061 wt% Pt/FC10 spheres

Temperature = 170 °C Flowrate = 230 mL/min Inlet Conc. = 2764 ppm MeOH

Time (hours)	Methanol Conversion (%)
0.42	88.4
0.75	88.2
1.00	87.9
2.83	86.1
4.66	84.8
6.49	83.9
8.32	83.4
10.15	82.3
11.98	81.9
13.81	81.0
15.64	80.5
17.47	79.7
19.30	79.3
21.13	78.9
22.96	79.2
24.79	78.5

D.2 Data for Pt/FC28 catalyst (dry conditions)

Catalyst: 9.8051 g of 0.0051 wt% Pt/FC28 spheres

Temperature = 163 °C Flowrate = 231 mL/min Inlet Conc. = 2751 ppm MeOH

Time (hours)	Methanol Conversion (%)
1.75	82.9
2.08	80.9
3.92	73.4
4.25	72.6
6.08	69.5
6.42	68.8
8.25	67.0
8.58	66.3
10.42	65.3
10.75	65.4
12.58	63.5
12.92	63.1
14.75	61.8
15.08	61.5
16.92	61.0
17.25	60.5
19.08	60.5
19.42	60.4
21.25	60.0
21.58	60.2
23.42	61.1
23.75	60.9
25.58	61.5
25.92	61.1

D.3 Data for Pt/FC65 catalyst (dry conditions)

Catalyst: 20.1281 g of 0.0026 wt% Pt/FC65 spheres

Temperature = 176 °C Flowrate = 231 mL/min Inlet Conc. = 2867 ppm MeOH

Time (hours)	Methanol Conversion (%)
0.08	57.5
0.33	52.2
0.58	49.3
0.83	48.1
2.58	43.1
4.33	40.4
6.08	37.8
7.83	36.2
9.58	35.2
11.33	34.6
13.08	34.5
14.83	34.7
16.58	34.1
18.33	34.2
20.08	33.9
21.83	34.3
23.58	34.1

D.4 Data for Pt/Al_2O_3 catalyst (dry conditions)

D.4-1 Catalyst: 6.7369 g of 0.0028 wt% Pt/Al_2O_3 spheres

Temperature = 72 °C Flowrate = 230 mL/min Inlet Conc. = 2670 ppm MeOH

Time (hours)	Methanol Conversion (%)
2.58	89.9
4.33	90.2
6.08	90.4
7.83	89.8
9.58	89.4
11.33	88.8
13.08	88.0
14.83	87.5
16.58	86.8
18.33	86.3
20.08	85.8
21.83	85.3
23.58	85.1

D.4-2 Catalyst: 5.1137 g of 0.0028 wt% Pt/Al_2O_3 spheres

Temperature = 161 °C Flowrate = 230 mL/min Inlet Conc. = 2670 ppm MeOH

Time (hours)	Methanol Conversion (%)
1.75	92
4.25	89
6.75	87
9.25	85
11.75	83
14.25	81
16.75	79
19.25	77
21.75	75
24.25	73

D.4-3 Catalyst: 2.3860 g of 0.0028 wt% Pt/Al_2O_3 spheres

Temperature = 206 °C Flowrate = 230 mL/min Inlet Conc. = 2670 ppm MeOH

Time (hours)	Methanol Conversion (%)
1.75	88
4.25	86
6.75	84
9.25	82
11.75	81
14.25	79
16.75	78
19.25	76
21.75	76
24.25	74

E. THEORETICAL CALCULATION OF THE EFFECTIVENESS FACTOR

E.1 Calculation of the Active Phase Layer Thickness

Data: $\rho_s = 3.363$ g/cm³ $\quad D_{avg} = 0.546$ cm $\quad V_s = \frac{\pi}{6} D_{avg}^3 = 0.0852$ cm³/sphere

$\rho_{fc} = 0.1$ g/cm³

Catalyst X: 0.034 wt%Pt/FC28/spheres

0.0352 g of 10% Pt/FC28 supported on 10.1957 g of ceramic spheres.

vol. of support = 10.1957 ÷ 3.363 = 3.0317 cm³

vol. of powder = 0.0352 ÷ 0.1 = 0.352 cm³

vol. of powder per sphere = 0.352 ÷ 3.0317 × 0.0852 = 9.8922×10^{-3} cm³/sphere

vol. of powder = $\frac{4}{3}\pi\left(r_o^3 - r_i^3\right)$

where r_o = the outside radius of the catalyst

r_i = the radius of the ceramic sphere

Therefore, $\quad 9.8922 \times 10^{-3} = \frac{4}{3}\pi\left(r_o^3 - 0.273^3\right)$

$r_o = 0.28318$ cm

Thickness of the Active Layer = $r_o - r_i = 0.28318 - 0.273 = 0.01018$ cm

Catalyst Y: 0.0094 wt%Pt/FC28/spheres

0.0191 g of 10%Pt/FC28 supported on 20.3925 g of ceramic spheres

vol. of support = 6.0638 cm³

vol. of powder = 0.191 cm³

vol. of powder per sphere = 2.6837×10^{-3} cm³/sphere

$r_o = 0.27584$ cm

Thickness of the Active Layer = 0.00284 cm

Catalyst Z: 0.0023 wt%Pt/FC28/spheres

0.0101 g of 10%Pt/FC28 supported on 43.8294 g of ceramic spheres

vol. of support = 13.0328 cm^3

vol. of powder = 0.101 cm^3

vol. of powder per sphere = 6.6027×10^{-4} cm^3/sphere

r_o = 0.27370 cm

Thickness of the Active Layer = 0.00070 cm

E.2 Calculation of the Effective Diffusivity

Approximation of the Diffusion Coefficient

To approximate the diffusivity of methanol in air within the active phase layer, it is assumed that only Knudsen diffusion is occurring over the range of pores. This is a good approximation considering that there is also counter current diffusion of products within the active layer. The counter current diffusion of products hinders the diffusion of the methanol in the pores. Therefore, a Knudsen diffusion coefficient better represents the diffusion occurring in the pores than a bulk diffusion coefficient for a binary mixture. The diffusion coefficient for Knudsen diffusion is given by;

$$D_k = 9700 r_e \sqrt{\frac{T}{M}}$$

where D_k = the Knudsen diffusion coefficient (cm^2/s)

r_e = pore radius (cm)

T = temperature (K)

M = molecular weight (32.04 for methanol)

For a range of pore sizes,

$$r_e = \frac{\int r dv}{v2 - v1}$$

Using the pore size distribution for 10%Pt/FC28 shown in Table 3.1,

$r_e = 1.203 \times 10^{-6}$ cm

Combining the terms,

$D_k = 2.0615 \times 10^{-3} \sqrt{T}$

Estimating the Effective Diffusivity

$$D_{k,eff} = \frac{D_k \varepsilon_p \sigma}{\tau}$$

where ε_p = the porosity of the active phase layer (void vol/total vol)

σ = the shape factor

τ = the tortuosity

Fogler[1] gives the typical values of σ and τ as 0.8 and 3.0 respectively. The porosity of the active layer is calculated from the values of the bulk density and the true density of the FC28. These values were obtained from the supplier.

bulk density = 0.1 g/cm^3 $\Rightarrow$ 10 cm^3/g

true density = 2.1 g/cm^3 $\Rightarrow$ 0.4762 cm^3/g

Therefore,

$$\varepsilon_p = \frac{(10 - 0.4762)}{10} = 0.9524$$

Combining the terms,

$D_{k,eff} = 0.2540 D_k$

The diffusion coefficient of methanol in the pores of the active phase layer can be estimated by the following temperature relationship,

$D_{k,eff} = 5.2362 \times 10^{-4} \sqrt{T}$

where T is in Kelvin and $D_{k,eff}$ is in cm^2/s.

E.3 Calculation of the Thiele Modulus and the Effectiveness Factor

Since the thickness of the active phase layer is small compared to the radius of curvature of the ceramic sphere, the active phase layer can be modeled as a semi-infinite flat plate. The equation for the Thiele modulus, as shown in Chapter 7, is given by;

$$\phi = L\sqrt{\frac{k_v}{D_{k,eff}}}$$

where L = the thickness of the active phase layer (cm)

k_v = the intrinsic rate constant per unit volume of active phase (s^{-1})

The only unknown parameter is k_v. This parameter is a function of temperature and is related to the catalyst through the activation energy. This makes the value of k_v dependent on the catalyst being tested. For the purpose of estimating the effectiveness factor, k_v was calculated from the reaction data for Catalyst Z (i.e. the catalyst with the thinnest active phase layer). By using this value of k_v, it is assumed that Catalyst Z has no internal mass transfer limitations. This assumption will be validated by comparing the activation energy found using Catalyst Z with those from literature. The activation energy is a good indication if mass transfer limitations are present during the kinetic study. The highest temperature used in the kinetic study was 385 K. This represents the largest k_v value and, therefore, the lowest effectiveness factor in the kinetic experiments. Table F.3-3 in Appendix F shows the value of ln k for the reaction at 385 K for Catalyst Z. The units of k are mol/(s·cm² Pt·mmHg). To obtain the value of k_v, the following unit conversion is required.

$$k_v = k \times 1954\frac{\text{cm}^2\text{Pt}}{\text{cm}^3\text{vol}} \times 82.06\frac{\text{cm}^3\cdot\text{atm}}{\text{gmol}\cdot\text{K}} \times 760\frac{\text{mmHg}}{\text{atm}} \times 298.15\text{K}$$

Therefore, k_v = 43.4235 s^{-1} @ 385 K.

The first unit conversion term is the surface area of the platinum per volume of porous powder. This value is calculated using the XRD results shown in Table 3.2 for 10%Pt/FC28. Using the above data, one can calculate the Thiele modulus for Catalyst X, Y, and Z.

Catalyst	Thickness (L) (cm)	$D_{k,eff}$ (cm^2/s)	k_v (s^{-1})	ϕ
X	0.01018	0.01027	43.4235	0.6619
Y	0.00284	0.01027	43.4235	0.1847
Z	0.00070	0.01027	43.4235	0.0455

The equation relating the Thiele modulus to the effectiveness factor for a first order reaction with a flat plate geometry is shown in Chapter 7.

$$\eta = \frac{\tanh \phi}{\phi}$$

Using the values of the Thiele modulus calculated above, the theoretical effectiveness factor for Catalysts X, Y, and Z are 0.876, 0.989, and 1.000 respectively.

References

1. Fogler, H. S., *Elements of Chemical Reaction Engineering*, Prentice-Hall Inc., **1986**, 562.

F. EXPERIMENTAL DATA FROM THE KINETIC STUDY

The following is a list of definitions used to simplify the interpretation of the data.

1. The inlet and outlet concentrations have the units of mol/cm^3 at 150 °C.
2. The total flowrate (F_T) has the units of cm^3/s at 23 °C.
3. The mass balance shown in the tables is a carbon balance given by,

$$\text{Mass. Bal.} = \frac{(\text{inlet carbon} - \text{outlet carbon})}{\text{inlet carbon}} \times 100\%$$

4. P_{MeOH} is used to describe the partial pressure of methanol (mmHg) in the outlet stream.

F.1 Data for Catalyst X

Catalyst: 11.8473 g of 0.034 wt%Pt/FC28/spheres

Table F.1-1 Kinetic Data for Catalyst X

Run NO.	Temp. (°C)	F_T (cm^3/s)	Inlet Conc. (mol/cm^3)	Outlet Concentration (mol/cm^3)					Mass. Bal. (%)
			CH_3OH	CH_3OH	$HCOOCH_3$	CO_2	CH_2O	H_2O	
X-1	63.2	231	2.4028E-8	1.0179E-8	2.5638E-9	6.4739E-9	1.2393E-9	2.7024E-8	4.2
X-2	63.8	231	5.3121E-8	2.8092E-8	5.2912E-9	1.1966E-8	3.1710E-9	5.9966E-8	-1.3
X-3	63.7	231	1.0186E-7	5.9244E-8	9.7403E-9	1.7360E-8	4.7461E-9	9.4763E-8	1.0
X-4	75.6	231	2.4347E-8	8.4383E-9	2.3110E-9	8.4544E-9	2.2556E-9	3.4951E-8	2.4
X-5	76.3	231	5.4762E-8	2.3071E-8	4.7091E-9	1.7065E-8	5.1056E-9	7.6456E-8	0.2
X-6	76.2	232	1.0519E-7	5.0304E-8	9.3552E-9	2.7842E-8	8.3416E-9	1.3861E-7	0.0
X-7	88.4	231	2.4292E-8	7.3661E-9	1.8930E-9	1.0111E-8	3.0068E-9	4.1298E-8	0.1
X-8	88.8	231	5.4872E-8	1.9028E-8	3.6482E-9	2.1523E-8	6.811E-9	9.0625E-8	0.6
X-9	89.2	231	1.0114E-7	3.8568E-8	6.9603E-9	3.8156E-8	1.1058E-8	1.6740E-7	-0.6
X-10	101.1	231	2.5602E-8	6.4484E-9	1.4965E-9	1.1779E-8	3.6124E-9	4.5643E-8	3.0
X-11	102.0	231	5.6911E-8	1.7239E-8	2.7793E-9	2.6169E-8	7.9563E-9	1.0583E-7	0.0
X-12	102.2	231	1.0495E-7	3.4399E-8	5.1847E-9	4.7895E-8	1.3576E-8	2.0188E-7	-1.2
X-13	114.3	231	2.5341E-8	5.2426E-9	1.1934E-9	1.3446E-8	3.9417E-9	5.1420E-8	1.3
X-14	115.1	231	6.0053E-8	1.5307E-8	2.0904E-9	3.0911E-8	9.0109E-9	1.2263E-7	1.1
X-15	114.8	231	1.0528E-7	2.9893E-8	3.693E-9	5.4475E-8	1.4858E-8	2.2103E-7	-1.3

Table F.1-2 Rate Data for Catalyst X

Run NO.	Temperature (K)	P_{MeOH} (mmHg)	$-r_{MeOH}$ (mol/cm² Pt·s)
X-1	336.4	0.2686	9.6804E-11
X-2	337.0	0.7413	1.7512E-10
X-3	336.9	1.5635	2.9787E-10
X-4	348.8	0.2227	1.1120E-10
X-5	349.5	0.6088	2.2151E-10
X-6	349.4	1.3275	3.8528E-10
X-7	361.6	0.1944	1.1830E-10
X-8	362.0	0.5021	2.5055E-10
X-9	362.4	1.0179	4.3732E-10
X-10	374.3	0.1702	1.3389E-10
X-11	375.2	0.4549	2.7729E-10
X-12	375.4	0.9078	4.9313E-10
X-13	387.5	0.1383	1.4048E-10
X-14	388.3	0.4039	3.1277E-10
X-15	388.0	0.7889	5.2695E-9

Table F.1-3 Data Obtained from the Plot of $\ln(P_{MeOH})$ vs $\ln(-r_{MeOH})$ for Catalyst X

Temperature (K)	ln k	α	R^2
336.8	-22.2391	0.64	0.9968
349.2	-21.8782	0.70	0.9999
362.0	-21.5640	0.79	1.0000
375.0	-21.3698	0.78	0.9989
387.9	-21.1895	0.76	0.9999

F.2 Data for Catalyst Y

Catalyst: 6.5678 g of 0.0094 wt%Pt/FC28/spheres

Table F.2-1 Kinetic Data for Catalyst Y

Run NO.	Temp. (°C)	F_T (cm^3/s)	Inlet Conc. (mol/cm^3)	Outlet Concentration (mol/cm^3)					Mass. Bal. (%)
			CH_3OH	CH_3OH	$HCOOCH_3$	CO_2	CH_2O	H_2O	
Y-1	68.3	230	2.6295E-8	2.2124E-8	9.8433E-10	2.4869E-9	3.3542E-10	-	-2.4
Y-2	68.2	231	6.6301E-8	5.7011E-8	1.5675E-9	3.9101E-9	2.0748E-9	-	0.3
Y-3	67.7	231	1.0414E-7	9.1732E-8	1.9753E-9	4.9945E-9	3.8426E-9	2.2717E-8	-0.4
Y-4	81.3	233	2.6833E-8	2.0951E-8	1.0491E-9	3.6896E-9	1.3829E-9	-	-4.8
Y-5	81.4	232	6.6359E-8	5.1855E-8	1.8136E-9	7.3306E-9	4.8214E-9	3.2020E-8	-1.9
Y-6	80.8	236	1.0546E-7	8.3060E-8	2.8685E-9	1.0233E-8	8.3516E-9	4.8316E-8	-1.8
Y-7	94.6	236	2.7499E-8	1.8686E-8	1.0738E-9	5.0466E-9	2.5317E-9	1.8289E-8	-3.3
Y-8	95.1	239	6.6095E-8	4.4083E-8	1.8933E-9	1.2061E-8	8.2899E-9	5.0919E-8	-3.2
Y-9	95.2	237	1.0500E-7	6.9510E-8	3.0322E-9	1.8804E-8	1.4236E-8	8.6224E-8	-3.4
Y-10	108.1	231	2.6678E-8	1.5462E-8	1.0537E-9	6.5608E-9	3.8748E-9	2.5562E-8	-5.0
Y-11	108.3	233	6.4551E-8	3.6358E-8	1.7927E-9	1.7056E-8	1.1675E-8	7.3684E-8	-6.4
Y-12	108.6	231	1.0470E-7	5.5401E-8	2.7583E-9	2.8420E-8	1.9022E-8	1.2764E-7	-3.5

Table F.2-2 Rate Data for Catalyst Y

Run NO.	Temperature (K)	P_{MeOH} (mmHg)	$-r_{MeOH}$ (mol/cm² Pt·s)
Y-1	341.5	0.5839	1.8943E-10
Y-2	341.4	1.5046	4.2366E-10
Y-3	340.9	2.4208	5.6602E-10
Y-4	354.5	0.5529	2.7057E-10
Y-5	354.6	1.3685	6.6429E-10
Y-6	354.0	2.1920	1.0437E-9
Y-7	367.8	0.4931	4.1060E-10
Y-8	368.3	1.1633	1.0386E-9
Y-9	368.4	1.8344	1.6604E-9
Y-10	381.3	0.4080	5.1149E-10
Y-11	381.5	0.9594	1.2969E-9
Y-12	381.8	1.4620	2.2490E-9

Table F.2-3 Data Obtained from the Plot of $\ln(P_{MeOH})$ vs $\ln(-r_{MeOH})$ for Catalyst Y

Temperature (K)	ln k	α	R^2
341.3	-21.9503	0.78	0.9942
354.4	-21.4466	0.98	0.9999
368.2	-20.8565	1.07	0.9999
381.5	-20.3761	1.15	0.9978

F.3 Data for Catalyst Z

Catalyst: 21.5820 g of 0.0023 wt%Pt/FC28/spheres

Table F.3-1 Kinetic Data for Catalyst Z

Run NO.	Temp (°C)	F_T (cm^3/s)	Inlet Conc. (mol/cm^3)	Outlet Concentration (mol/cm^3)					Mass. Bal. (%)
			CH_3OH	CH_3OH	$HCOOCH_3$	CO_2	CH_2O	H_2O	
Z-1	59.4	234	3.5189E-8	3.2432E-8	9.8084E-10	6.2461E-10	-	-	0.5
Z-2	59.0	231	9.1131E-8	8.5811E-8	1.6151E-9	1.3300E-9	6.6879E-10	8.4044E-9	0.1
Z-3	59.3	232	1.5240E-7	1.4465E-7	2.2253E-9	1.6828E-9	1.3650E-9	1.1473E-8	0.2
Z-4	72.1	234	3.4254E-8	2.9488E-8	1.0731E-9	1.2452E-9	5.8883E-10	-	2.3
Z-5	72.1	232	9.0164E-8	7.8136E-8	2.0041E-9	2.8971E-9	2.7634E-9	1.6522E-8	2.6
Z-6	72.1	231	1.3646E-7	1.2049E-7	2.7524E-9	3.7133E-9	4.0220E-9	2.1144E-8	2.0
Z-7	85.5	234	3.4155E-8	2.7067E-8	1.2387E-9	2.3431E-9	1.9852E-9	1.0443E-8	0.8
Z-8	85.5	232	8.8631E-8	7.0289E-8	2.4398E-9	5.7248E-9	6.3975E-9	2.7248E-8	1.5
Z-9	85.5	231	1.4865E-7	1.2033E-7	3.9782E-9	8.2527E-9	1.0314E-8	4.7713E-8	1.2
Z-10	98.6	234	3.4428E-8	2.5136E-8	1.2201E-9	3.0526E-9	3.0651E-9	1.2277E-8	2.1
Z-11	98.5	232	8.5678E-8	6.1537E-8	2.4644E-9	8.4779E-9	9.7032E-9	4.0916E-8	1.2
Z-12	98.7	231	1.4762E-7	1.0594E-7	4.2368E-9	1.5141E-8	1.7750E-8	7.0215E-8	0.2
Z-13	112.1	228	7.0106E-8	4.4231E-8	1.9776E-9	1.1142E-8	1.1131E-8	4.5640E-8	-0.5
Z-14	112.2	229	1.2485E-7	7.7037E-8	3.6705E-9	2.0981E-8	2.0881E-8	8.6397E-8	-1.1
Z-15	112.3	229	1.7732E-7	1.0516E-7	6.1776E-9	3.1250E-8	3.1157E-8	1.2999E-7	-1.5
Z-16	123.4	231	3.4598E-8	2.2300E-8	1.1023E-9	5.1497E-9	5.3424E-9	1.9456E-8	-1.2
Z-17	124.1	232	8.9231E-8	5.2564E-8	2.1396E-9	1.6577E-8	1.6035E-8	6.4838E-8	-0.3
Z-18	124.5	229	1.4449E-7	7.4298E-8	2.9630E-9	2.4808E-8	2.3074E-8	1.1351E-7	-2.2
Z-19	136.4	233	3.3125E-8	1.9450E-8	9.9737E-10	6.3631E-9	6.3923E-9	2.3735E-8	-3.2
Z-20	136.7	231	8.7485E-8	4.6212E-8	1.8123E-9	2.0540E-8	1.7772E-8	7.5857E-8	-0.8
Z-21	136.8	231	1.2561E-7	6.5586E-8	2.4208E-9	3.0520E-8	2.4860E-8	1.1194E-7	-0.2
Z-22	161.9	232	3.2904E-8	1.5940E-8	8.3877E-10	8.8953E-9	7.7282E-9	3.0965E-8	1.0
Z-23	162.0	231	8.3888E-8	3.6628E-8	1.2884E-9	2.9086E-8	2.0396E-8	1.0129E-7	-5.7
Z-24	162.0	230	1.4404E-7	5.8382E-8	1.8033E-9	5.0285E-8	3.1222E-8	1.7180E-7	0.4
Z-25	186.9	230	3.2633E-8	1.2059E-8	-	1.2374E-8	8.2113E-9	4.0701E-8	0.0

Z-26	187.1	228	8.5319E-8	2.6870E-8	9.7883E-10	3.6975E-8	2.0767E-8	1.2017E-7	-1.5
Z-27	187.2	228	1.4073E-7	4.3858E-8	1.2575E-9	6.2604E-8	3.1415E-8	2.0549E-7	0.2
Z-28	210.4	232	3.2607E-8	9.7292E-9	-	1.3051E-8	7.4363E-9	4.6816E-8	1.2
Z-29	210.7	228	8.3058E-8	2.0854E-8	-	4.4045E-8	1.9037E-8	1.3721E-7	-1.1
Z-30	210.9	228	1.3736E-7	3.3895E-8	9.4958E-10	7.2024E-8	2.9961E-8	2.2789E-7	-0.3

Table F.3-2 Rate Data for Catalyst Z

Run NO.	Temperature (K)	P_{MeOH} (mmHg)	$-r_{MeOH}$ (mol/cm² Pt·s)
Z-1	332.6	0.8559	1.5842E-10
Z-2	332.2	2.2646	3.0176E-10
Z-3	332.5	3.8173	4.4143E-10
Z-4	345.3	0.7782	2.7383E-10
Z-5	345.3	2.0620	6.8521E-10
Z-6	345.3	3.1797	9.0580E-10
Z-7	358.7	0.7143	4.0725E-10
Z-8	358.7	1.8549	1.0448E-9
Z-9	358.7	3.1755	1.6064E-9
Z-10	371.8	0.6633	5.3391E-10
Z-11	371.7	1.6240	1.3752E-9
Z-12	371.9	2.7958	2.3640E-9
Z-13	385.3	1.1673	1.4486E-9
Z-14	385.4	2.0330	2.6885E-9
Z-15	385.5	2.7752	4.0575E-9
Z-16	396.6	0.5885	6.9758E-10
Z-17	397.3	1.3872	2.0888E-9
Z-18	397.7	2.2518	3.3267E-9
Z-19	409.6	0.5133	7.8236E-10
Z-20	409.9	1.2195	2.3410E-9
Z-21	410.0	1.7308	3.4046E-9
Z-22	435.1	0.4207	9.6635E-10
Z-23	435.2	0.9666	2.6807E-9

Z-24	435.2	1.5407	4.8373E-9
Z-25	460.1	0.3182	1.1619E-9
Z-26	460.3	0.7091	3.2722E-9
Z-27	460.4	1.1574	5.4231E-9
Z-28	483.6	0.2568	1.3033E-9
Z-29	483.9	0.5504	3.4826E-9
Z-30	484.1	0.8945	5.7925E-9

Table F.3-3 Data Obtained from the Plot of $\ln(P_{MeOH})$ vs $\ln(-r_{MeOH})$ for Catalyst Z

Temperature (K)	ln k	α	R^2
332.5	-22.4647	0.68	0.9990
345.3	-21.7841	0.87	0.9940
358.7	-21.2944	0.93	0.9970
371.8	-20.9204	1.04	0.9998
385.4	-20.5450	1.18	0.9979
397.3	-20.4361	1.18	0.9950
409.9	-20.1458	1.22	0.9994
435.2	-19.6874	1.24	1.0000
460.3	-19.1762	1.20	0.9970
483.9	-18.8038	1.20	0.9970

F.4 Data for Pt/FC10 Catalyst

Catalyst: 1.4152 g of 0.0061 wt%Pt/FC10/spheres

Table F.4-1 Kinetic Data for Pt/FC10 Catalyst

Run NO.	Temp. (°C)	F_T (cm^3/s)	Inlet Conc. (mol/cm^3)	Outlet Concentration (mol/cm^3)					Mass. Bal. (%)
			CH_3OH	CH_3OH	$HCOOCH_3$	CO_2	CH_2O	H_2O	
FC1-1	40.0	227	2.8575E-8	1.9760E-8	3.6709E-9	1.6959E-9	3.6194E-10	-	-2.0
FC1-2	39.8	228	5.7304E-8	4.0071E-8	6.2942E-9	2.3661E-9	9.3780E-10	-	2.3
FC1-3	41.0	227	1.0948E-7	8.6043E-8	9.4278E-9	2.5078E-9	1.0131E-9	3.3826E-8	1.0
FC1-4	52.3	228	2.5063E-8	1.5568E-8	3.2183E-9	1.8707E-9	9.5665E-10	-	0.9
FC1-5	52.7	227	5.9939E-8	3.9471E-8	6.9523E-9	3.0345E-9	2.1489E-9	2.9933E-8	2.3
FC1-6	52.7	226	1.0542E-7	7.5632E-8	1.2196E-8	4.1418E-9	2.9549E-9	5.2506E-8	-1.6
FC1-7	64.8	226	2.4866E-8	1.4486E-8	2.9683E-9	2.3199E-9	1.9900E-9	-	0.5
FC1-8	65.2	227	6.0827E-8	3.6503E-8	7.0779E-9	4.2724E-9	4.5243E-9	3.5447E-8	2.3
FC1-9	65.6	226	1.0586E-7	6.6437E-8	1.3428E-8	7.1314E-9	7.0540E-9	7.1240E-8	-1.5
FC1-10	77.1	226	2.6048E-8	1.3192E-8	2.6223E-9	3.4603E-9	3.6101E-9	-	2.1
FC1-11	77.8	226	5.9596E-8	3.2575E-8	6.4673E-9	6.8752E-9	8.2122E-9	4.7621E-8	-1.7
FC1-12	77.8	226	1.0605E-7	5.7530E-8	1.2477E-8	1.2107E-8	1.3040E-8	9.4927E-8	-1.5
FC1-13	90.4	226	2.6876E-8	1.2328E-8	1.9893E-9	5.0907E-9	5.0570E-9	-	1.6
FC1-14	90.0	226	6.1333E-8	3.0777E-8	4.8176E-9	1.0664E-8	1.0986E-8	5.7767E-8	-1.2
FC1-15	88.7	226	1.1070E-7	5.5799E-8	9.3495E-9	1.9497E-8	1.7795E-8	1.1246E-7	-1.0
FC1-16	101.4	229	2.7124E-8	1.1551E-8	1.5124E-9	6.7775E-9	5.3433E-9	2.8628E-8	1.6
FC1-17	102.3	231	6.1977E-8	2.7952E-8	3.0445E-9	1.5881E-8	1.2305E-8	7.3218E-8	-0.4
FC1-18	101.9	233	1.1195E-7	4.9885E-8	5.6707E-9	3.0858E-8	2.0937E-8	1.4546E-7	-1.0

Table F.4-2 Rate Data for Pt/FC10 Catalyst

Run NO.	Temperature (K)	P_{MeOH} (mmHg)	$-r_{MeOH}$ (mol/cm² Pt·s)
FC1-1	313.2	0.5215	3.4180E-9
FC1-2	313.0	1.0575	6.7118E-9
FC1-3	314.2	2.2707	9.0890E-9
FC1-4	325.5	0.4108	3.6983E-9
FC1-5	325.9	1.0416	7.9372E-9
FC1-6	325.9	1.9959	1.1501E-8
FC1-7	338.0	0.3823	4.0075E-9
FC1-8	338.4	0.9633	9.4325E-9
FC1-9	338.8	1.7533	1.5221E-8
FC1-10	350.3	0.3481	4.9633E-9
FC1-11	351.0	0.8597	1.043E-8
FC1-12	351.0	1.5182	1.8734E-8
FC1-13	363.6	0.3253	5.6168E-9
FC1-14	363.2	0.8122	1.1797E-8
FC1-15	361.9	1.4726	2.1197E-8
FC1-16	374.6	0.3048	6.0919E-9
FC1-17	375.5	0.7376	1.3427E-8
FC1-18	375.1	1.3165	2.4706E-8

Table F.4-3 Data Obtained from the Plot of $\ln(P_{MeOH})$ vs $\ln(-r_{MeOH})$ for Pt/FC10 Catalyst

Temperature (K)	ln k	α	R^2
313.5	-18.9928	0.66	0.9442
325.8	-18.7445	0.72	0.9909
338.4	-18.4765	0.88	0.9985
350.8	-18.1956	0.89	0.9961
362.9	-18.0325	0.87	0.9971
375.1	-17.7999	0.95	0.9980

F.5 Data for Pt/FC65 Catalyst

Catalyst: 39.2712 g of 0.0026 wt%Pt/FC65/spheres

Table F.5-1 Kinetic Data for Pt/FC65 Catalyst

Run NO.	Temp. (°C)	F_T (cm^3/s)	Inlet Conc. (mol/cm^3)	Outlet Concentration (mol/cm^3)					Mass. Bal. (%)
			CH_3OH	CH_3OH	$HCOOCH_3$	CO_2	CH_2O	H_2O	
FC6-1	58.3	225	3.3771e-8	2.5192e-8	1.5985e-9	2.3055e-9	2.4258e-9	1.2982e-8	1.9
FC6-2	59.1	225	7.0502e-8	5.5365e-8	3.1345e-9	3.6386e-9	5.1252e-9	1.5137e-8	0.1
FC6-3	59.1	225	1.2184e-7	9.8585e-8	5.2051e-9	4.3898e-9	7.1444e-9	2.3256e-8	1.1
FC6-4	69.3	225	3.5932e-8	2.2293e-8	1.9801e-9	3.7906e-9	5.2354e-9	1.3639e-8	1.8
FC6-5	69.9	225	7.7412e-8	5.1330e-8	4.0966e-9	6.6335e-9	1.0404e-8	2.6082e-8	1.1
FC6-6	70.0	225	1.2415e-7	8.5851e-8	6.9200e-9	8.8729e-9	1.4663e-8	3.8302e-8	0.7
FC6-7	80.5	225	3.6378e-8	1.7850e-8	2.2296e-9	6.1715e-9	8.4570e-9	1.8529e-8	-1.5
FC6-8	81.6	226	8.0058e-8	4.1282e-8	4.5970e-9	1.1534e-8	1.7050e-8	3.8776e-8	1.2
FC6-9	81.9	224	1.2650e-7	6.8317e-8	7.5977e-9	1.6040e-8	2.4421e-8	5.8178e-8	2.0
FC6-10	92.0	231	4.0797e-8	1.4401e-8	2.1996e-9	9.6609e-9	1.1409e-8	2.6396e-8	2.3
FC6-11	92.9	229	8.5414e-8	3.2014e-8	4.6595e-9	1.9102e-8	2.2951e-8	5.3400e-8	2.4
FC6-12	93.1	228	1.3798e-7	5.5278e-8	8.5165e-9	2.8221e-8	3.5629e-8	8.2705e-8	1.3
FC6-13	103.5	228	4.1794e-8	9.6906e-9	1.8935e-9	1.4852e-8	1.2518e-8	3.2103e-8	2.3
FC6-14	104.2	228	8.6947e-8	2.1827e-8	3.8842e-9	3.2104e-8	2.5139e-8	6.5119e-8	0.1
FC6-15	103.4	228	1.4553e-7	3.9351e-8	7.7665e-9	4.8901e-8	4.0673e-8	1.0617e-7	0.7

Table F.5-2 Rate Data for Pt/FC65 Catalyst

Run NO.	Temperature (K)	P_{MeOH} (mmHg)	$-r_{MeOH}$ (mol/cm² Pt·s)
FC6-1	331.5	0.6648	3.2590e-10
FC6-2	332.3	1.4611	5.7505e-10
FC6-3	332.3	2.6017	8.8349e-10
FC6-4	342.5	0.5883	5.1814e-10
FC6-5	343.1	1.3546	9.9085e-10
FC6-6	343.2	2.2656	1.4551e-9
FC6-7	353.7	0.4711	7.0391e-10
FC6-8	354.8	1.0894	1.4796e-9
FC6-9	355.1	1.8029	2.2004e-9
FC6-10	365.2	0.3800	1.0295e-9
FC6-11	366.1	0.8448	2.0647e-9
FC6-12	366.3	1.4588	3.1838e-9
FC6-13	376.7	0.2557	1.2359e-9
FC6-14	377.4	0.5760	2.5068e-9
FC6-15	376.6	1.0385	4.0872e-9

Table F.5-3 Data Obtained from the Plot of $\ln(P_{MeOH})$ vs $\ln(-r_{MeOH})$ for Pt/FC65 Catalyst

Temperature (K)	ln k	α	R^2
332.0	-21.5484	0.73	0.9999
342.9	-20.9715	0.77	0.9999
354.5	-20.4247	0.85	0.9991
365.8	-19.8731	0.84	0.9993
376.9	-19.3422	0.85	0.9998

F.6 Data for Pt/Al_2O_3 Catalyst

Catalyst: 2.3224 g of 0.0028 wt%Pt/Al_2O_3/spheres

Table F.6-1 Kinetic Data for Pt/Al_2O_3 Catalyst

Run NO.	Temp. (°C)	F_T (cm^3/s)	Inlet Conc. (mol/cm^3)	Outlet Concentration (mol/cm^3)					Mass. Bal. (%)
			CH_3OH	CH_3OH	$HCOOCH_3$	CO_2	CH_2O	H_2O	
AL-1	32.6	228	4.5852E-8	3.6095E-8	4.7160E-9	6.8110E-10	-	1.2104E-8	-0.8
AL-2	33.3	228	1.0648E-7	8.9709E-8	8.1321E-9	1.4872E-9	-	1.7934E-8	-0.9
AL-3	33.0	228	1.5300E-7	1.3277E-7	8.5531E-9	1.5024E-9	-	2.0074E-8	1.1
AL-4	32.4	230	4.4655E-8	3.5380E-8	4.1999E-9	5.3987E-10	-	9.0522E-9	0.8
AL-5	45.1	226	4.6827E-8	3.2478E-8	7.1370E-9	2.0547E-9	-	1.7979E-8	-4.2
AL-6	45.0	227	1.0218E-7	7.4958E-8	1.3753E-8	3.6007E-9	6.9869E-10	3.5575E-8	-4.5
AL-7	45.0	228	1.8632E-7	1.3842E-7	2.0396E-8	5.0700E-9	1.0725E-9	5.3518E-8	0.5
AL-8	58.0	230	4.3796E-8	2.5982E-8	7.4805E-9	3.5442E-9	1.0972E-9	2.4561E-8	-4.1
AL-9	58.8	230	1.2205E-7	7.4584E-8	2.0037E-8	7.9863E-9	3.0118E-9	6.5466E-8	3.0
AL-10	58.9	227	2.1435E-7	1.3017E-7	3.3264E-8	1.2332E-8	4.2899E-9	1.0681E-7	0.5
AL-11	71.3	232	4.1566E-8	1.9678E-8	6.5267E-9	5.6906E-9	2.1640E-9	3.1471E-8	2.4
AL-12	70.9	232	9.6841E-8	5.1666E-8	1.6762E-8	1.1595E-8	5.2266E-9	7.2334E-8	-5.3
AL-13	71.4	232	1.6026E-7	8.6400E-8	2.8148E-8	1.7807E-8	7.7627E-9	1.1589E-7	-5.0
AL-14	84.5	229	4.2329E-8	1.8291E-8	6.1123E-9	9.5180E-9	3.6131E-9	3.8802E-8	-3.1
AL-15	85.0	229	9.4649E-8	4.1489E-8	1.3968E-8	1.8491E-8	7.8700E-9	8.6046E-8	-1.2
AL-16	85.1	229	1.6047E-7	7.2412E-8	2.5216E-8	3.0153E-8	1.2350E-8	1.4851E-7	-3.0

Table F.6-2 Rate Data for Pt/Al_2O_3 Catalyst

Run NO.	Temperature (K)	P_{MeOH} (mmHg)	$-r_{MeOH}$ (mol/cm² Pt·s)
AL-1	305.8	0.9525	4.0378E-9
AL-2	306.5	2.3674	6.9418E-9
AL-3	306.2	3.5038	8.3720E-9
AL-4	305.6	0.9337	3.8720E-9
AL-5	318.3	0.8571	5.8861E-9
AL-6	318.2	1.9781	1.1216E-8
AL-7	318.2	3.6529	1.9823E-8
AL-8	331.2	0.6857	7.4368E-9
AL-9	332.0	1.9683	1.9816E-8
AL-10	332.1	3.4352	3.4684E-8
AL-11	344.5	0.5193	9.2170E-9
AL-12	344.1	1.3635	1.9023E-8
AL-13	344.6	2.2801	3.1102E-8
AL-14	357.7	0.4827	9.9915E-9
AL-15	358.2	1.0949	2.2096E-8
AL-16	358.3	1.9110	3.6602E-8

Table F.6-3 Data Obtained from the Plot of $\ln(P_{MeOH})$ vs $\ln(-r_{MeOH})$ for Pt/Al_2O_3 Catalyst

Temperature (K)	ln k	α	R^2
306.2	-19.3110	0.58	0.9970
318.2	-18.8378	0.83	0.9970
332.0	-18.3640	0.95	0.9996
344.2	-17.9850	0.81	0.9959
358.2	-17.7273	0.95	0.9996

G. CONVERSION AND SELECTIVITY DATA

G.1 Data for Pt/FC10 catalyst

Catalyst: 1.4152 g of 0.0061 wt% Pt/FC10 spheres

Run NO.	Temp. (°C)	F_T (cm^3/s)	Inlet Conc. (mol/cm^3)	Outlet Concentration (mol/cm^3)					Mass. Bal. (%)
			CH_3OH	CH_3OH	$HCOOCH_3$	CO_2	CH_2O	H_2O	
FC1-2	39.8	228	5.7304E-8	4.0071E-8	6.2942E-9	2.3661E-9	9.3780E-10	-	2.3
FC1-5	52.7	227	5.9939E-8	3.9471E-8	6.9523E-9	3.0345E-9	2.1489E-9	2.9933E-8	2.3
FC1-8	65.2	227	6.0827E-8	3.6503E-8	7.0779E-9	4.2724E-9	4.5243E-9	3.5447E-8	2.3
FC1-11	77.8	226	5.9596E-8	3.2575E-8	6.4673E-9	6.8752E-9	8.2122E-9	4.7621E-8	-1.7
FC1-14	90.0	226	6.1333E-8	3.0777E-8	4.8176E-9	1.0664E-8	1.0986E-8	5.7767E-8	-1.2
FC1-17	102.3	231	6.1977E-8	2.7952E-8	3.0445E-9	1.5881E-8	1.2305E-8	7.3218E-8	-0.4
FC1-19	119.2	234	7.0049E-8	2.6558E-8	2.0534E-9	2.5575E-8	1.5325E-8	1.0888E-7	-2.2
FC1-20	148.2	230	6.2698E-8	1.6546E-8	1.1497E-9	2.9577E-8	1.3630E-8	1.1702E-7	1.0
FC1-21	176.2	234	6.2698E-8	1.3681E-8	8.7321E-10	3.3332E-8	1.3329E-8	1.3117E-7	1.0

Temperature (°C)	CH_3OH Conversion (%)	Selectivity (%)		
		$HCOOCH_3$	CO_2	CH_2O
39.8	30.1	65.6	24.1	9.8
52.7	34.1	57.3	25.0	17.7
65.2	40.0	44.6	26.9	28.5
77.8	45.3	30.0	31.9	38.1
90.0	49.8	18.2	40.3	41.5
102.3	54.9	9.7	50.9	39.4
119.2	62.1	4.8	59.5	35.7
148.2	73.6	2.6	66.7	30.7
176.2	78.2	1.8	70.1	28.1

G.2 Data for Pt/FC28 catalyst

Catalyst: 21.5820 g of 0.0023 wt%Pt/FC28/spheres

Run NO.	Temp (°C)	F_T (cm^3/s)	Inlet Conc. (mol/cm^3)	Outlet Concentration (mol/cm^3)					Mass. Bal. (%)
			CH_3OH	CH_3OH	$HCOOCH_3$	CO_2	CH_2O	H_2O	
Z-2	59.0	231	9.1131E-8	8.5811E-8	1.6151E-9	1.3300E-9	6.6879E-10	8.4044E-9	0.1
Z-5	72.1	232	9.0164E-8	7.8136E-8	2.0041E-9	2.8971E-9	2.7634E-9	1.6522E-8	2.6
Z-8	85.5	232	8.8631E-8	7.0289E-8	2.4398E-9	5.7248E-9	6.3975E-9	2.7248E-8	1.5
Z-11	98.5	232	8.5678E-8	6.1537E-8	2.4644E-9	8.4779E-9	9.7032E-9	4.0916E-8	1.2
Z-31	111.4	232	8.8273E-8	5.8309E-8	2.4305E-9	1.2409E-8	1.3354E-8	5.2458E-8	-0.8
Z-17	124.1	232	8.9231E-8	5.2564E-8	2.1396E-9	1.6577E-8	1.6035E-8	6.4838E-8	-0.3
Z-20	136.7	231	8.7485E-8	4.6212E-8	1.8123E-9	2.0540E-8	1.7772E-8	7.5857E-8	-0.8
Z-23	162.0	231	8.3888E-8	3.6628E-8	1.2884E-9	2.9086E-8	2.0396E-8	1.0129E-7	-5.7
Z-26	187.1	228	8.5319E-8	2.6870E-8	9.7883E-10	3.6975E-8	2.0767E-8	1.2017E-7	-1.5
Z-29	210.7	228	8.3058E-8	2.0854E-8	-	4.4045E-8	1.9037E-8	1.3721E-7	-1.1

Temperature (°C)	CH_3OH Conversion (%)	Selectivity (%)		
		$HCOOCH_3$	CO_2	CH_2O
59.0	5.8	44.7	36.8	18.5
72.1	13.3	26.1	37.8	36.1
85.5	20.7	16.8	39.3	43.9
98.5	28.2	11.9	41.1	47.0
111.4	33.9	8.6	44.0	47.4
124.1	41.1	6.2	47.7	46.1
136.7	47.2	4.5	51.2	44.3
162.0	56.3	2.5	57.3	40.2
187.1	68.5	1.7	63.0	35.3
210.7	74.9	0.0	69.8	30.2

G.3 Data for Pt/FC65 Catalyst

Catalyst: 39.2712 g of 0.0026 wt%Pt/FC65/spheres

Run NO.	Temp. (°C)	F_T (cm^3/s)	Inlet Conc. (mol/cm^3)	Outlet Concentration (mol/cm^3)					Mass. Bal. (%)
			CH_3OH	CH_3OH	$HCOOCH_3$	CO_2	CH_2O	H_2O	
FC6-2	59.1	225	7.0502e-8	5.5365e-8	3.1345e-9	3.6386e-9	5.1252e-9	1.5137e-8	0.1
FC6-5	69.9	225	7.7412e-8	5.1330e-8	4.0966e-9	6.6335e-9	1.0404e-8	2.6082e-8	1.1
FC6-8	81.6	226	8.0058e-8	4.1282e-8	4.5970e-9	1.1534e-8	1.7050e-8	3.8776e-8	1.2
FC6-11	92.9	229	8.5414e-8	3.2014e-8	4.6595e-9	1.9102e-8	2.2951e-8	5.3400e-8	2.4
FC6-14	104.2	228	8.6947e-8	2.1827e-8	3.8842e-9	3.2104e-8	2.5139e-8	6.5119e-8	0.1
FC6-16	114.4	231	8.7637e-8	1.2916e-8	2.8609e-9	4.5828e-8	2.2337e-8	1.9555e-7	1.0

Temperature (°C)	CH_3OH Conversion (%)	Selectivity (%)		
		$HCOOCH_3$	CO_2	CH_2O
59.1	21.5	26.3	30.6	43.1
69.9	33.7	19.4	31.4	49.2
81.6	48.4	13.9	34.8	51.4
92.9	62.5	10.0	40.9	49.1
104.2	74.9	6.4	52.5	41.1
114.4	85.3	4.0	64.5	31.4

G.4 Data for Pt/Al_2O_3 Catalyst

Catalyst: 2.3224 g of 0.0028 wt%Pt/Al_2O_3/spheres

Run NO.	Temp. (°C)	F_T (cm^3/s)	Inlet Conc. (mol/cm^3)	Outlet Concentration (mol/cm^3)					Mass. Bal. (%)
			CH_3OH	CH_3OH	$HCOOCH_3$	CO_2	CH_2O	H_2O	
AL-2	33.3	228	1.0648E-7	8.9709E-8	8.1321E-9	1.4872E-9	-	1.7934E-8	-0.9
AL-6	45.0	227	1.0218E-7	7.4958E-8	1.3753E-8	3.6007E-9	6.9869E-10	3.5575E-8	-4.5
AL-9	58.8	230	1.2205E-7	7.4584E-8	2.0037E-8	7.9863E-9	3.0118E-9	6.5466E-8	3.0
AL-12	70.9	232	9.6841E-8	5.1666E-8	1.6762E-8	1.1595E-8	5.2266E-9	7.2334E-8	-5.3
AL-15	85.0	229	9.4649E-8	4.1489E-8	1.3968E-8	1.8491E-8	7.8700E-9	8.6046E-8	-1.2
AL-17	105.6	230	1.0936E-7	3.9238E-8	8.8061E-9	3.9026E-8	1.4490E-8	1.7589E-7	-0.9
AL-18	129.7	230	1.0739E-7	3.2904E-8	3.7408E-9	5.2316E-8	1.3475E-8	2.0196E-7	1.1
AL-19	154.0	229	9.3022E-8	2.4891E-8	1.6753E-9	5.6402E-8	1.0025E-8	1.6285E-7	-1.8
AL-20	178.2	229	9.6335E-8	2.3286E-8	1.1883E-9	6.3816E-8	8.2848E-9	1.9888E-7	-1.5
AL-21	212.7	229	9.0499E-8	2.0373E-8	-	6.6286E-8	6.2473E-9	1.8463E-7	-2.7

Temperature (°C)	CH_3OH Conversion (%)	Selectivity (%)		
		$HCOOCH_3$	CO_2	CH_2O
33.3	15.8	84.5	15.5	0.0
45.0	26.6	76.2	19.9	3.9
58.8	38.9	64.6	25.7	9.7
70.9	46.6	49.9	34.5	15.6
85.0	56.2	34.6	45.9	19.5
105.6	64.1	14.1	62.6	23.3
129.7	69.4	5.4	75.2	19.4
154.0	73.2	2.5	82.8	14.7
178.2	75.8	1.6	87.1	11.3
212.7	77.5	0.0	91.4	8.6

H. CATALYST STABILITY DATA (wet and dry conditions)

H.1-1 Data for Pt/FC10 catalyst (dry conditions)

Catalyst: 1.3744 g of 0.0061 wt% Pt/FC10 spheres

Temperature = 170 °C Flowrate = 230 mL/min Inlet Conc. = 2764 ppm MeOH

Time (hours)	Methanol Conversion (%)
0.42	88.4
0.75	88.2
1.00	87.9
2.83	86.1
4.66	84.8
6.49	83.9
8.32	83.4
10.15	82.3
11.98	81.9
13.81	81.0
15.64	80.5
17.47	79.7
19.30	79.3
21.13	78.9
22.96	79.2
24.79	78.5

H.1-2 Data for Pt/FC10 catalyst (wet conditions)

Catalyst: 1.3744 g of 0.0061 wt% Pt/FC10 spheres

Temperature = 170 °C Flowrate = 230 mL/min Inlet Conc. = 2427 ppm MeOH

Water Partial Pressure = 1.7 kPa

Time (hours)	Methanol Conversion (%)
0.08	75.1
0.42	72.0
0.75	70.2
1.00	69.2
2.83	64.7
4.66	62.0
6.49	60.2
8.32	58.8
10.15	58.9
11.98	58.8
13.81	57.4
15.64	56.5
21.33	57.9
22.33	57.5
23.66	57.5

H.1-3 Data for Pt/FC10 catalyst (cyclic behaviour figure 8.4)

Catalyst: 1.3744 g of 0.0061 wt% Pt/FC10 spheres

Temperature = 170 °C Flowrate = 230 mL/min Inlet Conc. = 2427 ppm MeOH

Water Partial Pressure = 1.7 kPa

Time (hours)	Methanol Conversion (%)		Time (hours)	Methanol Conversion (%)	
	Dry Feed	Wet Feed		Dry Feed	Wet Feed
0.42	88.4		48.53	61.4	
0.75	88.2		48.87	64.4	
1.00	87.9		49.20	64.9	
2.83	86.1		49.45	66.4	
4.66	84.8		51.28	68.9	
6.49	83.9		53.11	70.5	
8.32	83.4		54.94	71.2	
10.15	82.3		56.77	71.5	
11.98	81.9		58.60	72.3	
13.81	81.0		60.43	71.9	
15.64	80.5		62.26	71.7	
17.47	79.7		64.09	71.5	
19.30	79.3		65.92	71.8	
21.13	78.9		67.75	72.6	
22.96	79.2		69.58	72.9	
24.79	78.5		71.41	73.0	
24.87		75.1	71.49		67.3
25.21		72.0	71.83		63.3
25.54		70.2	72.16		61.5
25.79		69.2	72.41		61.2
27.62		64.7	74.24		59.9
29.45		62.0	76.07		59.3
31.28		60.2	77.90		58.9
33.11		58.8	79.73		58.7
34.94		58.9	81.56		58.6
36.77		58.8	83.39		58.0
38.60		57.4	85.22		56.7
40.43		56.5	87.05		56.6
46.12		57.9	88.88		56.3
47.12		57.5	90.71		56.6
48.45		57.5	92.54		57.0
			94.37		58.3

H.2-1 Data for Pt/FC28 catalyst (dry conditions)

Catalyst: 9.8051 g of 0.0051 wt% Pt/FC28 spheres

Temperature = 163 °C Flowrate = 231 mL/min Inlet Conc. = 2751 ppm MeOH

Time (hours)	Methanol Conversion (%)
1.75	82.9
2.08	80.9
3.92	73.4
4.25	72.6
6.08	69.5
6.42	68.8
8.25	67.0
8.58	66.3
10.42	65.3
10.75	65.4
12.58	63.5
12.92	63.1
14.75	61.8
15.08	61.5
16.92	61.0
17.25	60.5
19.08	60.5
19.42	60.4
21.25	60.0
21.58	60.2
23.42	61.1
23.75	60.9
25.58	61.5
25.92	61.1

H.2-2 Data for Pt/FC28 catalyst (wet conditions)

Catalyst: 9.8051 g of 0.0051 wt% Pt/FC28 spheres

Temperature = 162 °C Flowrate = 231 mL/min Inlet Conc. = 2263 ppm MeOH

Water Partial Pressure = 1.4 kPa

Time (hours)	Methanol Conversion (%)
0.08	46.2
0.42	40.2
0.75	36.8
1.00	34.9
2.83	32.7
4.67	31.8
6.50	31.0
8.33	30.3
10.17	28.5
12.00	26.9
13.83	26.1
15.67	26.3
17.50	26.7
19.33	26.5

H.2-3 Data for Pt/FC28 catalyst (cyclic behavior Figure 8.5)

Catalyst: 9.8051 g of 0.0051 wt% Pt/FC28 spheres

Temperature = 162 °C Flowrate = 231 mL/min Inlet Conc. = 2263 ppm MeOH

Water Partial Pressure = 1.4 kPa

Time (hours)	Methanol Conversion (%)		Time (hours)	Methanol Conversion (%)	
	Dry Feed	Wet Feed		Dry Feed	Wet Feed
1.75	82.9		46.76	44.5	
2.08	80.9		48.59	46.4	
3.92	73.4		50.43	47.2	
4.25	72.6		52.26	48.6	
6.08	69.5		54.09	49.4	
6.42	68.8		55.93	49.5	
8.25	67.0		57.76	48.8	
8.58	66.3		59.59	49.1	
10.42	65.3		61.43	49.0	
10.75	65.4		63.26	49.6	
12.58	63.5		65.09	49.4	
12.92	63.1		80.42	47.3	air purge 163 °C
14.75	61.8		81.87	47.8	air purge 163 °C
15.08	61.5		83.17	47.9	air purge 163 °C
16.92	61.0		107.17	59.9	air purge 205 °C
17.25	60.5		109.17	59.8	air purge 205 °C
19.08	60.5		109.58		43.4
19.42	60.4		109.91		41.4
21.25	60.0		110.25		39.1
21.58	60.2		110.58		37.5
23.42	61.1		112.41		33.5
23.75	60.9		114.25		31.5
25.58	61.5		116.08		28.4
25.92	61.1		117.91		26.7
26.00		46.2	119.75		26.2
26.33		40.2	121.58		26.1
26.67		36.8	123.41		25.7
27.00		34.9	125.25		26.4
28.83		32.7	125.67	34.0	
30.67		31.8	126.00	40.1	
32.50		31.0	126.34	40.8	
34.33		30.3	126.67	41.0	
36.17		28.5	128.50	43.3	
38.00		26.9	130.34	45.1	
39.83		26.1	132.17	46.0	
41.67		26.3	134.00	46.8	
43.50		26.7	135.84	47.8	
45.33		26.5	137.67	48.5	
45.76	38.9		161.67	58.3	air purge 205 °C
46.09	40.0		162.67	57.2	air purge 205 °C
46.43	40.7				

H.3-1 Data for Pt/FC65 catalyst (dry conditions)

Catalyst: 39.2712 g of 0.0026 wt% Pt/FC65 spheres

Temperature = 166°C Flowrate = 231 mL/min Inlet Conc. = 2828 ppm MeOH

Time (hours)	Methanol Conversion (%)
0.08	97.1
0.42	96.8
0.75	96.3
1.00	95.8
2.83	93.8
4.67	92.3
6.50	91.0
8.33	90.2
10.17	89.4
12.00	89.3
13.83	88.9
15.67	88.8
17.50	88.6
19.33	88.7
21.17	88.9
23.00	89.3

H.3-2 Data for Pt/FC65 catalyst (wet conditions)

Catalyst: 39.2712 g of 0.0026 wt% Pt/FC65 spheres

Temperature = 166 °C Flowrate = 231 mL/min Inlet Conc. = 2395 ppm MeOH

Water Partial Pressure = 1.4 kPa

Time (hours)	Methanol Conversion (%)
0.08	65.5
0.42	56.2
0.75	53.6
1.00	52.8
2.83	50.1
4.67	48.2
6.50	47.0
8.33	46.2
10.17	44.5
12.00	42.3
13.83	40.1
15.67	39.8
17.50	38.1
19.33	38.4
21.17	37.8
23.00	37.3
24.83	37.9

H.4-1 Data for Pt/SDB catalyst (cyclic behavior Figure 8.6)

Catalyst: 8.4859 g of 0.002 wt% Pt/FC10 spheres

Temperature = 160 °C Flowrate = 230 mL/min Inlet Conc. = 2314 ppm MeOH

Water Partial Pressure = 1.4 kPa

Time (hours)	Methanol Conversion (%)		Time (hours)	Methanol Conversion (%)	
	Dry Feed	Wet Feed		Dry Feed	Wet Feed
0.08	21.4		42.08		51.1
0.33	20.4		43.83		51.1
0.58	23.5		45.58		51.3
0.83	31.4		47.33		50.4
2.58	58.6		47.58	54.3	
4.33	68.1		47.83	61.3	
6.08	74.5		48.08	62.7	
7.83	77.5		48.33	63.1	
9.58	79.0		50.08	68.7	
11.33	79.9		51.83	71.8	
13.08	80.4		53.58	75.8	
14.83	80.9		55.33	75.8	
16.58	81.4		57.08	75.7	
18.33	81.7		58.83	75.6	
20.08	82.2		60.58	75.6	
21.83	82.4		62.33	76.2	
23.58	82.2		64.08	76.7	
25.33	82.1		65.83	77.0	
27.08	81.9		67.58	76.2	
27.33		65.8	69.33	76.7	
27.83		60.3	71.08	76.9	
28.08		60.9	72.83	76.6	
29.83		60.9	74.58	75.6	
31.58		57.2	76.33	76.4	
33.33		54.8	78.08	76.2	
35.08		52.5	79.83	76.4	
36.83		50.8	81.58	76.3	
38.58		49.6	83.33	76.3	
40.33		50.4			

H.5-1 Data for Pt/Al_2O_3 catalyst (dry conditions)

Catalyst: 4.7845 g of 0.0028 wt% Pt/Al_2O_3 spheres

Temperature = 71 °C Flowrate = 232 mL/min Inlet Conc. = 2247 ppm MeOH

Time (hours)	Methanol Conversion (%)
1.50	69.8
1.75	70.5
12.00	74.1
12.25	73.7
13.50	73.4
13.75	72.9
15.00	73.2
15.25	73.1
16.50	72.8
16.75	72.5
18.00	72.3
18.25	72.5
19.50	71.7
19.75	71.9
21.00	72.0
21.25	71.5
22.50	71.4
22.75	71.4
24.00	71.7
24.25	70.6

H.5-2 Data for Pt/Al_2O_3 catalyst (wet conditions)

Catalyst: 4.7845 g of 0.0028 wt% Pt/Al_2O_3 spheres

Temperature = 71 °C Flowrate = 231 mL/min Inlet Conc. = 2354 ppm MeOH

Water Partial Pressure = 1.4 kPa

Time (hours)	Methanol Conversion (%)
0.50	61.1
0.75	60.4
1.50	59.6
1.75	59.0
2.50	58.0
2.75	57.7
3.50	56.9
3.75	56.5
4.50	55.8
4.75	55.3
5.50	54.7
5.75	54.4
6.50	53.1
6.75	52.7
8.50	51.0
8.75	50.6
10.50	49.1
10.75	49.0
12.50	43.7
12.75	43.1
14.50	40.2
14.75	39.6
16.50	37.9
16.75	37.6
18.50	35.7
18.75	35.3

I. RATE DATA FOR WET FEED CONDITIONS

I.1 Data for Pt/FC10 catalyst

Catalyst: 1.4152 g of 0.0061 wt% Pt/FC10 spheres

Inlet water partial pressure = 1.1 kPa

Run NO.	Temp (°C)	F_T (cm^3/s)	Inlet Conc. (mol/cm^3)	Outlet Concentration (mol/cm^3)					Mass. Bal. (%)
			CH_3OH	CH_3OH	$HCOOCH_3$	CO_2	CH_2O	H_2O	
FC1-22	115.5	226	5.6032e-8	4.6039e-8	8.5893e-10	3.5711e-9	3.9710e-9	3.0514e-7	1.3
FC1-23	126.8	227	5.8299e-8	4.0422e-8	9.7387e-10	7.0998e-9	8.3729e-9	3.2784e-7	0.8
FC1-24	138.4	227	5.8832e-8	3.3483e-8	9.8721e-10	1.0742e-8	1.1556e-8	3.3127e-7	1.8
FC1-25	151.8	229	6.1382e-8	2.9684e-8	9.4868e-10	1.5018e-8	1.4159e-8	3.6162e-7	1.0
FC1-26	166.1	229	6.0765e-8	2.4331e-8	8.7211e-10	1.8532e-8	1.5041e-8	3.6154e-7	1.8
FC1-27	176.6	230	6.0765e-8	2.1287e-8	8.2554e-10	2.1956e-8	1.5410e-8	3.7140e-7	0.8

Temperature (°C)	Reaction Rate (mol/cm^2 Pt·s)	Selectivity (%)		
		$HCOOCH_3$	CO_2	CH_2O
115.5	3.8583e-9	10.2	42.5	47.3
126.8	6.9325e-9	5.9	43.2	50.9
138.4	9.8304e-9	4.2	46.1	49.6
151.8	1.2400e-9	3.1	49.9	47.0
166.1	1.4253e-8	2.5	53.8	43.7
176.6	1.5511e-8	2.2	57.5	40.3

I.2 Data for Pt/FC28 catalyst

Catalyst: 21.5820 g of 0.0023 wt%Pt/FC28/spheres

I.2-1 Dry feed after exposure to water

Run NO.	Temp (°C)	F_T (cm^3/s)	Inlet Conc. (mol/cm^3)	Outlet Concentration (mol/cm^3)					Mass. Bal. (%)
			CH_3OH	CH_3OH	$HCOOCH_3$	CO_2	CH_2O	H_2O	
Z-31	109.4	230	8.8706e-8	8.1135e-8	1.0287e-9	2.5948e-9	3.7587e-9	3.9540e-9	-0.9
Z-32	134.7	230	9.0090e-8	6.8369e-8	1.1940e-9	8.9256e-9	1.0100e-8	3.6010e-8	0.3
Z-33	161.1	230	8.9266e-8	5.6211e-8	1.0758e-9	1.6770e-8	1.5653e-8	6.1430e-8	-1.7
Z-34	185.7	225	8.7753e-8	4.3098e-8	9.1443e-10	2.4471e-8	1.9106e-8	8.4530e-8	-0.9
Z-35	209.6	228	8.4014e-8	3.4520e-8	-	3.0912e-8	1.9316e-8	1.011e-7	-0.9

Temperature (°C)	Reaction Rate (mol/cm^2 Pt·s)	Selectivity (%)		
		$HCOOCH_3$	CO_2	CH_2O
109.4	4.2471e-10	13.9	35.2	50.9
134.7	1.2185e-9	5.9	44.1	50.0
161.1	1.8543e-9	3.2	50.1	46.7
185.7	2.4505e-9	2.1	55.0	42.9
209.6	2.7523e-9	0.0	61.5	38.5

I.2-2 Inlet water partial pressure = 0.4 kPa

Run NO.	Temp (°C)	F_T (cm^3/s)	Inlet Conc. (mol/cm^3)	Outlet Concentration (mol/cm^3)					Mass. Bal. (%)
			CH_3OH	CH_3OH	$HCOOCH_3$	CO_2	CH_2O	H_2O	
Z-36	134.7	231	8.7500e-8	7.4400e-8	9.0400e-10	4.6800e-9	6.7800e-9	1.4220e-7	-0.3
Z-37	160.5	230	8.6900e-8	6.0800e-8	9.0200e-10	1.1700e-8	1.2800e-8	1.6150e-7	-0.1
Z-38	185.4	230	8.7363e-8	4.8947e-8	-	2.0129e-8	1.7869e-8	2.1250e-7	0.5
Z-39	209.5	228	7.7227e-8	3.4449e-8	-	2.6210e-8	1.7923e-8	2.1070e-7	-1.8

Temperature (°C)	Reaction Rate (mol/cm^2 Pt·s)	Selectivity (%)		
		$HCOOCH_3$	CO_2	CH_2O
134.7	7.3394e-10	7.3	37.9	54.8
160.5	1.4666e-9	3.6	46.0	50.4
185.4	2.1550e-9	0.0	53.0	47.0
209.5	2.3788e-9	0.0	59.4	40.6

I.2-3 Inlet water partial pressure = 2.2 kPa

Run	Temp	F_T	Inlet Conc.	Outlet Concentration					Mass. Bal.
NO.	(°C)	(cm^3/s)	(mol/cm^3)	(mol/cm^3)					(%)
			CH_3OH	CH_3OH	$HCOOCH_3$	CO_2	CH_2O	H_2O	
Z-40	135.3	229	8.5431e-8	8.1251e-8	-	6.3852e-10	1.2474e-9	6.2130e-7	2.7
Z-41	160.3	232	8.7814e-8	6.9656e-8	-	5.6048e-9	8.3159e-9	6.6990e-7	4.8
Z-42	185.4	231	8.3803e-8	5.6719e-8	-	1.2959e-8	1.4307e-8	7.2080e-7	-0.2
Z-43	210.8	230	7.9888e-8	4.2388e-8	-	2.0745e-8	1.6999e-8	7.0370e-7	-0.3

Temperature	Reaction Rate	Selectivity		
(°C)	(mol/cm^2 Pt·s)	(%)		
		$HCOOCH_3$	CO_2	CH_2O
135.3	2.3346e-10	0.0	33.9	66.1
160.3	1.02745e-9	0.0	40.3	59.7
185.4	1.5259e-9	0.0	47.5	52.5
210.8	2.1036e-9	0.0	55.0	45.0

I.2-4 Inlet water partial pressure = 3.5 kPa

Run NO.	Temp (°C)	F_T (cm^3/s)	Inlet Conc. (mol/cm^3)	Outlet Concentration (mol/cm^3)					Mass. Bal. (%)
			CH_3OH	CH_3OH	$HCOOCH_3$	CO_2	CH_2O	H_2O	
Z-44	160.5	229	8.0003e-8	7.2171e-8	-	3.1454e-9	5.3099e-9	1.0530e-6	-0.8
Z-45	185.2	227	8.1841e-8	6.1413e-8	-	9.9615e-9	1.2036e-8	1.0490e-6	-1.9
Z-46	210.7	226	7.6867e-8	4.7387e-8	-	1.6234e-8	1.4756e-8	1.0570e-6	-2.0

Temperature (°C)	Reaction Rate (mol/cm^2 Pt·s)	Selectivity (%)		
		$HCOOCH_3$	CO_2	CH_2O
160.5	4.3744e-10	0.0	37.2	62.8
185.2	1.1310e-9	0.0	45.3	54.7
210.7	1.6250e-9	0.0	52.4	47.6